CHAPTER ONE
INTRODUCTION

1.1Preface

Nanotechnology is one of the most promising technologies of the 21st century it is the ability to convert the nanoscience theory to useful applications by observing, measuring, manipulating, assembling, controlling and manufacturing matter at the nanometer scale [1].

Nanoparticles and structures have been used by humans in fourth century AD, by the Roman, which demonstrated one of the most interesting examples of nanotechnology in the ancient world [2]. The Lycurgus cup, from the British Museum collection, represents one of the most outstanding achievements in ancient glass industry [3, 4]. It is the oldest famous example of dichroic glass.

Dichroic glass describes two different types of glass, which change color in certain lighting conditions, this means that the Cup have two different colors [5]. The glass appears green in direct light and red-purple when light shines through the glass. In 1990, the scientists analyzed the cup using a transmission electron microscopy (TEM) to explain the phenomenon of dichroism [6, 7]. The observed dichroism (two colors) is due to the presence of nanoparticles with 50–100 nm, in diameter. X-ray analysis showed that these nanoparticles are silver-gold (Ag-Au) alloy, with a ratio of Ag:Au of about 7:3, containing in addition about 10% copper(Cu) disperse in a glass matrix[8].

The American physicist and Nobel Prize laureate Richard Feynman introduce the concept of nanotechnology in 1959. During the annual meeting of the American Physical Society [9], Feynman presented a lecture entitled “There’s Plenty of Room at the Bottom” at the California Institute of Technology (Caltech). In this lecture, Feynman made the hypothesis “Why can’t we write the entire 24 volumes of the Encyclopedia Britannica on the head of a pin?”, and described a vision of using machines to construct smaller machines and down to the molecular level.

This new idea demonstrated that Feynman's hypotheses have been proven correct, and for these reasons, he is considered the father of modern nanotechnology [7, 8]. After fifteen years, Norio Taniguchi, a Japanese scientist was the first to use and define the term "nanotechnology" in 1974 as: "nanotechnology mainly consists of the processing of separation, consolidation, and deformation of materials by one atom or one molecule". After Feynman had discovered this new field of research catching the interest of many scientists, two approaches have been developed describing the different possibilities for the synthesis of nanostructures. These manufacturing approaches fall under two categories: top-down and bottom-up, which differ in degrees of quality, speed and cost [10].

The initial history of nanotubes started in the 1970s. A preparation of the planned carbon filaments was completed by Morinobu Endo who was earning his Ph.D. at the University of Orleans, France. The growth of these carbon filaments were initially thought to be the first carbon nanotubes. However, they failed to meet the measurement requirements for width and thus were deemed, eventually, barrelenes [11].

In 1991 the true first invention of nanotube was finally made, He was credited with the first visual impression of the tubes of atoms that roll up and are capped with fullerene molecules by many scientists in the field. Some state that his discovery just wasn't taken very seriously at the time because science did not know how this discovery could impact scientific research. In 1993 that Iijima and Donald Bethune found single walled nanotubes known as buckytubes. This helped the scientific community make more sense out of not only the potential for nanotube research, but the use and existence of fullerenes [12].

Carbon nanotubes divide into two groups; single wall carbon nanotubes (SWNTs) and multi wall carbon nanotubes (MWNTs) depending on number of concentric graphene cylinder that tube contains. Some of carbon nanotube's excellent physical properties are high aspect ratio, high Young modulus, high tensile

strength, and high thermal and electrical conductivity. Because of their high young modulus and low weight they are useful as reinforcing agents in composite materials and in a variety of applications such as sensors, field emission devices, flat panel displays, energy storage, electrochemical devices and electronic devices Catalyst material is very important for CNT growth. Transition metals are appropriate for CNT growth but especially Fe, Co, Ni is the best ones according to many researchers [13].

1.2 Problem Statement

Carbon nanotubes have wide application in different area such as Energy storage, electronics, fabrics and fibers, air and water filtration and biomedical, there are materials that can be used to improve the limited properties of pure carbon nanotubes such as MgO, ZnO, CuO, TiO2, and CoO. In this research we choose TiO2 and CoO because they are available and cheap.

1.3 Objective

1.3.1 General objective

To synthase and determine structure, morphology and optical properties of carbon nanotubes doping by cobalt oxide and titanium dioxide at different concentration.

1.3.2 Specific Objectives

- To prepare carbon nanotubes (CNTs) doping with cobalt oxide (CoO) and titanium dioxide (TiO_2) using chemical vapour deposition technique (CVD).
- To calculate average diameter of CNTs from scanning electron microscope (SEM) images using imagej software.
- To determine crystal structure of CNTs using X-ray diffraction (XRD) technique.
- To identify functional groups of CNTs using Fourier transform infrared spectroscopy (FTIR) technique.
- To find optical properties of CNTs using UV-visible spectrometer.
- To compere characteristic of CNTs before and after doping with TiO_2 and CoO.

1.4 Methodology

The methodology of the research is based on using chemical vapor deposition (CVD) to synthesize carbon nanotubes (CNTs) doping by cobalt oxide CoO and Titanium dioxide TiO_2 at different concentration, implications of X-ray diffraction (XRD), scanning electron microscopic (SEM), Fourier transform infrared spectroscopy (FTIR) and UV-visible spectrometer to study structure and optical properties of carbon nanotubes (CNTs) doping by cobalt oxide CoO and titanium dioxide TiO_2.

1.5 Literature Review

1.5.1 Nitrogen-Doped Carbon Nanotube/Polypropylene Composites Krause with Negative Seebeck Coefficient

This work done by Beate and et al, This study describes the application of multi-walled carbon nanotubes that were nitrogen-doped during their synthesis (N-MWCNTs) in melt-mixed polypropylene (PP) composites. Different types of N-MWCNTs, synthesized using different methods, were used and compared. Four of the five MWCNT grades showed negative Seebeck coefficients (S), indicating n-type charge carrier behavior. All prepared composites (with a concentration between 2 and 7.5 wt% N-MWCNTs) also showed negative S values, which in most cases had a higher negative value than the corresponding nanotubes. The S values achieved were between 1.0 μV/K and −13.8 μV/K for the N-MWCNT buckypapers or powders and between −4.7 μV/K and −22.8 μV/K for the corresponding composites. With a higher content of N-MWCNTs, the increase in electrical conductivity led to increasing values of the power factor (PF) despite the unstable behavior of the Seebeck coefficient. The highest power factor was achieved with 4 wt% N-MWCNT, where a suitable combination of high electrical conductivity and acceptable Seebeck coefficient led to a PF value of 6.1×10^{-3} $\mu W/(m \cdot K^2)$. First experiments have shown that transient absorption spectroscopy (TAS) is a useful tool to study the carrier transfer process in CNTs in composites and to correlate it with the Seebeck coefficient [14].

1.5.2 Effect of Acetylene Rates and Temperature Variations of Iron Nanoparticles in Carbon nanotubes.

This work by H. Idriss and et al, This study using iron nano particles(Fe NP) with size of 2~3 nm and purity of 99.99% to synthesis carbon nano tubes of iron nanoclusters using low pressures chemical vapor deposition (LPCVD) at temperature range (650 to 950 ^{o}C) and gas flow rates (Argon, 100 standard cubic centimeters per minute (sccm), Hydrogen 50 sccm and Acetylene, 10, 20, 30sccm) were applied respectively, for each 20 minutes of the samples, the best obtained results of the CNTs at temperature 650 ^{o}C and ac aytelene 20sccm, the surface of the obtained CNTs samples was studied using scanning electron microscope (SEM) and their applications were discussed using fractional methods, it was found that the surface roughness of iron CNTs increased with increasing iron sub-particle sizes [15].

1.5.3 Optical Properties of Barium Borate (BaB_2O_4) Compound for Current Optoelectronic Applications.

this work done by Ibtehag Ali Sanosy and et al.This study aimed to study the characteristic of Barium borate (BO2)2 have to use it in optoelectronic applications, Barium borate was prepared by sol-gel synthesis depending on different molar (0.1, 0.2, 0.3 0.4 and 0.5) mole. The optical characteristics of the prepared samples have been investigated by UV/Vis spectrophotometer in the wavelength range of (370 – 620) nm the value of absorbance increase by Ba x increase, absorption of all sample at 467 nm (in the visible region), this means that the transition must be corresponding to a direct electronic transition. The samples have a direct allow electronic transition with optical energy (Eg) values decreased from (2.441) eV to (2.315) eV as the concentration of the samples increased .The value of the Extinction coefficient (K) at the visible region depended on the sample treatment method. The maximum value of (n) equal 2.153for all samples at 510 nm and the value of (n) begins to red shift in the region of the spectrum while Ba_x

increase, this means that the samples become more transparent in the (510 nm)region [16].

1.5.4 The Effect of Annealing Temperature, Doping Carbon Nanotubes with TiO_2, CuO, ZnO And MgO on Its Conductivity and Electrical Primitively

This work done by Azza Abdalwahab Abdalla et al. In this work graphite, potassium chlorate (KClO3) nitric acid (HNO3) and sulfuric acid (H2SO4) were used to form carbon nanotubes (CNTs), the formed CNTs were doped with TiO2, CuO, ZnO And MgO using different annealing temperatures (450,500,550 and 600 oC), It was found that the conductivity and dielectrics constants decrease when the temperature was increased for all samples except for MgO where they were increased [17].

1.5.5 The effect of Fe and Ni catalysts on the growth of multiwalled carbon nanotubes using chemical vapour deposition.

This work done by Joydip Sengupta and Chacko Jacob, The effect of Fe and Ni catalysts on the synthesis of carbon nanotubes (CNTs) using atmospheric pressure chemical vapor deposition (APCVD) was investigated using Field emission scanning electron microscopy (FESEM) analysis which suggests that the samples grow through a tip growth mechanism. High-resolution transmission electron microscopy (HRTEM) measurements show multiwalled carbon nanotubes (MWCNTs) with bamboo structure for Ni catalyst while iron filled straight tubes were obtained with the Fe catalyst. The X-ray diffraction (XRD) pattern indicates that nanotubes are graphitic in nature and there is no trace of carbide phases in both the cases. Low frequency Raman analysis of the bamboo-like and filled CNTs confirms the presence of radial breathing modes (RBM). The degree of graphitization of CNTs synthesized from Fe catalyst is higher than that from Ni catalyst as demonstrated by the high frequency Raman analysis. The study reveals that the catalyst strongly affects not only crystallinity but also the morphology and microstructure [18].

1.5.6 Effects of metallic cobalt crystal phase on catalytic activity of cobalt Catalysts supported on carbon nanotubes in Fischer–Tropsch synthesis.

This work by Ali Nakhaei Pour and Mohammad reza Housain dokht, A series of Co/CNT catalysts with various particle sizes was prepared and used to examine the structure sensitivity of the Fischer–Tropsch synthesis (FTS) reaction .The effects of metallic cobalt crystal phase on catalytic activity of cobalt catalysts in the Fischer– Tropsch synthesis were investigated in a continuous spinning basket reactor. The cobalt catalysts prepared by impregnation of the cobalt active phase in a micro emulsion system on multiwall carbon nanotube supports. A series of cobalt catalysts with different Co particle sizes was prepared by variation of the water-to-surfactant molar ratio from 2 to 12 in the micro emulsion system. The catalyst activity results show that the FTS reaction rate increased on increasing the reaction temperature and passed through a maximum by decreasing the catalyst particle size. The higher activity of catalysts with small particle size may be related to the greater hcp metallic cobalt content in the catalyst active phase, also the results show that larger cobalt particles exhibit more face-centered cubic and less hexagonal close-packed metallic cobalt. The catalysts with higher fractions of hexagonal close-packed phase exhibited higher conversion in the Fischer–Tropsch reaction [19].

1.5.7 Thermal Investigations on Carbon Nanotubes by Spectroscopic Techniques

this work by Maria Teresa Caccamo and et al. The main purpose of this work was to characterize the thermal behaviour of CNTs using Fourier Transform Infrared and Raman spectroscopy. CNTs purchased from Sigma Aldrich, held at different temperatures. More specifically, the CNTs were placed with a metal spatula inside glass containers, which in turn were placed on a heating plate. They were heated on electric hot plate to T = 25 ◦C, 50 ◦C, 100 ◦C, 150 ◦C, 200 ◦C, 250 ◦C, 300 ◦C, 350 ◦C, 400 ◦C, and 450 ◦C. The collected FTIR and Raman spectra were analysed by using two innovative procedures: spectral distance (SD) makes reference to spectral deviation at the lowest temperature, T = 25 ◦C. The second method wavelet cross correlation (XWT) based on the evaluation of the similarity

degree of the spectra, always taking as reference spectrum the lowest temperature, as T = 25 ◦C. From both these two analyses, a relaxation temperature value emerges, corresponding to the relaxation inflection point, of T = 206 ◦C for the IR and Raman spectra [20].

1.5.8 Synthesis and Characterization of Multi Walled Carbon Nanotubes (MWCNT).

This work by T.Arunkumar and et al, This work is about the large scale production of MWCNTs using thermal catalytic chemical vapor deposition (TC-CVD) and characterize using scanning electron microscope (SEM), X-ray diffraction (XRD), Energy Dispersive X-Ray Analysis (EDAX) and thermogravimetric analysis (TGA). The synthesis of MWCNTs was made by breakdown of acetylene (C2H2) gas and Fe / MgO act as catalyst, SEM analysis the growth of the MWCNTs was imaged and it has seen that the clusters are uniformly packed within one another and size of the MWCNTs was ranging from 20-30 nm. The XRD analysis gave the structure of produced MWCNTs as hexagonal and nature as crystalline. The crystalline size of the powder was also found through XRD. The purity of the powder produced was also checked using TGA. The EDAX analysis was taken in order to verify the amount of carbon and other impurities present in that powder. From TGA the purity of MWCNT remains high till 800 oC, which shows that the TC-CVD is appropriate method for the synthesis of MWCNT in large scale [21].

1.5.9 Effective Doping of Single-Walled Carbon Nanotubes with Polyethyleneimine.

This work by Monika Rdest and Dawid Janas, in this work, single-walled carbon nanotubes (SWCNTs) were doped with polyethyleneimine (PEI) to create such material. The microstructure of the films was studied using a scanning electron microscope (SEM). An online detector coupled to the microscope analyzed the chemical composition of the material by means of the energy-dispersive X-ray spectroscopy (EDX), Raman spectroscopy was used to detect electronic and

structural changes to the material. Electrical conductivity was measured using a 4-probe method with a source meter. Temperature of the samples was controlled by heating the sample on a hot plate and measuring its temperature with an infrared camera. Conductance was recalculated to conductivity by considering the sample area and thickness. The thickness was measured with a micrometer screw gauge .the results show that when thin free-standing films were produced directly from SWCNT dispersion containing the PEI dopant, the electrical conductivity of the obtained material was the highest. Values as high as 1301 ± 56 S/cm were registered. Conversely, when the SWCNT films were doped in a typical dipping fashion, the electrical conductivity amounted only to 593 ± 21 S/cm [22].

1.5.10 Mechanical, Electrical, and Thermal Properties of Carbon Nanotube Buckypapers/Epoxy Nanocomposites Produced by Oxidized and Epoxidized Nanotubes.

This work by George Trakakis and et al, High volume fraction carbon nanotube (CNT) composites (7.5–16% vol.) were fabricated by the impregnation of CNT buckypapers into epoxy resin. To enhance the interfacial reaction with the epoxy resin, the CNTs were modified by two different treatments, namely, an epoxidation treatment and a chemical oxidation. To determine the result of CNTs functionalization by terms of mass change, thermogravimetric analysis (TGA) measurements were carried out. Modified and unmodified CNTs were heated to 680 ◦C, by a rate of 10 ◦C/min, in Nitrogen atmosphere. The details of pores of the dry (empty) buckypapers were studied by mercury intrusion porosimetry. The architecture of the internal CNT network and the penetration quality of epoxy were explored by scanning electron microscope (SEM). The surface modification of CNTs was studied by X-Ray Photoelectron Spectroscopy (XPS). The mechanical properties of nanocomposites and pure resin were studied by three-point bending experiments, the electrical conductivity measurements, broadband dielectric measurements were performed, using an Alpha-N frequency response

analyser by Novocontrol Technologies GmbH . The thickness of the samples was between 1.5 and 2 mm, while the diameter of the specimens was 30 mm. Finally, the thermal conductivity of our samples was measured using a Hot Disk TPS 2500 S transient plane source. The measurements were performed at 23 ◦C. the results show that CNT buckypapers can convert epoxy resin from low mechanical performance material to high performance comparable to glass fiber/epoxy composites, from electrical insulator to semiconductor and from thermal insulator to thermal conductor [23].

5.1.11 Study of the Optical Properties of Isonitrosoacetophenone ($C_8H_7NO_2$) Using UV-Vis Spectroscopy

This work by Salma Fath Alrahman Ahmed and et al, the optical properties of the isonitrosoacetophenone (C8H7NO2) were studied using UV-Vis spectroscopy. It was shown that the value of the optical properties affected by the Isonitrosoacetophenone concentrations. The absorbance was shown to be decreased from 2.7×10^{-4} (a. u.) at 278 nm for pure isonitrosoacetophenone to 1×10^{-4} (a. u.) for mixed isonitrosoacetophenone with 2.0 ml at the same wavelength. The transmission of the $C_8H_7NO_2$ was showed to shift towards the shorter wavelength as the concentration of water is increased, starting from ~346 nm for pure $C_8H_7NO_2$and decreased to ~300 nm when the concentration of water was 2.0 ml. The absorption coefficients of the five isonitrosoacetophenone, was decreased as the concentration of water increased. The refractive index has a maximum value of 2.15 at 355 nm for the pure isonitrosoacetophenone, the refractive indices spectra are shifted to the left. Nevertheless, the strange results from those obtained when the concentration of the water has increased the value of the refractive indices of the mixed $C_8H_7NO_2$ in the wavelengths range of (220-300) nm. The value of band-gap (E_g) increased from (3.405) eV for pure $C_8H_7NO_2$ to (3.472) eV for mixed $C_8H_7NO_2$ with 2.0 ml water. Moreover, the results show that the band gap values of either pure or mixed $C_8H_7NO_2$were increased as (n)

increase, and it has higher values when n=3/2 than n=2 which corresponds to indirect allowed transition [24].

1.5.12 Diameter control of single-walled carbon nanotube forests from 1.3–3.0 nm by arc plasma deposition.

This work by Guohai Chen and et al, this work demonstrated the precise and continuous control of SWCNT average diameter in a forest ranging from 1.3 to 3.0 nm with, 1 A˚ resolution by using APD of catalyst nanoparticles. Through APD, the catalyst condition (size, density, and composition) was tuned and shown as an effective method for controlling the SWCNTs in a forest where Cr led to smaller diameters and Ni led to larger diameters .WCNT forests were synthesized in a 10 tube furnace by thermal CVD using helium as the carrier gas and 1% ethylene as the carbon source at 1000 sccm total flow. The catalyst nanoparticles were observed by AFM. The forest structures were characterized by SEM. The average diameter of SWCNTs was analyzed by FTIR spectroscopy. Transmission FTIR spectroscopy was performed, and the location of the absorption band (E (eV)) was converted to diameter (d (nm)) by the following relation, d =5 0.77/E, which was derived simply from the Kataura plot. It should be noted that while the shape of the FTIR absorption peak is dependent on the SWCNT dispersion, the peak position is highly consistent. Finally, the FTIR results were confirmed by TEM (TOPCON EM-002B) observation [25].

1.5.13 Carbon Nanotube Sheet-Synthesis and Applications

This work by Megha Chitranshi and et al, this paper gives an overview of different approaches to synthesize CNTs and then focuses on the floating catalyst method to form CNT sheets. The CNT sheet is modified to form a carbon nanotube hybrid (CNTH) sheet by incorporating metal, ceramic, or other types of nanoparticles into the high-temperature synthesis process to improve and customize the properties of the traditional nanotube sheet. This paper also discusses manufacturing obstacles and the possible commercial applications of

the CNT sheet and CNTH sheet. Applications for CNT sheet include air and water filtering, energy storage applications, and compositing CNTH sheets to produce apparel with anti-microbial properties to protect the population from infectious diseases. The paper also provides an outlook towards large scale commercialization of CNT material [26].

1.5.14 Carbon Nanotubes-Based Nanomaterials and Their Agricultural and Biotechnological Applications.

This work by Dinesh K. Pate and et al, This review paper highlighted some recent development on electrochemical platforms over single-walled CNTs (SWCNTs), multi-walled CNTs (MWCNTs), and nanocomposites as a promising biomaterial in the field of agriculture and biotechnology. Notably, the physicochemical properties of CNTs are profoundly affected by the diameter and helicity of the graphene sheet, as well as the number of graphene layers. The significant enhancement in the seeds germination/plant growth was noted in the presence of carbon-based nanomaterials compared with the control owing to the penetration of the seed coat, which allows more water uptake. The high adsorption potential of CNTs facilitates the extraction process and is widely explored in the extraction technique for the removal of contaminants from the samples. CNTs or their derivatives are often utilized in the nanotechnology sector to develop high efficient battery, fuel cells, electrode reactor for wastewater treatment, and energy storage. CNTs or their derivatives can be applied for the storage of hydrogen as an energy source, and this potential can be tuned by changing the electronic environment of CNTs [27].

1.5.15 The Advances in Biomedical Applications of Carbon Nanotubes

this work done by Timur Saliev, Unique chemical, physical, and biological features of carbon nanotubes make them an ideal candidate for myriad applications in industry and biomedicine. Carbon nanotubes have excellent electrical and thermal conductivity, high biocompatibility, flexibility, and

resistance to corrosion, nano-size, and a high surface area, which can be tailored and functionalized on demand. The important feature of CNTs is a large surface area that provides an opportunity to load and deliver therapeutic molecules to the affected tissues and organs. The unique needle-like shape of CNTs assists drug delivery through enhanced permeability and retention. In addition, CNTs possess a capacity for Raman scattering, photoluminescence, and photo acoustic response. CNTs morphology allows coupling with different. Nano-systems and fabrication of hybrid nano-carriers, which can be utilized as theranostics modalities for diagnostics and treating cancer and other pathologies [28].

1.5.16 Multi-walled carbon nanotube-based systems for improving the controlled release of insoluble drug dipyridamole

This work done by WENQUAN ZHU and et al, Applicability of multi-walled carbon nanotubes (MWCNTs) in loading dipyridamole (DDM), a poorly soluble drug, was evaluated. Additionally, the effect of drug-loading efficiency on the release behavior of the MWCNT-DDM system was also investigated. DDM as a model drug was incorporated into MWCNTs with different drug-loading rates (10, 25 and 50%) using the solvent deposition method. The MWCNT-DDM system was successfully established and characterized using common solid-state characterization methods. Scanning electron microscopy (SEM), transmission electron microscopy (TEM), nitrogen adsorption analysis and Fourier transform-infrared (FT-IR) spectroscopy were carried out to observe the progress of drug loading. X-ray diffraction (XRD) and differential scanning calorimetry (DSC) were used to systematically assess the crystalline state of the DDM after being loaded into the MWCNTs. Improvements in dissolution rate were evaluated by the dissolution test. The results revealed that with the increase of drug loading, the form of DDM in the MWCNTs changed from amorphous to crystalline state. Also, the release rate of DDM decreased upon increasing the drug-loading rate of carriers [29].

1.5.17 Carbon Nanotubes: Applications to Energy Storage Devices

This work by Ruhul Amin and et al. One-dimensional carbon nanotubes (CNTs) have been considered as potential candidates for the development of energy storage materials based on their unique chemical and physical properties. The architecture and quality of the CNTs plays a vital role on the electrochemical performances exhibited by both batteries and supercapacitors. It is observed that a slight modification (defects creation, heteroatoms doping & controlling the distribution of pore sizes) in the CNT structure brings out complementary properties that translate to excellent electrochemical performances. Anchored and directly grown aligned structure of CNTs trends to have high stability and fast ion transportation. The composite electrode with incorporated CNTs is being benefited from the high surface area, excellent conductivity, enhanced specific capacity, better cyclability and rate capability. CNTs can be used as an electrochemically active and inactive electrode component in energy storage systems. It turns out that all types of CNTs can serve as flexible supporting materials and can also enable next generation flexible energy storage devices. The extraordinarily high electronic conductivity also enables CNTs and graphite as an additive to the composite electrode and enable to activate poorly conducting electrode materials to make them electrochemically active. Moreover, the structures and morphologies of CNTs are beneficial for supercapacitors and as catalyst support for fuel cells [30].

1.5.18 facile growth of carbon nanotubes using microwave ovens: the emerging application of highly efficient domestic plasma reactors

This work by Yang Liu and et al, The facile growth of carbon nanotubes (CNTs) using microwave radiation reveals a new way for the cost effective synthesis of CNTs for a wide range of applications. A domestic microwave ovens can be used as convenient plasma reactors to grow CNTs in a very fast, simple, energy-saving and solvent-free manner. The special heating mechanism of microwaves can not

only accomplish the fast growth of high density CNT brushes within tens of seconds, but also eliminate the need for a flammable gaseous carbon source and an expensive furnace. By carefully selecting the substrate and catalyst, low-temperature growth of CNTs can also be achieved on low-melting point organic polymers at atmospheric pressure. Highly localized heating near the catalyst nanoparticles was observed under microwave irradiation, and this phenomenon can be utilized to grow CNTs at desired locations on the substrate to fabricate CNT-based nanoelectronics in situ. Finally, the microwave growth of CNTs is highly adaptive to different carbon sources, substrates and catalysts, showing enormous potential to generate functionalized CNT-based composites for emerging advanced applications [31].

1.5.19 the Construction of Carbon Nanotubes Containing an Anti-Bacterial Chemical Component and its Effect on MDR and XDR Isolates of Pseudomonas Aeruginosa

This work done by Kamelia Banihashemi and et al, In this study, a novel chemical component was synthesized and coated the CNT. The antimicrobial effects were then evaluated on MDR, XDR, and PDR strains of P. aeruginosa isolated from burn patients. Antibiotic susceptibility was evaluated using the disk diffusion test and minimum inhibitory concentration (MIC) testing. In order to determine the potential cytotoxicity, an MTT assay was performed on Human Dermal Fibroblasts. The effect of treatment on the expression of wound healing genes was analysed via qRT-PCR. Experimental data indicates that our CNT coated chemical compound had antibacterial properties, negligible cytotoxicity, and could accelerate the wound healing process. The CNT chemical compound has the potential to treat and reduce the occurrence of multi-drug resistant [32].

1.5.20 Preparation and transport properties of oriented buckypapers with single walled carbon nanotubes

This work done by Natalia P. Stepina and et al. The highly conductive oriented single walled carbon nanotube buckypapers were fabricated using the extrusion of the viscous suspension of protonated SWCNTs through the narrow (300 μm) slit. Two different regimes in the temperature dependence of conductance were observed: high temperature metallic-like behaviour and low temperature semiconductor behaviour. The low-temperature behaviour is related to the inter-SWCNT hopping, which is determined by the barrier magnitude that depends on the degree of CNT packing and, correspondingly, on the alignment. Doping affects the semiconductor behaviour and increases the intra-CNT conductance. As a result, the orientation results in the increase of buckypaper conductivity by more than one order of magnitude. In addition, one order conductance growth is observed after the iodine treatment at room temperature. The fluctuation-assisted tunnelling mechanism was used for the explanation of the experimental transport data. The obtained conductivity value for SWCNT buckypapers is suitable for many applications [33].

1.5.21 Microwave Absorption and Magnetic Properties of Cobalt Ferrites/Carbon Nanotubes Nanocomposites

Owing to the unique microstructure and the excellent dielectric properties, carbon nanotubes (CNTs) were decorated with $CoFe_2O_4$ nanoparticles to synthesize the $CoFe_2O_4$/CNTs nanocomposites by the solvothermal method. The phase structure, morphology, magnetic properties and microwave absorption performance of the as-prepared CoFe2O4/CNTs were characterized and discussed by X-ray diffraction (XRD), thermal gravity analysis (TGA), transmission electron microscope (TEM), vibrating sample magnetometer (VSM) and vector network analyser (VNA). All results indicated that the diameter of $CoFe_2O_4$ nanoparticles decorating on the surface of CNTs increased with the

solvothermal temperature. $CoFe_2O_4$/CNTs prepared at 180^oC, 200^oC and 220^oC exhibited superparamagnetism, while the other samples presented ferromagnetism at room temperature. And with the increasing solvothermal temperature, the saturation magnetization and coercivity increased up to 72 emu/g and 2000 Oe for the sample prepared at 260^oC (S-26). And the rejection loss of $CoFe_2O_4$/CNTs nanocomposites increased with the solvothermal temperature up to 15.7 dB for S-26 with the bandwidth of 2.5 GHz [34].

1.6 Thesis Layout

This thesis contains four chapters, Chapter one presents the introduction, history and objectives of the study and literature review. Chapter two gives a brief literature background about the properties of Carbon Nanotubes (CNTs) The techniques used to characterize carbon nanotubes production were also explained. The experimental work is presented in Chapter three. Chapter four contains the results, discussion and conclusion.

CHAPTER TWO

THEORETICAL BACKGROUND

2.1 Introduction

This chapter about Theoretical Background of carbon nanotubes, types, syntheses, properties and it is application, crystal structure, spectroscopy in addition to cobalt oxide and titanium dioxide.

2.2 Carbon nanotubes

Carbon nanotubes (CNTs) is smart carbon materials which significantly utilized for the potential applications, large-scale synthesis, structural evaluation, and physical as well as chemical properties of carbon nanotubes and/or related conjugated carbon materials [1]. It can be described as graphite sheets that are rolled up into cylindrical shapes. The length of CNTs is in the form of micro meters with a diameter of about 100 nm .Carbon nanotubes (CNTs) are considered as a derivative of both carbon fibers and fullerene with molecules composed of 60 atoms of carbons arranged in particular muffled tubes [35]. CNTs have a broad range of electronic, thermal, and structural properties because of their nanosize which may vary with their length, diameter, and chirality .Due to their unique properties, CNTs have wide range applications such as photovoltaic devices, sensors, transparent electrodes, supercapacitors, and conducting composites [10].

2.3 Type of Carbon Nanotubes

CNTs can be divided into three categories on the basis of the number of tubes present in the CNTs.

2.3.1 Single Wall Carbon Nanotubes (SWCNTs)

If carbon nanotube contains one graphene layer, it is named single wall nanotube (SWCNTs).

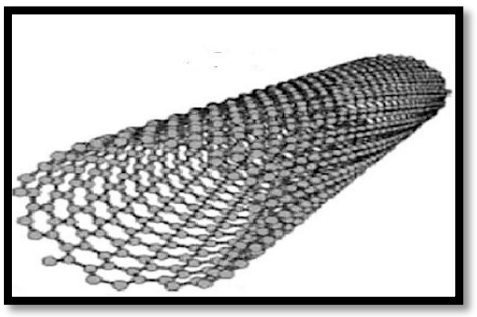

Figure (2.1) single wall carbon nanotubes (SWCNTs)

An important feature of SWCNTs relies on the high tensile strength parallel to the tube axis as a consequence of the strongly delocalized electron density, and the high aspect ratio (up to millions) makes SWCNTs suitable for improving the physical strength of polymers. Another important feature of SWCNTs is the semiconducting behaviour dependent on chiral indexes, the band-gap being inversely related to the tube diameter [36]. Besides the semiconducting properties, SWCNTs present high electron and hole motilities, improving short circuit currents in solar cell devices, through chemical doping of the graphitic structure, the band-gap is modified and permits the SWCNTs to serve as a chemical sensor where the response is generally interpreted as a current change when a probe molecule interacts with the doping agent in the graphitic structure. [35].

2.3.2 Multi Wall Carbon Nanotubes (MWCNTs)

Multi-walled carbon nanotubes (MWCNTs) are a special form of carbon nanotubes in which multiple single-walled carbon nanotubes are nested inside one another [37].

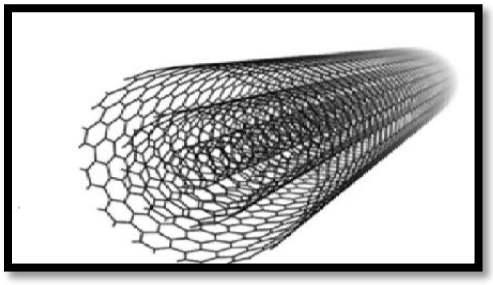

Figure (2.2) Multi wall carbon nanotubes (MWCNTs)

Graphite layer spacing consist of 2 to 30 concentric graphene, diameters of which range from 2.5 to 100 nm. MWNTs are stronger than SWNTs, but they have more defects than SWNTs. The diameter between tube walls within the MWNT is approximately 0.34 nm [30]. The carbon atoms of graphene are positioned either opposite to one another or opposite carbon atoms from the neighbouring graphene. These enable the carbon nanotube to have a 3-dimensional structure of graphite. The MWNT do not possess as high or varied properties however are easier to process because of their larger diameter ranging from 10 to 50 nm with a length of 1–20 μm [38].

2.4 Synthesis of Carbon Nanotubes

There are many techniques used to produce MWNTs or SWNTs. Methods such as electric arc discharge, laser ablation and chemical vapour deposition techniques are well established to produce a wide variety of CNTs. These methods are described in following sections.

2.4.1 Arc discharge method

The arc discharge method is a well-known method for the formation of CNTs .A buffer gas such as helium is introduced in a chamber containing a cathode, a graphite anode, and vaporized carbon molecules. The chamber also contains a small amount of metal catalysts such as nickel, cobalt or iron. Under applied pressure, the chamber is heated to 4000 K, and a direct current (DC) current is passed through the sample. In the progression of this technique, nearly half of the vaporized carbon solidifies on the tip of cathode in the form of a "hard cylindrical deposit". Condensation of the remaining carbon occurs, forming "cathode soot" on the cathode, and "chamber soot", which is present all over the walls of the chamber .The chamber and the cathode soot yield either SWCNTs or MWCNTs. The selection of the inert gas and the added metallic catalyst decides whether the resultant CNTs are SWCNTs or MWCNTs .For the production of SWCNTs, catalyst precursors are necessary for growth in the arc discharge, while the anode is immersed with a metal catalyst, such as Fe, Co, Ni, Y, or Mo. Studies have

revealed that SWCNTs with a diameter of 1.4 nm can be synthesized by Ni-Y graphite mixtures, giving yields of<90%. This mixture is nowadays used worldwide for the fabrication of SWCNTs at high yield [8]. The advantage of this method is the high yield of nanotubes. However, the little control over the orientation of the nanotubes is the key disadvantage that ultimately affect their activity. Furthermore, due to the involvement of a catalyst in the production of SWCNTs, the products need to be purified later on [30].

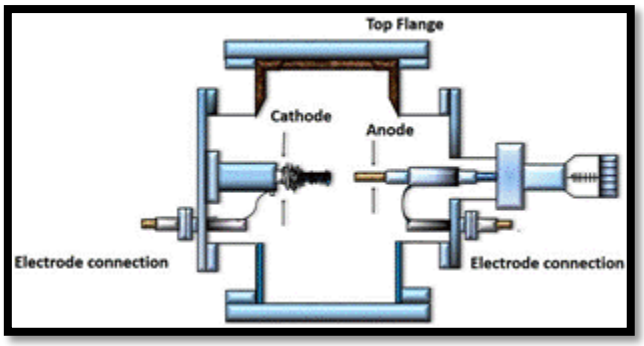

Figure (2.3) Schematic diagram show the Arc discharge method

2.4.2 Laser ablation technique

Laser ablation technique was first used by Smalley's group at Rice University in 1995 for the production of single-wall carbon nanotubes. Laser ablation process involves vaporization of material from a solid target [10]. Pulsed laser ablation is a Physical Vapor Desorption (PVD) method, where carbon atoms are evaporated from a heated graphite specimen (the target) in an inert atmosphere by intense pulsed laser irradiation .The product is deposited on a cooled substrate positioned adjacent to the target. The method was originally used to produce fullerene, but doping the graphite target with catalyst materials enable the formation of SWCNT with a narrow diameter size distribution. The catalysts may be Fe, Co, Ni, Pt, Rh or $NiCo$ alloy. If using Fe as a catalyst, the reactor atmosphere must contain either O_2 or H_2 to activate the catalytic process. It is also possible to produce MWCNT with this technique, but currently this procedure is not competitive for MWCNT [11]. Due to the high energy consumption, laser ablation process is expensive. However, the method is still attractive due to the capability to yield very well defined materials of high purity. Consequently, based on current techniques, the laser ablation method is not likely to become a procedure for major CNT production [38].

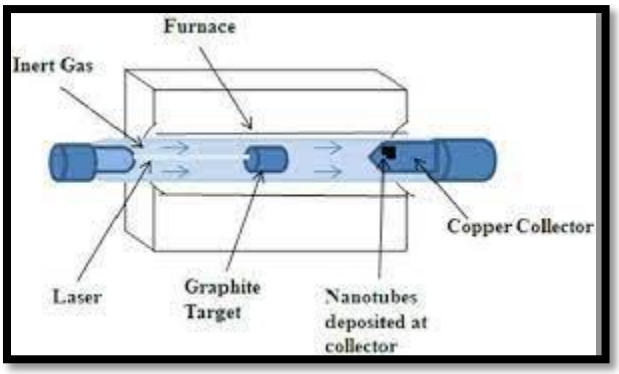

Figure (2.4) Schematic diagram of laser ablation apparatus

2.4.3 Chemical Vapour Deposition (CVD)

Thermally activated CVD (TACVD) is a conventional CVD process in which the chemical reactions are initiated by thermal energy in a hot wall or cold wall reactor using inorganic chemical precursors, usually, the gas phase is heated to create reactive species and promote the kinetics. The thermal energy can be provided by several methods, e.g.: direct resistance heating of the substrate or substrate holder, RF-induction of the substrate holder or subsector, thermal radiation heating and photo-radiation heating. Normally, the temperature supplied by these methods can reach up to 800–2000 °C. The major advantage of TACVD is that it can be operated at normal pressure with high growth rate and the operation is relatively simple. Now, this technique has been used widely in industry for surface coatings, particularly suited to high volume continuous growth process. However, the use of thermal sources can also be is advantageous. For example, heat input may damage the temperature-sensitive substrates and limit the range of precursors that can be used. In addition, the poor efficiency of the gas heating precursor process leads to a great waste of energy. Therefore, alternative forms of energy input were developed to allow deposition at lower temperatures [42, 43].

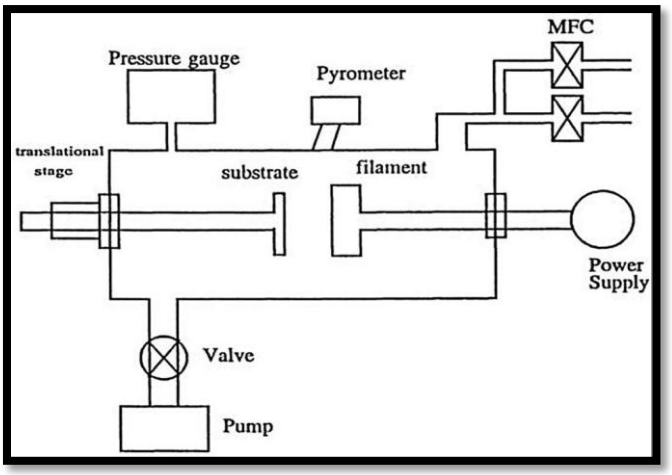

Figure (2.5) Schematic diagram of the thermally activated chemical vapour deposition

2.4.3.2 Plasma enhanced CVD

One way of reducing growth temperatures is to use plasma enhanced CVD (PECVD). PECVD is also known as glow discharge chemical vapour deposition. It uses electron energy (plasma) rather than thermal energy as the activation method to initiate reactions for the production of chemically active ions and radicals that can participate in heterogeneous reactions, which in turn, enable deposition occur at a low temperature and at a reasonable rate, in which, the multitile push–pull plasma source was used to deposit high-quality SiN_x films. The multi-tile push–pull electrodes consist of five pairs of electrically floating electrodes, and each pair comprises two adjacent push–pull (alternating ± voltage) electrodes. These electrodes were connected with a matcher/ power splitter, which enabled delivering equal power to each electrode pair by inductive coupling to the radio frequency (rf) power generator. Compared with the TACVD, plasma enhanced deposition can occur at very low temperatures, even close to ambient. This allows temperature-sensitive substrates to be deposited, such as aluminium, organic polymers, metals or metal alloys In addition, due to high-energy transfer to the relative species, PECVD is considered as the most powerful CVD technique. PECVD processes have been widely used for the deposition of a large range of materials with standard and novel properties; both inorganic and organic materials, as well as polymers, have been prepared by

PECVD. However, also due to its great energy input, it tends to catalyze reaction too quickly which bring complication in the final results. For example, some fragile substrates can easily be damaged by ion bombardment from the plasma, particularly if the ion energy exceeds 20 eV. Furthermore, some polymerization process travels too fast to allow the molecules on the substrate to restructure which resulting in low crosslinking. What's more, it is difficult to obtain a pure deposition using this method as the low-temperature condition resulted in desorption of by-products and other incomplete gas. Also, the PECVD needs to be carried out at a vacuum condition to generate plasma, so a more complicated reactor is needed which makes the PECVD system more expensive which lays a big obstacle on the large scale commercial application process[44].

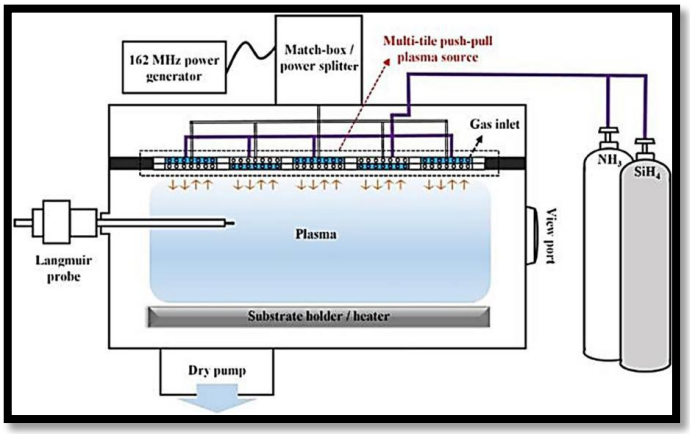

Figure (2.6) the schematic diagram of very high frequency-PECVD using multi-tile push–pull plasma used to deposit high quality $\boldsymbol{SiN_x}$ films

2.4.3.3 Photo-induced CVD

CVD process that makes use of high-energy photons is known as photo-induced CVD (PICVD). There are a variety of light sources for PICVD such as arc lamp, CO_2 lasers, $Nd-YAG$ lasers, excimer lasers, argon-ion and ultraviolet (UV) or vacuum ultraviolet (VUV) lights. The process of photo-induced CVD involves the interaction of light radiation with precursor molecules either in the gas phase or on the growth surface. Precursor molecules must absorb energy to break the chemical bonding in molecules driven by ultraviolet radiation or visible photons from an excimer lamp. Essentially, the mechanism of PICVD coating is the

interaction between light, precursor and the substrate. It is related to the light absorption and excitation of the reactant molecules, intermolecular energy transfer, single or multiphoton dissociation, and adsorption and desorption of the molecules on the solid surface, surface diffusion, surface nucleation as well as film growth kinetics. Due to the different gas source, light source and process conditions for different film deposition, different reaction mechanisms and growth patterns exist in the PICVD process. Studies have shown that the PICVD have generally the following six patterns: UV excited gaseous phase dissociation; UV excited surface adsorbate decomposition; energy transfer of photosensitive reaction; vibrational excitation infrared multiphoton dissociation; light-induced photo thermal decomposition and light-induced surface nucleation and growth, which includes a UVC mercury lamp, a long quartz reactor, precursor tanks (CO and H_2), photoinitiator tank (H_2O_2), as well as argon inert gas (used to purge the reactor before experiments to remove oxygen)[45] . The PICVD process can be performed at atmospheric or reduced pressure ($e.g.$, $0.01-1\ atm$), which greatly cut the cost of the system. In addition to the advantages noted above for gas-phase coating methods, PICVD has other potential advantages, including the fact that it can be achieved in a room temperature, which can effectively prevent and eliminate the adverse impact of migration of impurities, self-doped gas miscellaneous, reaction system contamination and radiation damage to the substrate in the high-temperature and plasma process. In addition, light excitation can induce photolysis, photosensitization and reduce the reaction activation energy of the gas molecules or the surface adsorbed molecules, resulting in an accelerated process of reaction kinetics and high quality of deposited films. The addition of excimer lamps requires only minor modifications of the gas-phase nanoparticle synthesis systems. PICVD is also attractive because it can be operated faster and easier on a continuous mode. It has a better control on the reaction and tends to produce more cross-linked structures than PECVD. Moreover, there is no constraint on the type of substrate, which can be opaque,

absorbent, or transparent. However, there are also some limitations for PICVD. As light is applied in this technology, there are two sides of consideration in the system: high energy of light and transparent-to-light reactor walls. High energy lights (vacuum ultraviolet excimer lamps with wavelength$10-200\ nm$) normally has low penetration ability, but those lights with good penetration (shortwave ultraviolet with wavelength$200-280\ nm$) have lower energy. So when a high energy light source is applied, materials with good light transmittance, such as MgF_2, LiF or CaF_2 should be used as windows, which are expensive. If the light source with good light transmittance but less energy is used, the reactive mixture has to be photosensitive or added with photo initiator to improve the reaction efficiency. Thus exploring photosensitive coating precursors or photo initiators is a perspective way to make up the limitations of PICVD. [44, 46].

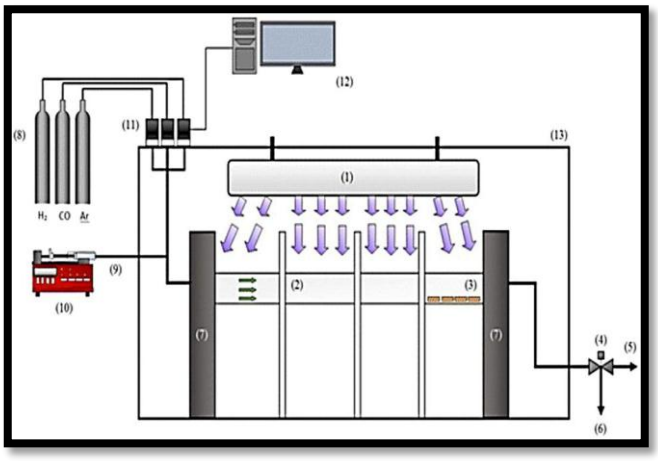

Figure (2.7) Schematic of a PICVD setup (1) UV source, (2) quartz tube reactor, (3) treated samples, (4) solenoid proportional valve, (5) ventilation, (6) vacuum, (7) sealing plates, (8) syngas and argon, (9) hydrogen peroxide [H_2O_2], (10) syringe pump, (11) mass flow controllers, (12) computer, (13) protective box

2.4.4 Flame pyrolysis

This technique is presented very uniquely by the research group of Liu et al. as a new method for mass CNTs production using simple equipment and experimental conditions. The authors called it V-type pyrolysis flame. They captured successfully CNTs with less impurities and high yield using carbon monoxide as the carbon source. Acetylene/air premixed gas provided heat by combustion.

Pentacarbonyl was used as the catalyst and hydrogen/helium premixed gas acted as diluted and protection gas. The diameter of obtained CNTs was approximately between 10 nm and 20 nm, and its length was dozens of microns.156 Moreover they studied the effect of sampling time, hydrogen and helium to the CNTs growth process [47].

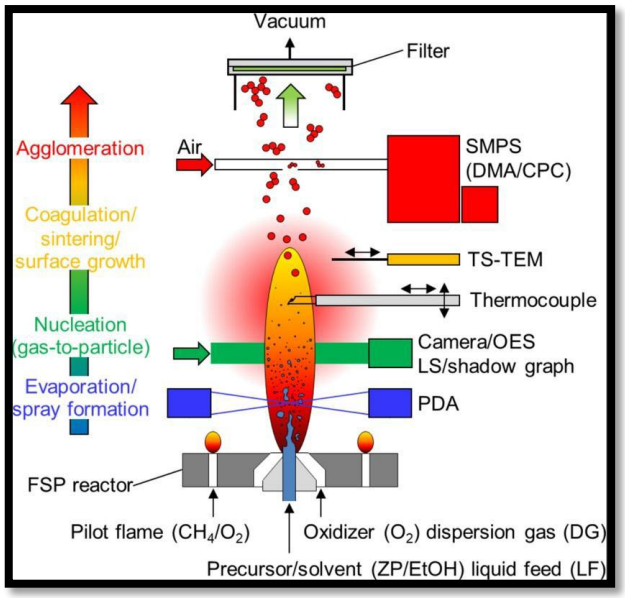

Figure (2.8) Flame pyrolysis system

2.4.5 Bottom-up approach

Bottom-up approach or self-assembly, approaches to nanofabrication use chemical or physical forces operating in nanoscale to assemble basic unit into larger structure. As a component size decreases in nanofabrication, bottom-up approach provide an increasingly important complement to top down techniques. Inspiration for bottom-up approach comes from biological systems, where nature has harnessed chemical forces to create essentially all the structure needed by life. A number of bottom-up approaches have been developed for producing nanoparticles, ranging from condensation of atomic vapours on surfaces to coalescence of atoms in liquids [48].

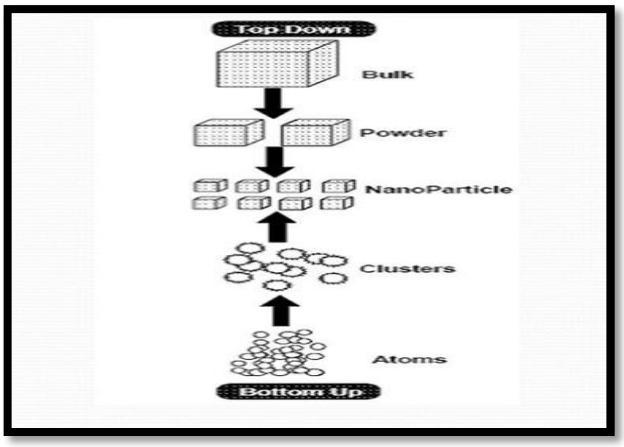

Figure (2.9) Bottom-up approach

2.4.6 Ball milling

Ball milling and subsequent annealing is a simple method for the production of CNTs. Although it is well established that mechanical attrition of this types can lead to fully nano porous, microstructure. Essentially the method consist of placing graphite powder into a stainless steel container along with four hundred steel balls. The container is burged, and argon is introduced, the milling is carried out at room temperature for up to 150 hours. Following milling, the powder is annealed under an inert gas flow at temperature of 1400 ◦C for six hours. The mechanism of this process is not known, but it is thought that the ball milling process forms nano tubes nuclei, and the annealing process activates nanotubes growth. Research has shown this method produces more multi walled carbon nanotubes and few single wal led carbon nanotubes [47, 49].

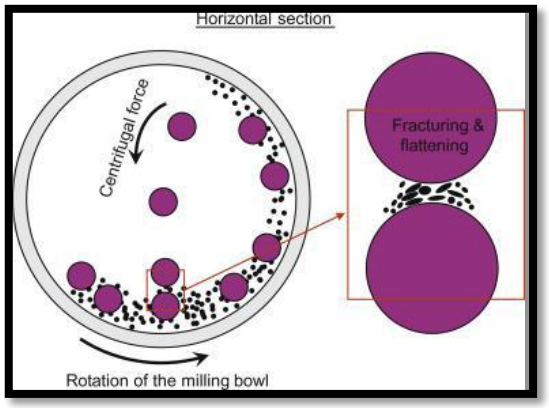

Figure (2.10) Ball milling system

2.5 Properties of Carbon Nanotubes

CNTs reportedly have extremely high surface areas, large aspect ratios, and remarkably high mechanical strength. The tensile strength of CNTs is 100 times greater than that of steel, and the electrical and thermal conductivities approach those of copper .These unique properties make CNTs good candidates as fillers in different polymers and ceramics to realize desirable consumer products. It has also been predicted that CNT-based field-effect transistors (FETs) will so supplant their silicon-based analogy counterparts CNTs are also good incorporating agents due to their unique electrical, mechanical and thermal properties [33].

2.5.1 Electrical property

The electronic structure of a CNT can be obtained from 2D graphite. But since carbon nanotubes are one-dimensional structures, they exhibit electronic properties that are directly dependent on their diameter and helicity. They have got extremely low electric resistance. Resistance occurs only when an electron collides with few defects in the crystal structure through which it is passing. The defect may be an impurity in the atom or in the crystal structure. Such collisions deflect the electron from its path. Due to the very small diameter and high aspect ratio of CNT, the electrons inside a carbon nanotube are not so easily scattered [36]. CNT has a very high current carrying capacity exceeding superconductors. CNT with particular combinations of n and m can be semiconducting or metallic. This allows the formation of semiconductor–semiconductor junctions and semiconductor–metal junctions useful in device fabrication. Armchair nanotubes are metallic while others can be metallic or semiconducting in nature but high curvature in small diameter tubes can strongly affect the electrical properties which cause many exceptions. Conductivity in MWNT is more complex than SWNT. Also, the electrical properties of CNT are strongly related to the method of their treatment and the state of aggregation of CNT. It has been reported theoretically that ideal nanotubes behave as ballistic conductors for micron range

distances. The one dimensional confinement of electrons combined with the requirements for energy and momentum conservation lead to ballistic conduction which causes efficient and fast conduction of electrons and carry current with zero resistance [33].

2.5.2 Mechanical Properties

Mechanical properties of nanotubes cannot be measured, primarily due to difficulties in obtaining pure, homogeneous, and uniform CNT samples. Theoretical as well as experimental results show that CNT is stiffer than diamond and exhibits the maximum Young's modulus of 1.4 TPa and tensile strength of around 100 GPa [13]. The outer wall in MWNT not only protects the inner CNT from chemical interactions but also improves the tensile strength in comparison to SWNT. Since CNT have sp2 bonds between individual carbon atoms, they possess greater tensile strength than Kevlar and steel [10]. This bond is considerably stronger than the sp3 bond in a diamond. Theoretically, SWNT may have a tensile strength hundreds of times stronger than steel. Experimental Young's modulus of SWNT is 1002 GPa .Another amazing property of carbon nanotube is its elasticity. On exposure to axial compressive forces, CNT can be bended, twisted, kinked, and buckled without damaging them. They are elastic and can return to their original structure. However, their elasticity has a limit and can be temporarily deformed under a powerful force. In terms of Young's modulus and tensile strength ratios, CNT has a significant mechanical advantage as compared to other materials. This makes CNT a very promising material for mechanical applications such as in CNT–polymer composites. However, the presence of structural defects actually reduces their mechanical properties [12].

2.5.3 Thermal Properties

As rolled graphitic structures, CNTs are of great importance and interest not only for their electronic and mechanical properties, but also for their thermal properties. Although their size is very small, the quantum effects are important and the low temperature specific heat and thermal conductivity show direct

evidence of the 1-D quantization of the phonon band structure in CNTs .The incorporation of pristine and functionalized nanotubes to different materials can double the thermal conductivity for a loading of only 1%, showing that nanotube composite materials may be useful for thermal management applications in industries. Kim et al. measured the thermal conductivity of individual MWNTs and found it to be 3,000 W/K (higher than that of graphite) at room temperature. Beside this they also determined that the value is two orders higher than the magnitude those obtained for bulk MWNTs. A similar study was carried for SWNTs, with this result being greater than 200 W/m K for SWNTs .There are several factors which influence the thermal properties such as the number of phonon-active modes, the length of the free path for the phonons, and boundary surface scattering .These properties also depend on the atomic arrangement, the diameter and length of the tubes, the number of structural defects and the morphology, as well as the presence of impurities in the CNTs [7].

2.5.4 Optical Properties

The optical properties of CNTs are related to their one dimensional nature. Theoretical information explains that Optical activity of CNTs disappear if nanotubes become large therefore it is expected that other physical properties are influenced by these parameters. Use of optical activity results in Optical devices in which CNTs play an important role [2].

2.5.4.1 Absorption

The intensity of the net absorbed radiation is dependent on the character of the medium as well as the path length within. The intensity of transmitted or non-absorbed radiation continuously decreases with distance x that the light traverses:

$$I_T = I_o e^{-\beta x} \qquad (2.1)$$

Where is the intensity of the non-reflected incident radiation and ß the absorption Coefficient (in mm-1), is characteristic of the particular material; furthermore, varies with wavelength of the incident radiation. The distance parameter x is

measured from the incident surface into the material. Materials that have large values are considered highly absorptive.

2.5.4.2 Absorption coefficients

A measure of the rate decreases in the intensity electromagnetic radiation when it pass through substance and much of the information about the properties of materials is obtained when they interact with electromagnetic radiation, the intensity is expressed by the Lambert-Beer-Lambert law

$$I = I_o\, e^{(-\alpha l)} \qquad (2.2)$$

Where (I) is transmitted intensity, (I_o) is incident intensity and (l) is the optical path length substance.

From equation (1)

$$\frac{I}{I_o} = e^{(-\alpha d)}$$

$$log\left(\frac{I_o}{I}\right) = \alpha l(\log(e))$$

$$log\left(\frac{I_o}{I}\right) = Absorbance$$

Then: $A = \alpha l(\log(e))$

$\alpha = \frac{A}{l(\log(e))}$, log (e) 0.4343

Therefore

$$\alpha = 2.303 * \frac{A}{l} \qquad (2.2)$$

2.5.4.3 Extinction coefficient

Extinction coefficient is measure of how strongly a substance absorbs light at a particular wavelength. It is an intrinsic of a chemical species that is dependent upon their chemical composition and structure. The absorbance of light at given wavelength of a substance is dependent on the mass density or molar

concentration of the specific substance, Extinction coefficient can be calculated by relation

$$k = \frac{\alpha\lambda}{4\pi} \quad (2.3)$$

Where α is absorption coefficient and λ is wavelength.

2.5.4.4 Transmission

The phenomena of transmission is the passage of electromagnetic radiation through a medium, the material which have high value of absorption have small value of transmission and vies versa .transmission can be estimated by relation

$$T = \frac{I}{I_0} \text{ or } T = 1 - A - R \quad (2.4)$$

R is the reflection of the electromagnetic radiation.

2.5.4.5 Reflection

Reflection is the process by which electromagnetic radiation returned either at the boundary between two media or the interior of a medium The reflectivity R represents the fraction of the incident light that is reflected at the interface or

$$R = \frac{I_R}{I_o} \quad (2.5)$$

Where I_o and I_R are the intensities of the incident and reflected beams, respectively. If the light is normal (or perpendicular) to the interface, then

$$R = \left(\frac{n_2 - n_1}{n_{2+} n_1}\right)^2 \quad (2.6)$$

Where n_1 and n_2 are the refractive indices of the two media. If the incident light is not normal to the interface, R will depend on the angle of incidence. When light is transmitted from a vacuum or air into a solid s, then

$$R = \left(\frac{n_s - 1}{n_s + 1}\right)^2 \quad (2.7)$$

2.5.4.6 Refractive index

The refractive index n of a material is defined as the ratio of the velocity in a vacuum to the velocity in the medium or

$$n = \frac{c}{\upsilon} \tag{2.8}$$

The magnitude of n will depend on the wavelength of the light. Just as Equation (3.8) gives the magnitude of c, an equivalent expression gives the velocity of light in a medium as

$$\nu = \frac{1}{\sqrt{\varepsilon\mu}} \tag{2.9}$$

Where ε and μ are, respectively, the permittivity and permeability of the particular substance. Then Equation (3.8) becomes

$$n = \frac{c}{\nu} = \frac{\sqrt{\varepsilon\mu}}{\sqrt{\varepsilon_o\mu_o}} = \sqrt{\varepsilon_r\mu_r} \tag{2.10}$$

Where ε_r and μ_r are the dielectric constant and the relative magnetic permeability respectively.

2.5.4.7 Optical Energy Band Gap

Optical Energy Band Gaps measurement the exaction state of electrons from the valance band to conduction band using photon of selected frequency. The energy band gap of the material related to it is absorption coefficient and can be calculated by Tauc equation

$$(\alpha h\upsilon)^n = C(h\upsilon - E_g) \tag{2.11}$$

Where n refer to type of transition (direct or indirect) and C constant.

2.5.4.8 Optical conductivity

The optical conductivity is the extension of electrical transport to high optical frequencies and it is directly depends on the absorption coefficient and the refractive index of the materials. Optical conductivity using formula

$$\sigma_{opt} = \frac{\alpha nc}{4\pi} \quad (2.12)$$

α Is the absorption coefficient of the material.

2.5.4.9 Electrical conductivity

The electrical conductivity refer to the measure of high electric current move within the material.

The electrical conductivity can be estimated using the following relation.

$$\boldsymbol{\sigma_{ele} = \frac{2\lambda\delta_{opt}}{\alpha}} \quad (2.13)$$

2.5.4.10 Dielectric constant

The dielectric constant of a material is the ratio of its permittivity to the permittivity of the vacuum, it express the extent to which material can hold electric flux on it. Dielectric constant is a complex number consist of real part and imaginary part, the real dielectric constant $\varepsilon_1$can be calculated from relation

$$\varepsilon_1 = n^2 - K^2 \quad (2.14)$$

N is refractive index and k is Extinction coefficient, and imaginary dielectric constant can be calculated from relation

$$\varepsilon_2 = 2nK \quad (2.15)$$

2.6 Application of carbon nanotubes

2.6.1 Medical Application of CNTs

The unique properties and characteristics of CNTs enable scientists to develop new areas in nanomedicine. SWNTs and MWNTs have already proven their potential to serve as safer and effective alternatives to previous drug delivery methods. They can pass through membranes, carrying therapeutic drugs,

vaccines, and nucleic acids deep into the cell to the substrate targets. They serve as ideal non-toxic vehicles, which in some cases, increase the solubility of the drug, resulting in greater efficiency and safety. Overall, recent studies of CNTs have shown a very promising future for them in medicine [12].

2.6.2 Energy Storage

The intrinsic properties of CNTs make them the preferred material for use as electrodes in capacitors and batteries. CNTs possess good electrical conductivity, an extremely high surface area (~1000 m /g), and most importantly, their linear geometry makes their surface very accessible to the electrolyte. Research has demonstrated that CNTs have the highest reversible capacity of any carbon material for use in lithiumion batteries. Moreover, CNTs are excellent materials for supercapacitor electrodes and are currently being marketed for this application. In addition, CNTs hold applications in various fuel cell components. They have several properties, such as high thermal conductivity and surface area, making them valuable as electrode catalyst supports in PEM fuel cells. Owing to their high electrical conductivity, they may also be used in gas diffusion layers, besides current collectors. The high strength and toughness to weight characteristics of CNTs may also prove useful as part of composite components in fuel cells that are used in transport applications, where durability is paramount. [10].

2.6.3 Electronic devices

One of the potential application of nanotubes is the field of electronics, due to its highly conducting nature. Out of two types, single walled nanotubes are the most conducting type. Twisting and bending of nanotube makes it highly conducting. With high conductivity and small size, nanotubes may be an alternate option to copper which is generally used, but has limitation of ineffective at size less than 40 nm.

2.6.4 Sensors

Carbon nanotubes have been reported to a good gas sensor, because of its elongated shape. They have reported to an excellent oxygen gas sensor. They measured DC electrical resistance and the thermoelectric power of bundles and thin films of SWNTs. The sensitivity of carbon nanotubes to $NO_3$and NH_3 was reported by Dai and co-workers, by measuring conductivity of MWNT upon exposure to $NO_3$and NH_3 at variable time periods and temperature. Functionalized MWNT have also been used for gas sensing. Robert Haddon and colleagues found that functionalized SWNTs experienced a much greater change of resistance upon exposure to NH_3 than did pristine tubes, giving them greater sensitivity as sensors [1].

2.7 Crystal structure

Crystal structure is adscription of the ordered arrangement of atoms, ions or molecules in crystalline material. Ordered structure occur from the intrinsic nature of the constituent particles to form symmetric pattern that repeat along the principal directions of three dimensional space in matter. The smallest group of particles in the material that constitutes this repeating pattern is the unit cell of the structure .the unit cell defined as the smallest repeating unit having the full symmetry of the crystal structure of the entire crystal which is built up by repetitive translation of the unite cell along it is principle axes the length of principal axes or the edge of the unit cell is and the angels between them are the lattice constant (lattice parameter). The geometry of unit cell is defined as a parallelepiped providing six lattice parameters taken as the length of the cell edges (a,b,c)and the angels between them is (α,β,γ) and the positions of the atoms inside the unit cell are described by the set of atomic positions (x_i,y_i,z_i) measured from the lattice point. The symmetry properties of the crystal are embodied in its space group. A crystal structure and symmetry play a role in determine many of it is physical properties, such as cleavage, electronic band structure and optical transparency [50, 51, 52 and 53].

2.8 Miller Indices

Miller indices is a group of three number (h,k,l) that indicates the orientations of plane or set of parallel planes of atoms in the crystal, if each atom in the crystal is represented by a points and these points are connected by lines, the resulting lattice may be divided into number of identical blocks or unit cells, the intersecting edges of one of the unit cells defines a set of crystallographic axes, and the miller indices are determined by the intersection of the plane with this axes[54, 55].

2.9 Bravais lattices

Bravais lattices is the most fundamental way to describe lattice, it is an array of discrete with an agreement and orientation that look exactly the same from any of the discrete points, that is the lattice points are indistinguishable from one another. The bravais lattices refer can refer to one of the 14 different of the unit cells that a crystal structure can be made up of [56].

2.10 Types of Bravais lattices

2.10.1 Cubic system

It has three types of Bravais lattices (primitive, body cantered and face cantered), for cubic system a=b=c and $\alpha=\beta=\gamma=90^{o}$.

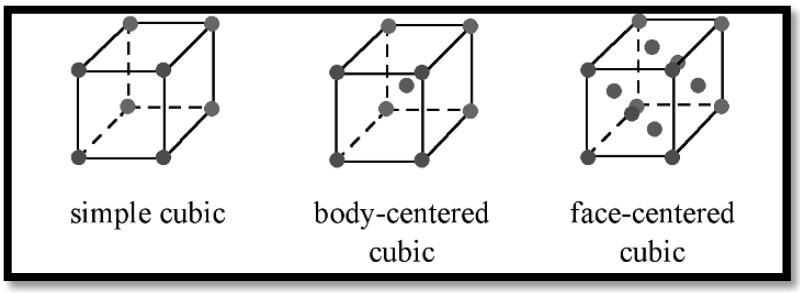

Figure (2.11) cubic system

2.10.2 Tetragonal system

It has two types of Bravais lattices (primitive and body cantered), for tetragonal system a=b≠ c and $\alpha=\beta=\gamma=90^{o}$.

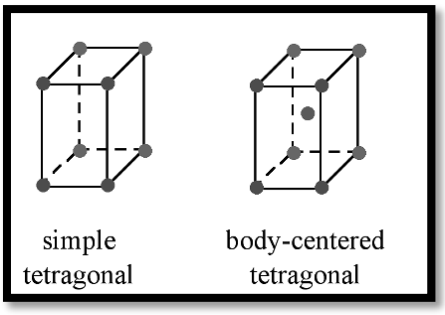

Figure (2.12) Tetragonal system

2.10.3 Orthorhombic system

It has four types of Bravais lattices (primitive, base centred, face centred and body centred), for orthorhombic system a≠ b≠ c and α=β=γ=90◦.

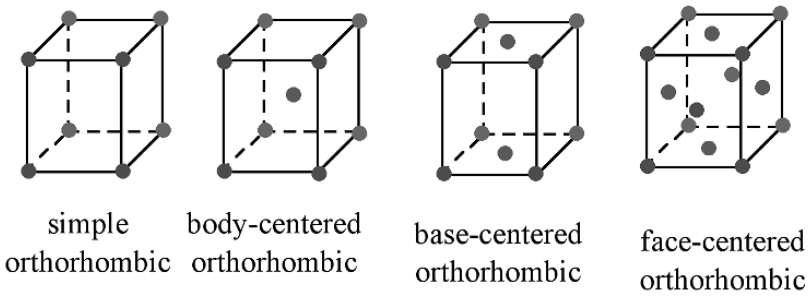

Figure (2.13) orthorhombic system

2.10.4 Hexagonal system

It has only one type of Bravais lattice which is primitive, for hexagonal system a=b≠ c and α=120 ◦ β=γ=90◦.

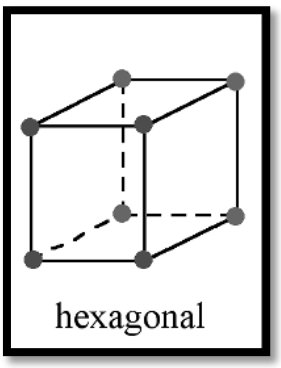

Figure (2.14) Hexagonal system

2.10.5 Rhombohedral system

It has only one type of Bravais lattice which is primitive, for Rhombohedral system a=b=c and α=120 ◦ β=γ≠90◦.

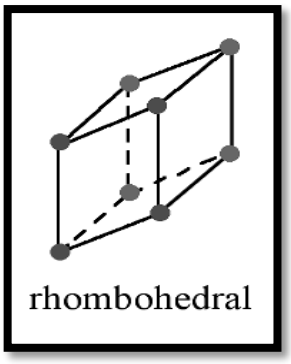

Figure (2.15) rhombohedral system

2.10.6 Monoclinic system

It has two types of Bravais lattices (primitive and base centred), for monoclinic system a=b≠ c and α≠90° β=γ=90°.

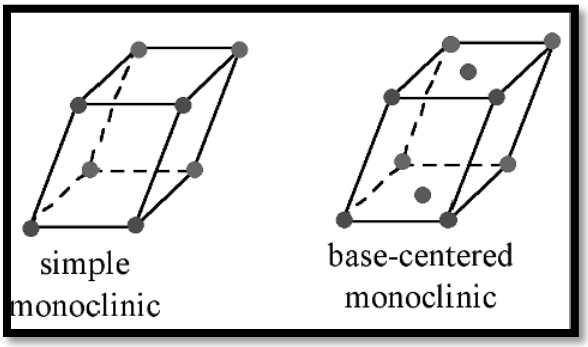

Figure (2.16) monoclinic system

2.10.7 Triclinic system

It has only one type of Bravais lattice which is primitive, for triclinic system a≠ b≠ c and α≠ β≠γ≠90° [57, 58 and 59].

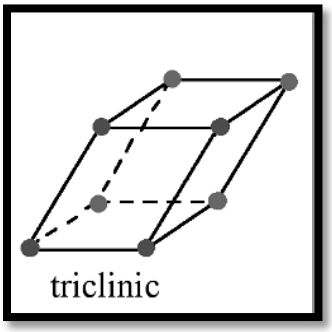

Figure (2.17) triclinic system

2.11 Spectroscopy

Spectroscopy is the study of interaction between light and matter where the absorption and emission of the light or other radiation by the matter are be measured, spectroscopy mainly deals with the dispersion of light and other radiation caused by an objective which allowed to study various properties of the object, the measurement in the spectroscopy is a function of the wavelength of the radiation being observed. Spectroscopy has been widely exploited as it allows the determination of composition, physical and electronic structure to be determined of various particles of molecular or atomic levels [60, 61].

2.12 Interaction of light with matter

Light interacts with matter in four ways:

2.12.1 Absorption

is the process in which light absorbed by matter and converted into energy, absorption depends on the electromagnetic frequency of the light and object's nature of atoms, the absorption of light directly proportional to the frequency, if they are complementary, light is absorbed, if they are not complementary, then the light passes through material or gets reflected. Absorption depends on the state of an object's electron, all electrons vibrate at specific frequency which is known as their natural frequency, when light interacts with an atom of the same frequency, the electrons of the atoms become excited and start vibrating. During this vibration, the electrons of the atoms interact with the neighbouring atoms and convert this vibrational energy into thermal energy.

2.12.2 Transmission

The phenomena of transmission is the passage of electromagnetic radiation through a medium, if the material has high absorption it will has low transmission.

2.12.3 Reflection

Is the change in the direction of the wavefront at interface between two different media so that the wavefront returns into the medium from which it originated.

2.12.4 Emission

It is the process of elements releasing different photons of colors as their atoms returns to their lower energy levels, the color of light that is emitted by an atoms depends on how much energy the electron release as its move down different energy levels. When the electrons return to the lower energy levels, they release extra energy and that can be in the form of light causing the emission of the light [62].

2.13 Cobalt Oxide (CoO)

Cobalt oxide is an organic material compound that has been described as olive green or grey solid. It has 74.9326g/mol molecular weight and density 6.45g/cm^3, it is melting at 1933 ^oC (2206 ^oK) and it is insoluble in water, it has cubic face centred crystal structure with lattice constant 4.2637A_o, it is antiferromagnetic below 16 ^oC. Cobalt oxide is prepared by oxidation of cobalt powder with air by thermal decomposition of cobalt (II) nitrate or the carbonate. Cobalt oxide used extensively in ceramics industry as additive to create blue colored glazes and enamels as well as chemical industry for producing cobalt (II) powder [63].

2.14 Titanium dioxide

Titanium dioxide also known as titanium (IV) or titania, their molecular weight is 79.866g/mol and 4.23 g/cm^3 density, it is melt at 1843 ^oC (2116 ^oK) and boil at 2973 ^oC (3245 ^oK), it is insoluble in water and it has energy gap about 3.05 eV, their magnetic susceptibility is $+5.9\times10^{-6}$ cm^3/mol and it has refractive index equal to 2.488. Titanium dioxide has wide range of applications including paint, sunscreen and food coloring [64].

CHAPTER THREE

EXPERIMENTAL

3.1 Introduction

The experimental details were given in this chapter. The first section about synthesis of carbon nanotubes doping with cobalt oxide (CoO) and titanium dioxide (TiO_2) at different concentrations, and the second part about characterization techniques which were UV-Visible spectrometer, Fourier Transferred Infrared spectrometer ,Scanning electron microscope ,and X-ray diffractometer.

3.2 Materials

The materials used in this research were graphite, sodium chlorite (NaClO3 106.44g/mole, 99%, ZEUS), Cobalt oxide (CoO 74.9326 G/mole, LOBA), titanium dioxide (TiO2 79.866 g/mole, LOBA), nitric acid (HNO3 63.01g/mole, 65%, ZEUS), sulphuric acid (H2SO4, ZEUS) and Deionized water (DI).

3.3 Experimental Tools

The tools used in this research were magnetic stirrer (model: IKA C-MAG MS, 3582600), digital water bath (model: Prime digital water bath-22l, LWB-122DL), filtered paper (size15 mm), UV/VIS spectrometer (model: JENWAY 720), Fourier Transferred Infrared spectrometer (FTIR: model FTIR-8100), scanning electron microscope (SEM: model VEGA3 TESCAN) and X-ray diffraction (XRD: model D2 PHASE XRD).

3.4 Characterizations Methods

The characterization techniques used in this research were:

3.4.1 Fourier Transform Infrared Spectrometer

An FTIR analysis measure the range of wavelengths in the infrared region that are absorbed by a material, the sample's absorbance of the infrared light's energy

at various wavelengths is measured to determine the material's molecular composition and structure. Unknown materials are identified by searching the spectrum against a database of reference spectrums [65].

Figure (3.1): FTIR spectrometer instrument

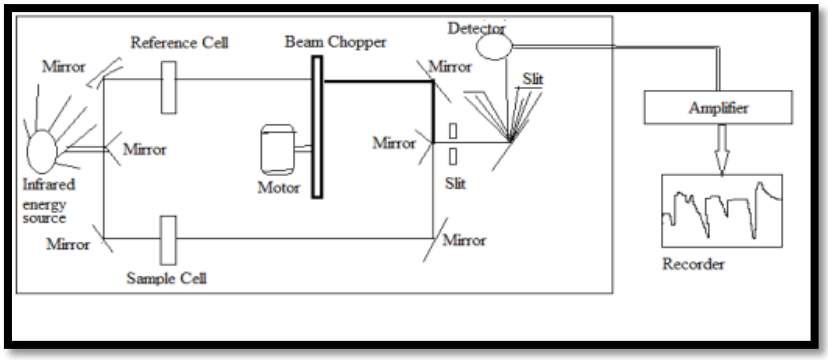

Figure (3.2): schematic diagram of FTIR spectrometer

Figure (3.2) show schematic diagram of FTIR spectrometer, a simple device called an interferometer is used to identify samples by producing an optical signal with all the IR frequencies encoded into it. The signal can be measured quickly. Then, the signal is decoded by applying a mathematical technique known as Fourier transformation. This computer-generated process then produces a mapping of the spectral information. The resulting graph is the spectrum which is then searched against reference libraries for identification [66].

3.4.2 UV-Visible Spectrometer

UV-Visible spectroscopy is used to study the optical Properties of materials, it refers to absorption spectroscopy or reflectance spectroscopy in part of the ultraviolet and the full, adjacent visible regions of the electromagnetic spectrum. This means it uses light in the visible and adjacent ranges.

Figure (3.3): UV-VIS instrument

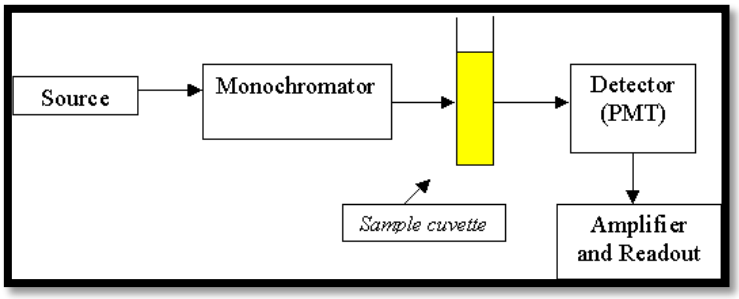

Figure (3.4): schematic diagram of UV-VIS spectrophotometer

Figure (3.4): show schematic diagram of UV-VIS spectrophotometer, electromagnetic radiation is emitted within the wavelength range of about 200 to 800 nm from the source. The source is often a Deuterium (or hydrogen) lamp, a tungsten filament lamp, or a xenon arc lamp. The radiation from the source is then passed through a wavelength selector (either a diffraction grating or filter) through which a narrow band of wavelengths can pass. The sample is dissolved in some solvent which is contained in a sample container which is made of plastic,

glass, or quartz. The beam from the wavelength selector passes through the sample and is absorbed by the sample according to Beer's law. The light passed into a photomultiplier tube where the light intensity is recorded [67].

3.4.3 Scanning Electron Microscope (SEM)

A scanning electron microscope (SEM) is a type of electron microscope that produces images of a sample by scanning the surface with a focused beam of electrons to render high resolution, three-dimensional images. These images provide information about topography, morphology and composition.

Figure (3.5): A scanning electron microscope instrument

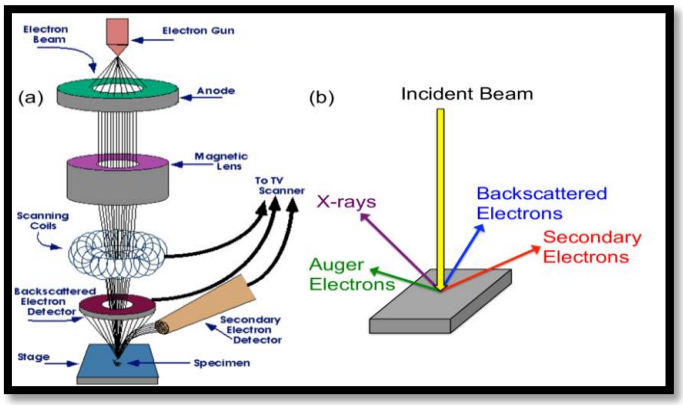

Figure (3.6): schematic diagram of scanning electron microscope

A schematic representation of an SEM is shown in Figure (3.6). Electrons are generated at the top of the column by the electron source and then accelerated down the column that is under vacuum, which helps to prevent any atoms and molecules present in the column from interacting with the electron beam and ensures good quality imaging. Electromagnetic lenses are used to control the path of the electrons. The condenser defines the size of the electron beam (which defines the resolution), while the objective lens' main role is the focusing of the beam onto the sample. Scanning coils are used to raster the beam onto the sample. Different types of electrons are emitted from samples upon interacting with the electron beam. A Backscattered Electron (BSE) detector is placed above the sample to help detect backscattered electrons. Images show contrast information between areas with different chemical compositions as heavier elements (high atomic number) will appear brighter. A Secondary Electron (SE) detector is placed at the side of the electron chamber, at an angle, in order to increase the efficiency of detecting secondary electrons which can provide more detailed surface information [68].

3.4.4 X-ray diffraction (XRD)

X-ray diffraction analysis (XRD) is a technique used in materials science to determine the crystallographic structure of a material. XRD works by irradiating a material with incident X-rays and then measuring the intensities and scattering angles of the X-rays that leave the material [69].

Figure (3.7) XRD instrument

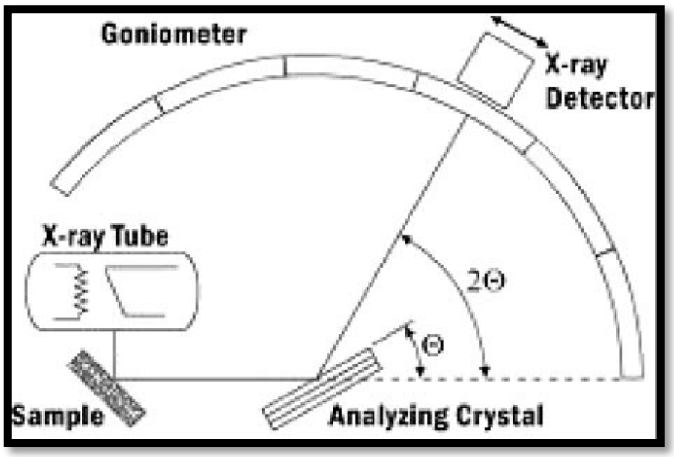

Figure (3.8): schematic diagram of X-ray diffraction (XRD)

Figure (3.8) show schematic diagram of (XRD), X-ray diffractometers consist of three basic elements: an X-ray tube, a sample holder, and an X-ray detector. X-rays are generated in a cathode ray tube by heating a filament to produce electrons, accelerating the electrons toward a target by applying a voltage, and bombarding the target material with electrons. When electrons have sufficient energy to dislodge inner shell electrons of the target material, characteristic X-ray spectra are produced, the specific wavelengths are characteristic of the target material (Cu, Fe, Mo, Cr). Filtering, by foils or crystal monochrometers, it is required to produce monochromatic X-rays needed for diffraction, Copper is the

most common target material for single-crystal diffraction, with Cu radiation = 1.5418Å. These X-rays are collimated and directed onto the sample. As the sample and detector are rotated, the intensity of the reflected X-rays is recorded. When the geometry of the incident X-rays impinging the sample satisfies the Bragg Equation, constructive interference occurs and a peak in intensity occurs. A detector records and processes this X-ray signal and converts the signal to a count rate which is then output to a device such as a printer or computer monitor, the geometry of an X-ray diffractometer is such that the sample rotates in the path of the collimated X-ray beam at an angle θ while the X-ray detector is mounted on an arm to collect the diffracted X-rays and rotates at an angle of 2θ.

3.5 ImageJ software

ImageJ is a public domain Java image processing and analysis program inspired by NIH Image for the Macintosh. It runs, either as an online applet or as a downloadable application, on any computer with a Java 1.5 or later virtual machine. Downloadable distributions are available for Windows, Mac OSX and Linux. It can read many image formats including TIFF, GIF, JPEG, BMP, DICOM, FITS and 'raw'. It supports 'stacks' (and hyperstacks), a series of images that share a single window. It is multithreaded, so time-consuming operations such as image file reading can be performed in parallel with other operations. It can calculate area and pixel value statistics of user-defined selections. It can measure distances and angles. It can create density histograms and line profile plots. It supports standard image processing functions such as contrast manipulation, sharpening, smoothing, edge detection and median filtering. It does geometric transformations such as scaling, rotation and flips. Image can be zoomed up to 32: 1 and down to 1: 32. All analysis and processing functions are available at any magnification factor. The program supports any number of windows (images) simultaneously, limited only by available memory. Spatial calibration is available to provide real world dimensional measurements

in units such as millimetres. Density or grey scale calibration is also available. ImageJ was designed with an open architecture that provides extensibility via Java plugins. Custom acquisition, analysis and processing plugins can be developed using ImageJ's built in editor and Java compiler. User-written plugins make it possible to solve almost any image processing or analysis problem [71].

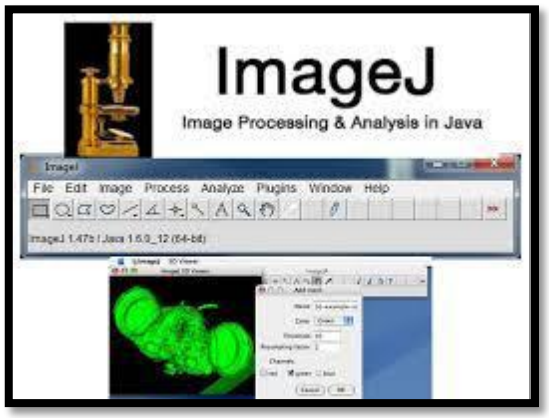

Figure (3.9) Imagej software

3.6 Origin Software

Origin is a powerful data analysis and publication-quality graphing software, tailored to the needs of scientists and engineers. What sets Origin apart from other applications is the ease with which you can customize and automate your data import, analysis, graphing and reporting tasks. Data analysis in origin including statistics, signal process, Curve fitting and peal analysis. Origin's Curve Fitting is performed by nonlinear least squares fitter which is based on the Levenberg-Marquardt algorithm. Origin imports data files in various formats such as JPEG, GIF, EPS TIFF, etc [72].

3.7 Methodology

Chemical vapor deposition (CVD) was used to synthesis carbon nanotubes doping with cobalt oxide (CoO) and titanium dioxide (TiO_2) at different concentration, firstly, six samples of carbon nanotubes were Prepared by adding 5 g of graphite powder to a mixture of (50 ml) sulfuric acid and (25 ml) of nitric acid. Because the reaction produces an amount of heat, it was cooled to 5 ° C with

an ice bath. 25 g of sodium chlorate was added to the solution in addition to cobalt oxide and Titanium dioxide (0.5, 0.75, 1.00.1.25and 1.5) molar. The solution was heated to 70 °C in a water bath for 24 hours and then placed in air for 3 days. Most of the graphite was bottom predicted but some carbon was floating. The floating carbon material was transferred to 1 litter of Deionized water (DI). After stirring for an hour, the solution is filtered and dried.

Fourier Transform Infrared spectroscopy analysis (FTIR) was used to characterize functional groups, bonding types, nature of compounds, the surface morphology for each sample of the carbon nanotubes were studied by scanning electron microscope (SEM), UV-Visible spectrometer that used to study the optical properties of prepared CNTs, and X-ray diffractometer (XRD) which used to determine the crystallographic structure of a material, origin Lab and Imagej Programs were used to obtain surface roughness and size distribution from SEM images.

CHAPTER FOUR

RESULTS, DISCUSSIONS and CONCLUSION

4.1 Introduction

In this chapter the main results that have been obtained from the experiments made of Carbon Nano Tube (CNT) doping with cobalt Oxide (CoO) and titanium dioxide (TiO_2) at different concentration (0.5, 1.00 and 1.5) . The data of X-ray diffraction (XRD) have been analysed by to obtain crystal structure and lattice parameters of samples, Scanning electron microscope analysis have applied to study surface morphology and to determine the diameter of the samples. The FT-IR data have been carried to investigate the chemical bonds within atoms, and the data of UV-visible used to evaluate the optical parameters.

4.2 XRD Results

X-ray diffraction (XRD) was used to study the structure and to calculate lattice constants for reference sample, CNTs+CoO and CNTs+TiO_2 at concentration (0.5, 0.75, 1.00, 1.25 and 1.5) molar as shown below.

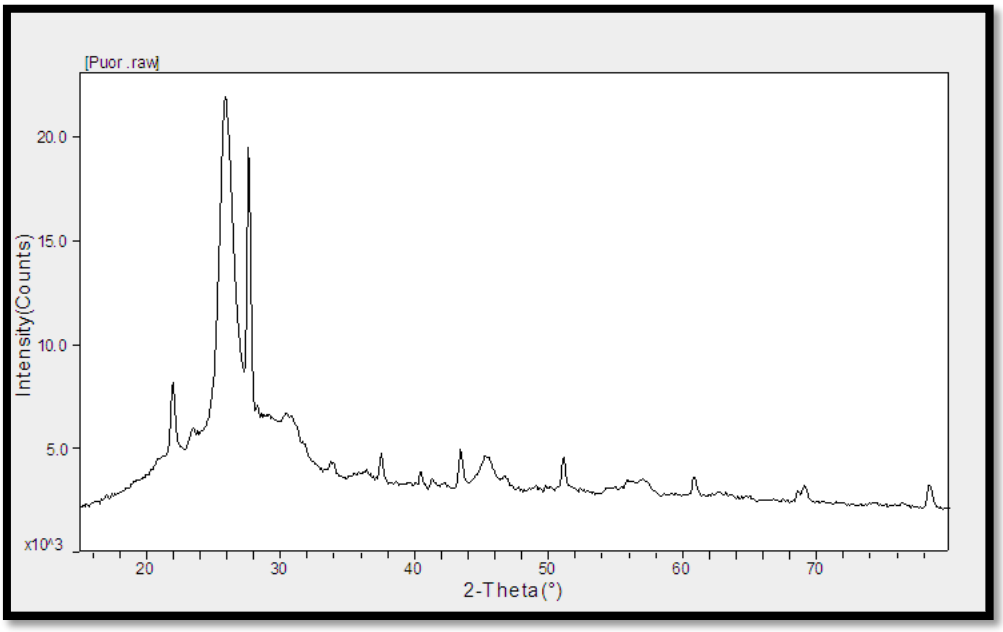

Figure (4.1) XRD spectrum of reference sample

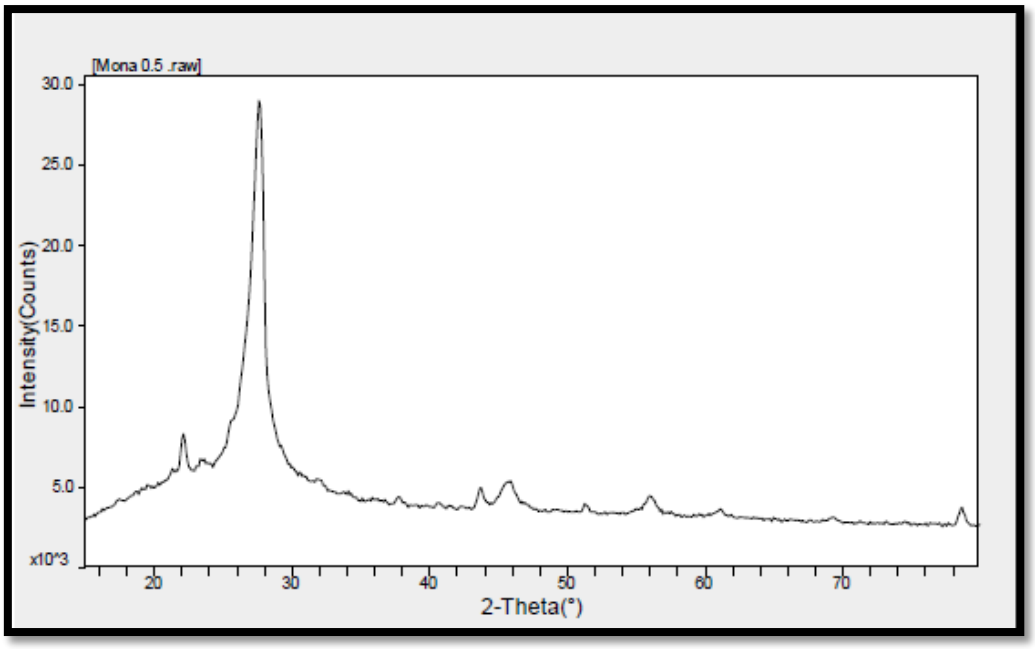

Figure (4.2) XRD spectrum of CNTs+CoO (0.5)

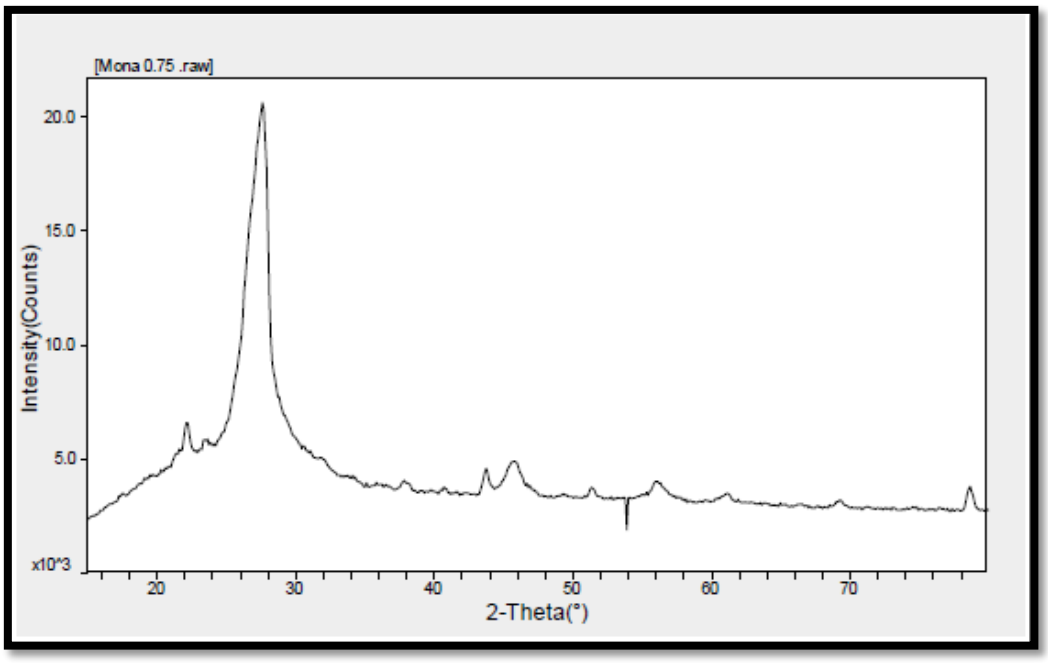

Figure (4.3) XRD spectrum of CNTs+CoO (0.75)

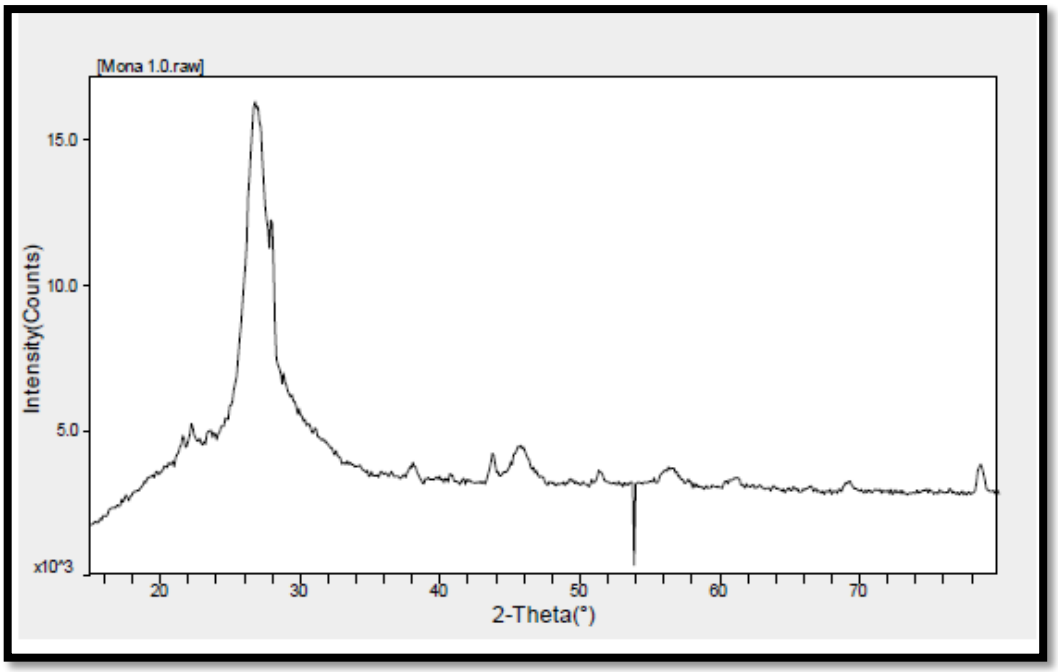

Figure (4.4) XRD spectrum of CNTs+CoO (1.00)

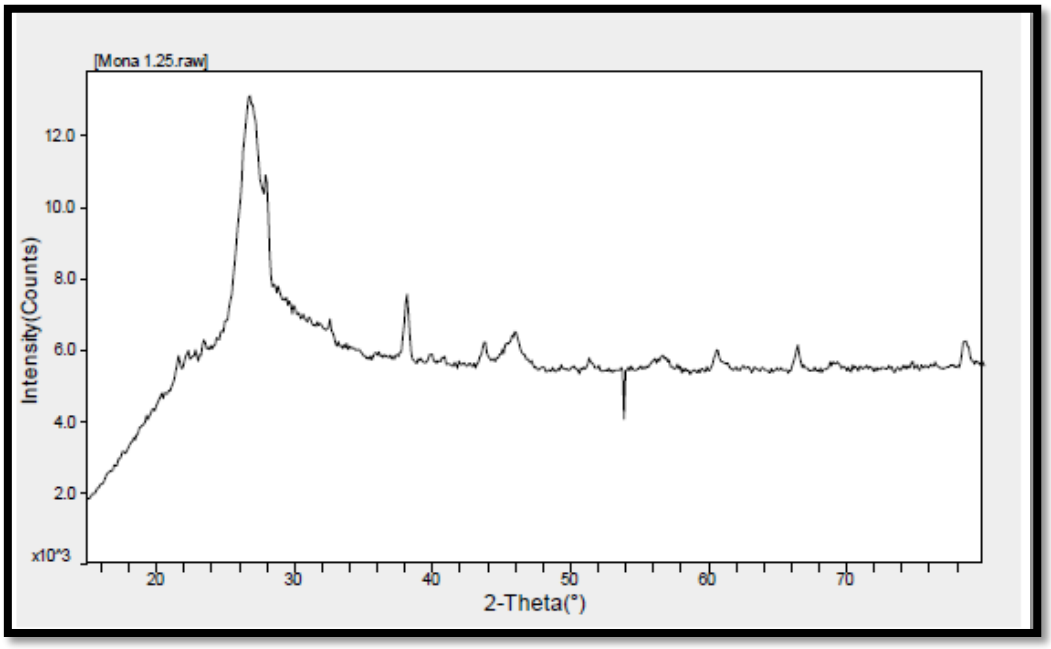

Figure (4.5) XRD spectrum of CNTs+CoO (1.25)

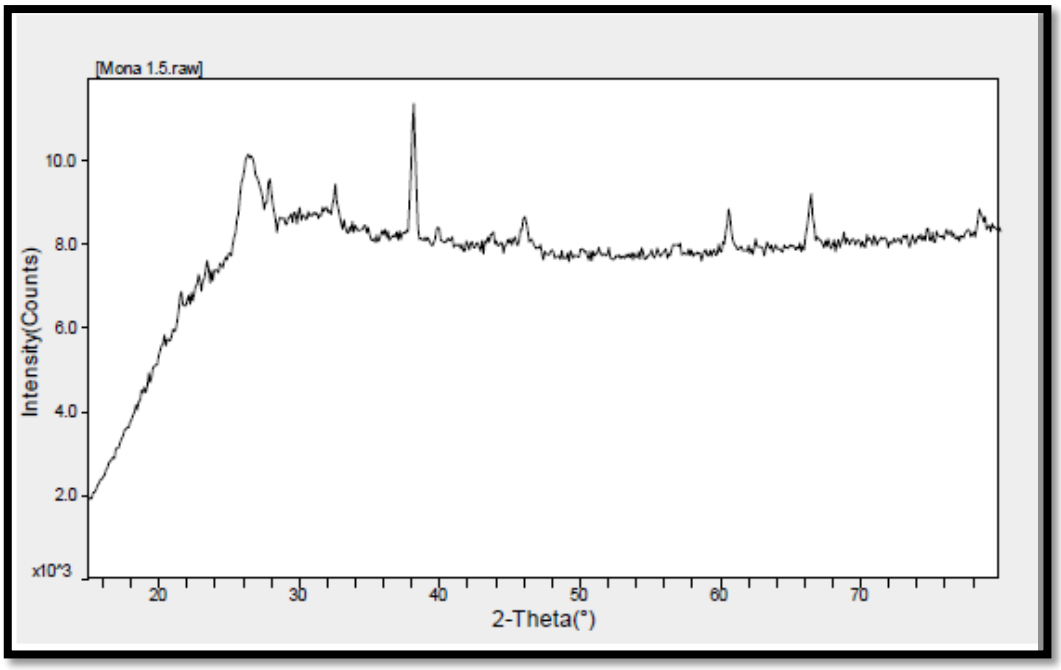

Figure (4.6) XRD spectrum of CNTs+CoO (1.50)

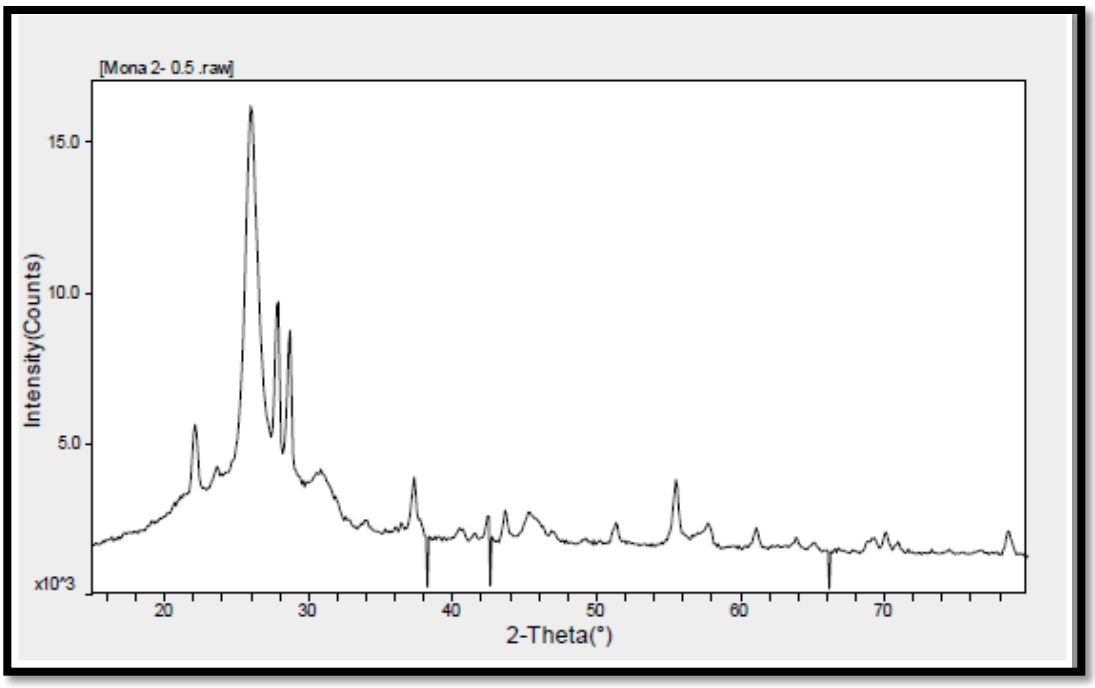

Figure (4.7) XRD spectrum of CNTs+TiO_2 (0.5)

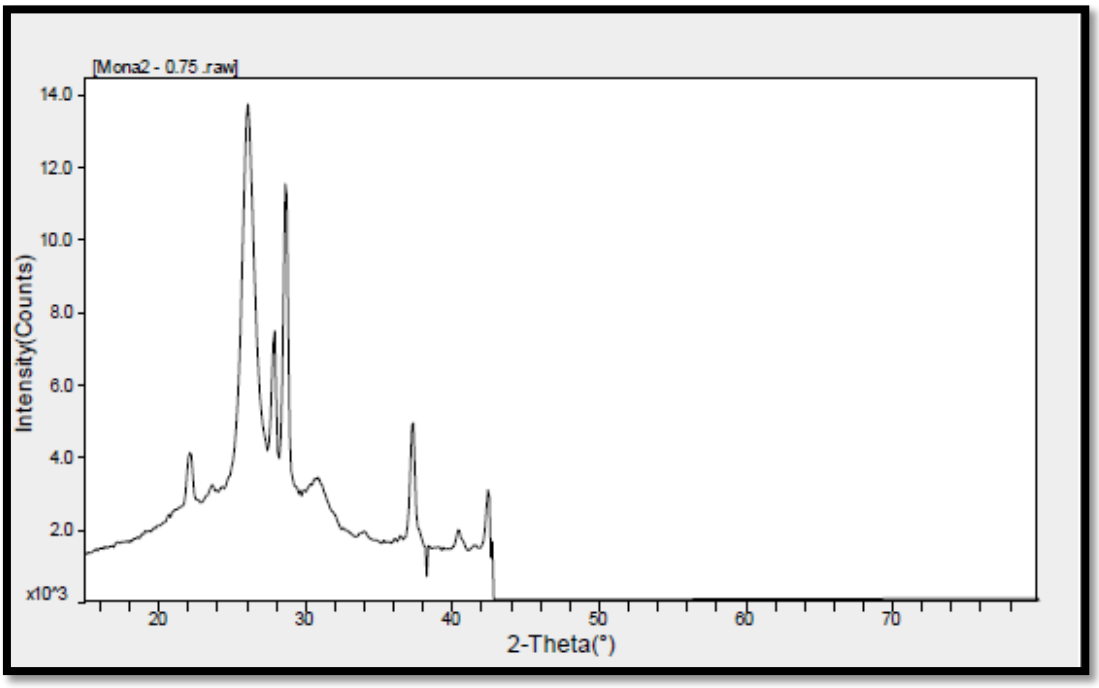

Figure (4.9) XRD spectrum of CNTs+TiO_2 (0.75)

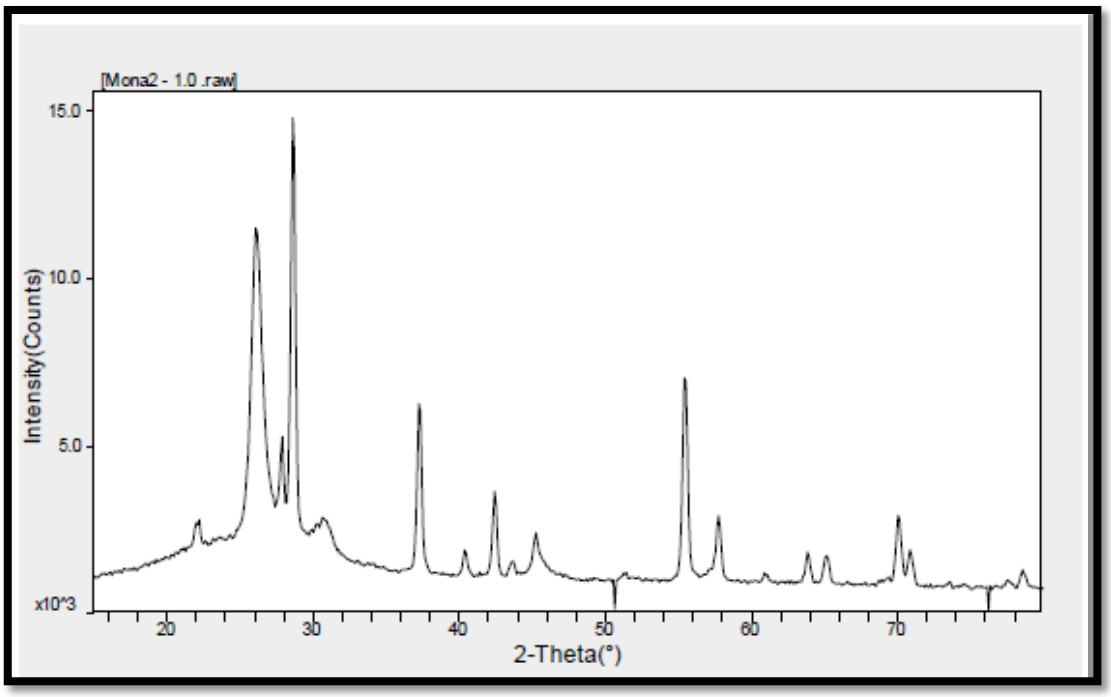

Figure (4.10) XRD spectrum of CNTs+TiO_2 (1.00)

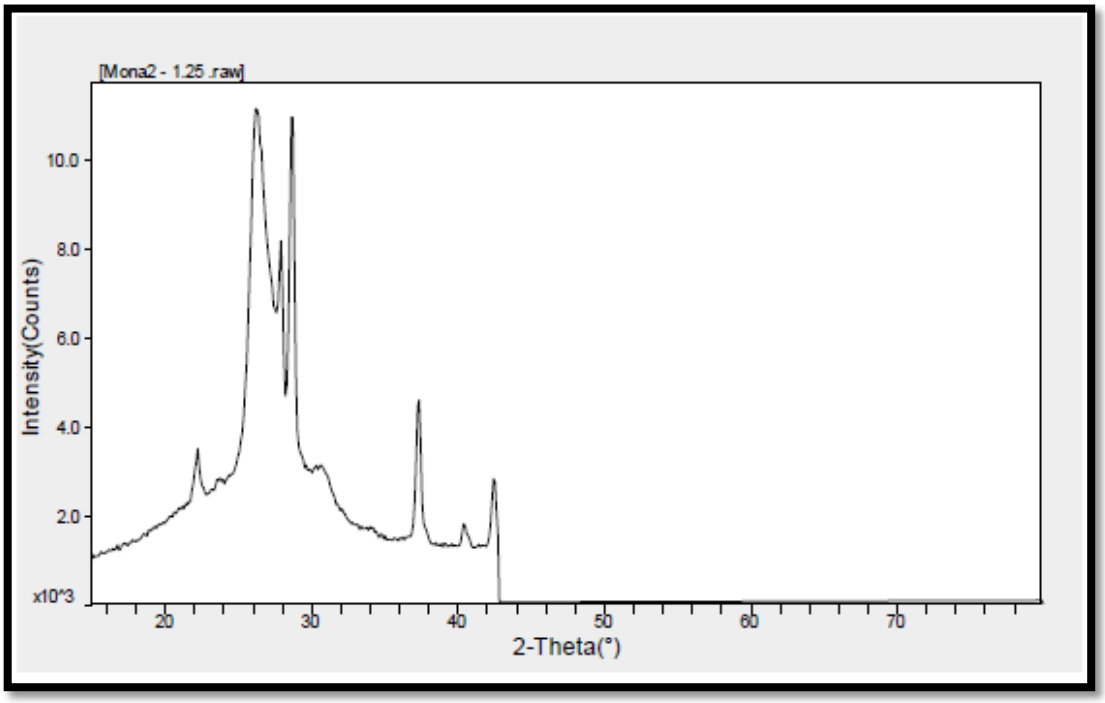

Figure (4.11) XRD spectrum of CNTs+TiO_2 (1.25)

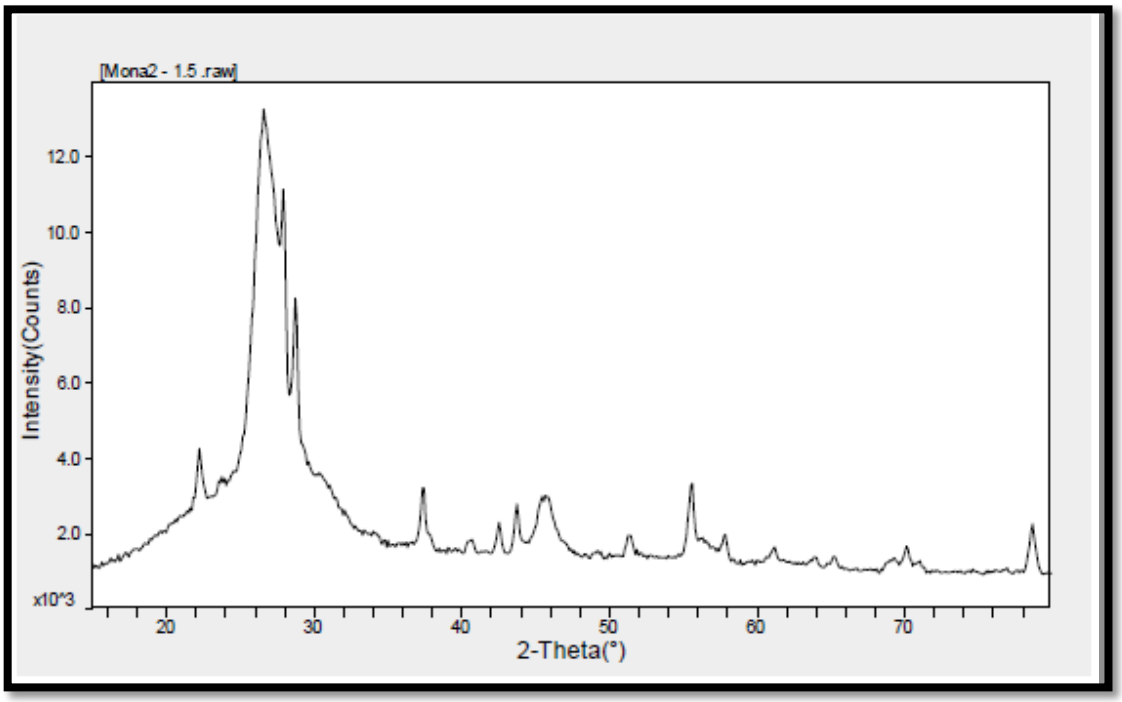

Figure (4.12) XRD spectrum of CNTs+TiO_2 (1.50)

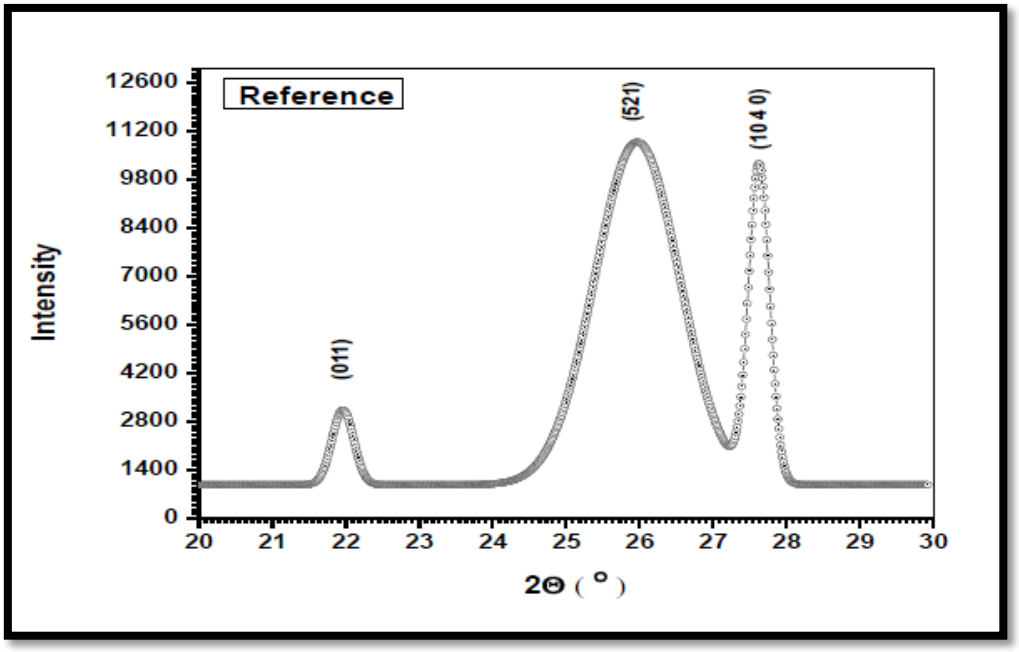

Figure (4.12) XRD spectrum of reference sample

Table (4.1) XRD parameters of reference sample

Samples	Type of cell	2θ(^{O})	d(A^{0})	X_s(nm)	h k l	δ($mg.cm^{-3}$)
reference CNTs	monoclinic-primitive	21.942	4.0475	21.3	0 1 1	6.9310
		25.873	3.4454	6.9	5 1 1	3.5550
		27.601	3.2291	49.1	1 0 4	3.5550

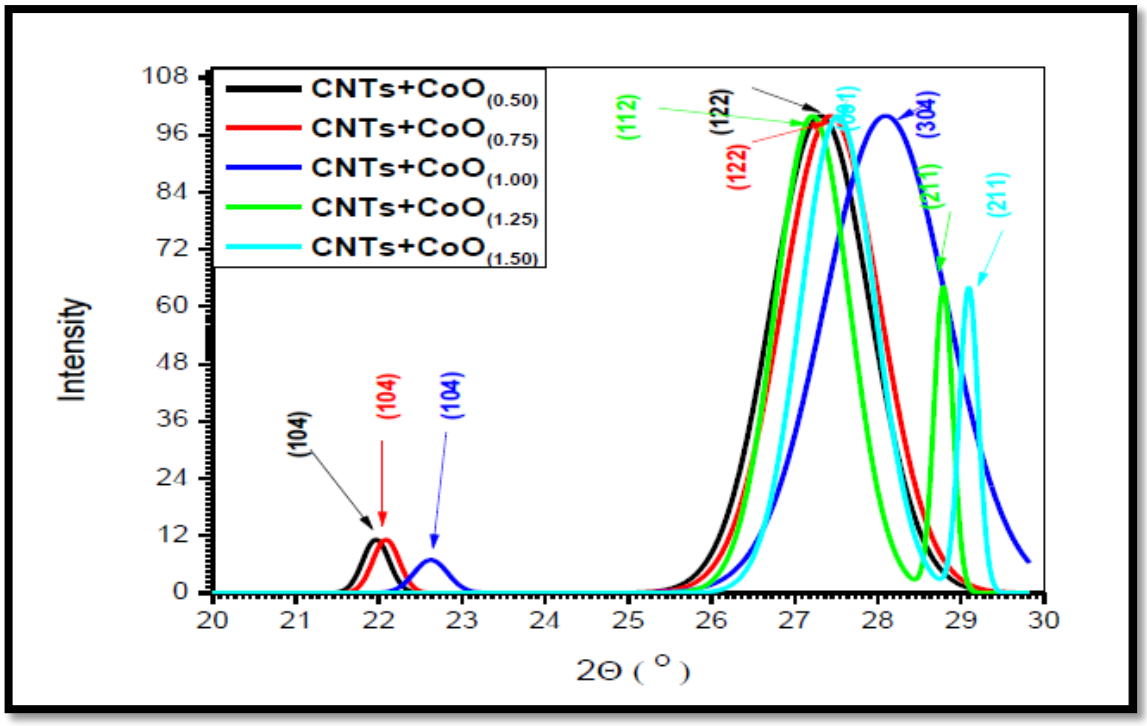

Figure (4.13) XRD spectrum of CNTs+CoO samples

Table (4.2) XRD parameters of CNTs+CoO samples

Samples	Type of cell	2θ(°)	d(A⁰)	Xs(nm)	h k l	δ(mg.cm⁻³)
CNTs+CoO(0.5)	Monoclinic-primitive	22.092	4.0204	22.6	1 0 4	3.7315
		27.589	3.2305	9.5	1 2 2	3.7315
CNTs+CoO(0.75)	Monoclinic-primitive	22.092	4.0204	22.6	1 0 4	3.7315
		27.589	3.2305	9.5	1 2 2	3.7315
CNTs+CoO(1.00)	Monoclinic-primitive	22.208	3.9997	40.4	1 0 4	4.6559
		27.937	3.1911	28.5	3 0 4	4.6559
CNTs+CoO(1.25)	Monoclinic-B-center	26.687	3.3376	7.5	1 2 2	2.6198
		27.994	3.1847	33.2	2 1 1	2.6198
CNTs+CoO(1.50)	Hexagonal-primitive	26.182	3.4008	9.3	0 0 1	7.2335
		27.873	3.1983	61.4	2 1 1	7.2335

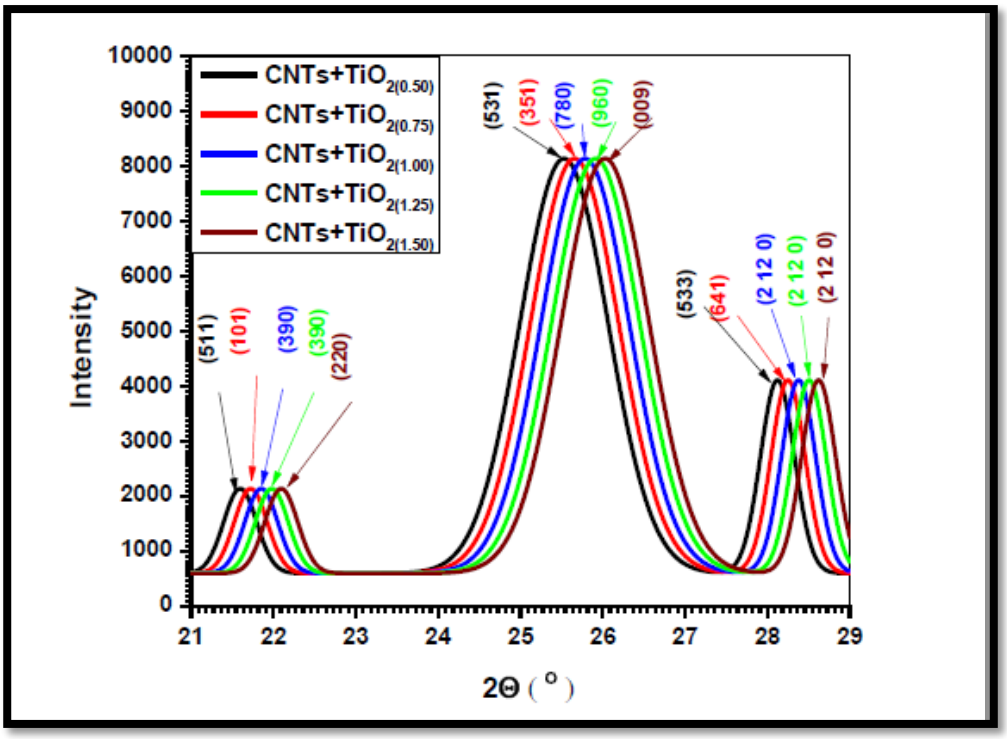

Figure (4.14) XRD spectrum of CNTs+TiO2 samples

Table (4.3) XRD parameters of CNTs+TiO2 samples

Samples	Crystal	2θ(^{O})	d(A^{0})	X_s(nm)	h k l	δ(mg.cm^{-3})
$CNTs+TiO_{2(0.5)}$	Cubic-F-center	22.088	4.1804	22.4	5 1 1	4.4372
		25.902	3.4370	10.6	5 1 1	4.4372
		28.691	3.1089	22.6	5 3 3	4.4372
$CNTs+TiO_{2(0.75)}$	Orthorhombic-primitive	22.094	4.0200	20.6	1 0 1	6.7421
		26.061	3.4164	10.7	3 5 1	6.7421
		28.608	3.1177	25.4	6 4 1	6.7421
$CNTs+TiO_{2(1.00)}$	Monoclinic-primitive	22.128	4.0139	25.3	3 9 0	6.9310
		26.072	3.4149	11.6	7 8 0	6.9310
		28.603	3.1182	27	2 12 0	6.9310
$CNTs+TiO_{2(1.25)}$	Monoclinic-primitive	22.2178	4.0050	26	3 9 0	9.9310
		26,173	3.4020	7.4	6 9 0	9.9310
		28.613	3.1172	22.6	2 12 0	9.9310
$CNTs+TiO_{2(1.50)}$	Triclinic-primitive	22.199	4.0012	31.3	2 2 0	4.3187
		26.375	3.3514	7.2	2 2 0	4.3187
		28.694	3.1988	22.5	2 12 0	4.3187

The XRD charts reference sample was shown in fig (4.1), CNTs+CoO samples shown from fig (4.2) to fig (4.6) and for the all CNTs+TiO_2 samples from fig (4.7) to fig (4.11). Miller indices provided in fig (4.12),fig(4.13) and fig(4.14) for reference, CNTs+CoO and CNTs+TiO_2 respectively , crystal with (monoclinic – primitive) crystal structure for pure CNTs (a=b=8.948 and c=14.078 / $\alpha = 90^o$ $\beta = 90.33^o$, and $\gamma = 90^o$)and the XRD parameters for reference CNTs listed in table(4.1) .All peaks determine transformation of Carbon Nano Tube (CNT) samples doping by Cobalt Oxide (CoO) (0.5, 0.75, 1.00, 1.25 and 1.5) Molar. crystallites with (Monoclinic – primitive)(a = 14.72 , b=7.23 and c = 16.64 / α $90^o = \beta = 90.6^o, \gamma = 90^o$) for CNTs+$CoO_{(0.5)}$, while for CNTs+$CoO_{(0.75)}$ (Monoclinic – primitive)crystal structure (a = 14.72 , b=7.23 and c = 16.64 / α $90^o = \beta = 90.6^o \gamma = 90^o$), crystal with (Monoclinic – primitive) crystal structure(a = 10.037 , b=8.862 and c = 10.186 / α $90^o = \beta = 90.95^o \gamma = 90^o$) for CNTs+$CoO_{(1.00)}$, the crystallites with (Monoclinic – B-center) crystal structure for CNTs+$CoO_{(1.25)}$ (a = 8.758 , b=4.869 and c = 10.717 / $\alpha = \beta = \gamma = 90^o$) and with (hexagonal – primitive) crystal structure (a =b= 6.02 and c = 3.418 / $\alpha = \beta = 90^O$ and $\gamma = 120^o$) for CNTs+$CoO_{(1.50)}$, the XRD parameters for all CNTs+CoO listed in table (4.2). The crystallites with (Cubic – F-center) crystal structure for the sample (a = b = c = 20.52 / $\alpha = \beta = \gamma = 90^o$) CNTs+$TiO_{2\,(0.5)}$ and for CNTs+$TiO_{2\,(0.75)}$ (orthorhombic – primitive) crystal structure (a = 34.067, b = 38.085 and c = 4.056 / $\alpha = \beta = \gamma = 90^o$). Crystallites with (monoclinic – primitive) crystal structure (a = 34.34, b = 38.05 and c = 4.06 / $\alpha = 90^o = \beta = 90.33^o = \gamma = 90^o$) for CNTs+$TiO_{2(1.00)}$, Crystallites with (monoclinic – primitive)crystal structure (a = 34.067 ,b = 38.085 and c = 4.056 / $\alpha = \beta = \gamma = 90^o$) for CNTs+$TiO_{2(1.25)}$ and finally Crystallites with (triclinic – primitive) crystal structure (a = 8.3678, b = 9.6916 and c = 6.9613 / $\alpha = 106.872^o = \beta = 101.726^o = \gamma = 96.743^o$) for CNTs+$TiO_{2(1.50)}$. The XRD parameters for all CNTs+TiO_2 listed in table (4.3).

4.3 SEM Results

Scanning electron microscope (SEM) was used to study diameter and surface morphology of reference sample, CNTs+CoO and CNTs+ TiO2 at concentration (0.5,0.75, 1.00,1.25 and 1.5) molar as shown in figures (4.15) , figure (4.16) and figure (4.17) respectively.

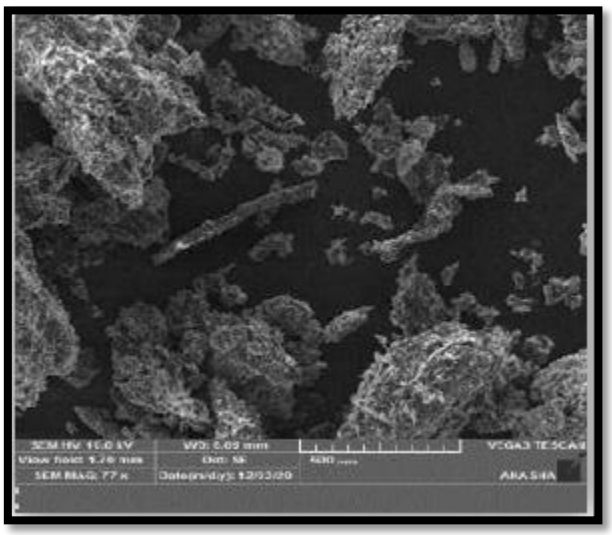

Figure (4.15) SEM for reference CNTs

Figure (4.16) SEM for CNTs+CoO samples

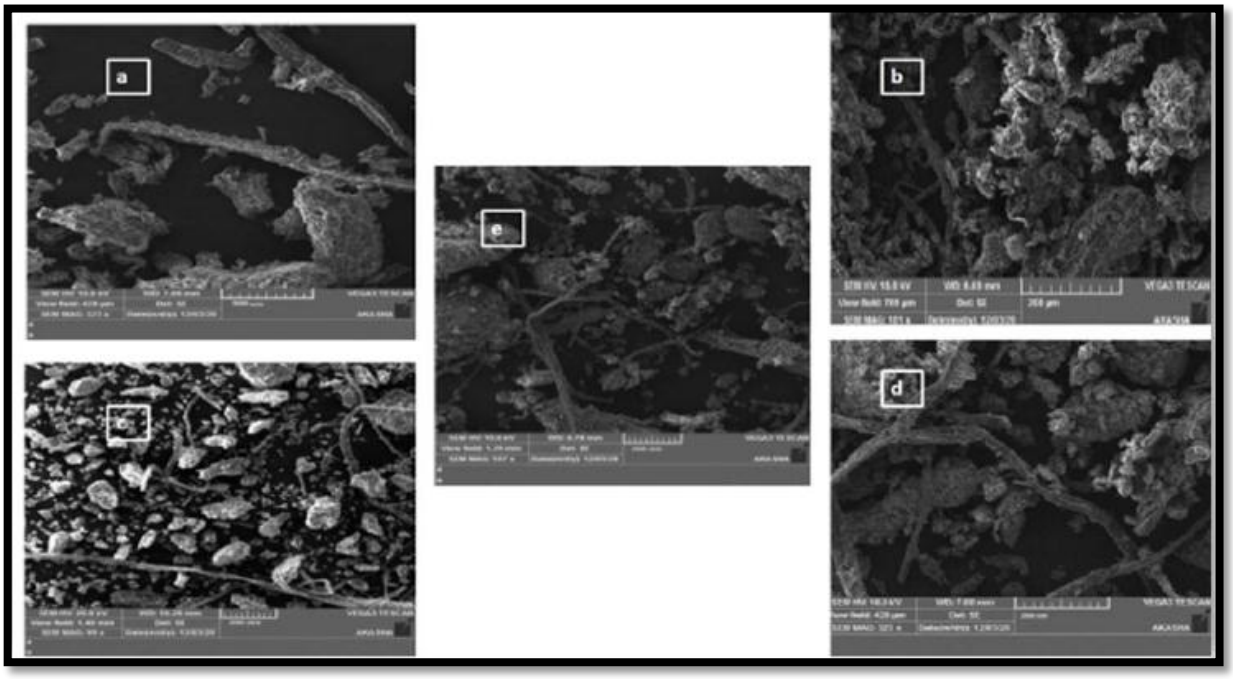

Figure (4.17) SEM for CNTs+TiO_2 samples

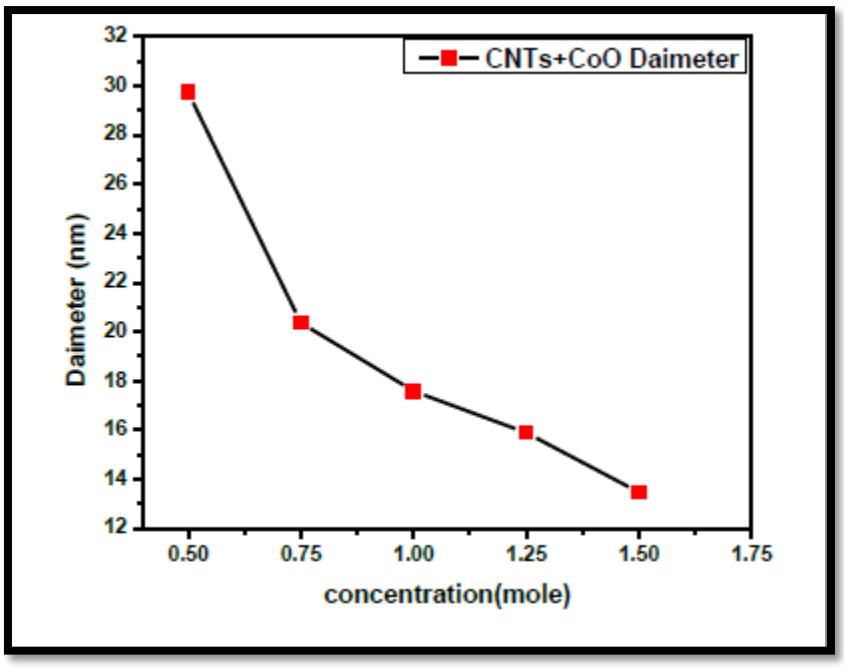

Figure (4.18) the variation of CNTs average diameter with Cobalt oxide (CoO) concentration

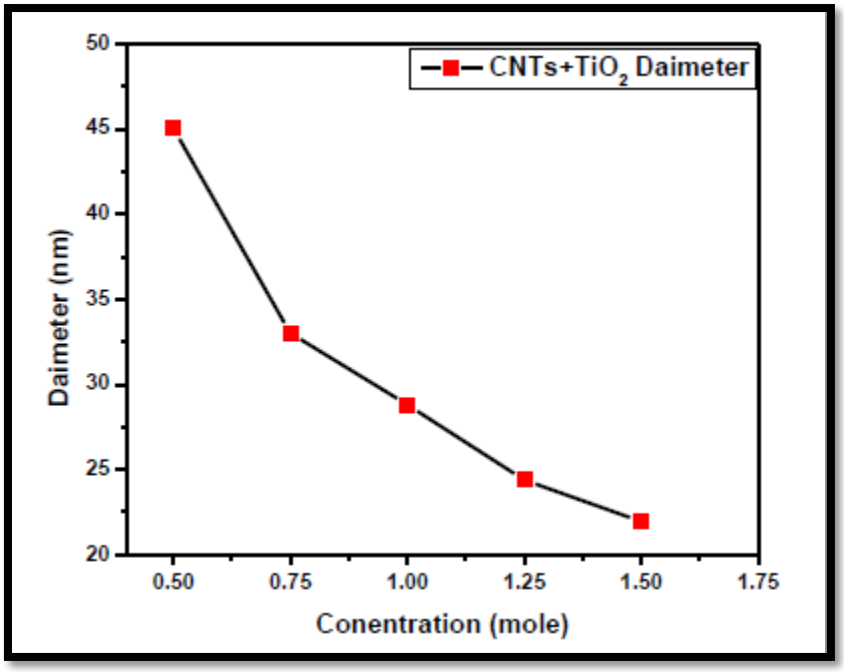

Figure (4.19) the variation of CNTs average diameter titanium dioxide (TiO_2) with concentration

Fig (4.18) and (4.19) showing the variation of CNTs average diameter with Cobalt oxide (CoO) and titanium dioxide (TiO_2) with concentrations (0.5, 0.75, 1.00, 1.25 and 1.5) which was calculated using imagej and origin software, the average diameter reference sample is 51.021nm it was observed that the diameter of CNTs decreases with concentration of CoO and TiO_2 increase, the diameter for CNTs+CoO (0.50) is 29.736nm, for CNTs+CoO(0.75) is 20.368 nm, for CNTs+CoO (1.00) is 17.588nm, for CNTs+CoO(1.25) is 15.8971 nm and for CNTs+CoO (1.5) 13.485nm. , The diameter for CNTs+TiO_2 (0.5) is 29.73645.032 nm, for CNTs+TiO_2 (0.75) is 33.014 nm, for CNTs+TiO_2 (1.00) is 28.813 nm, for CNTs+TiO_2 (1.25) is 24.387 nm and CNTs+TiO_2(1.5) is 21.951nm. From figure (4.20), it is clear that cobalt oxide decreased the diameter of CNTs more than titanium dioxide do.

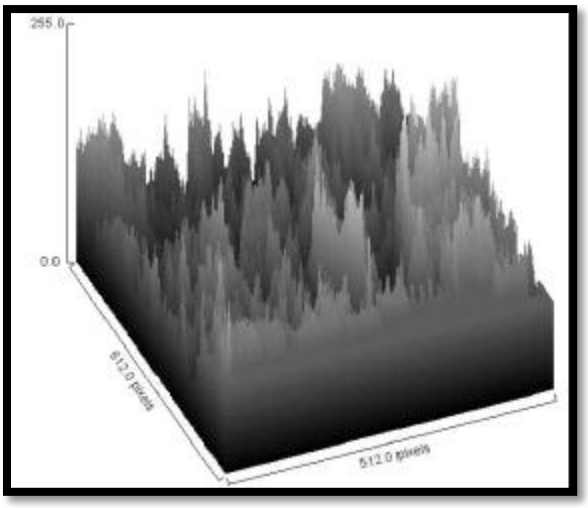

Figure (4.20) surface roughness of reference sample

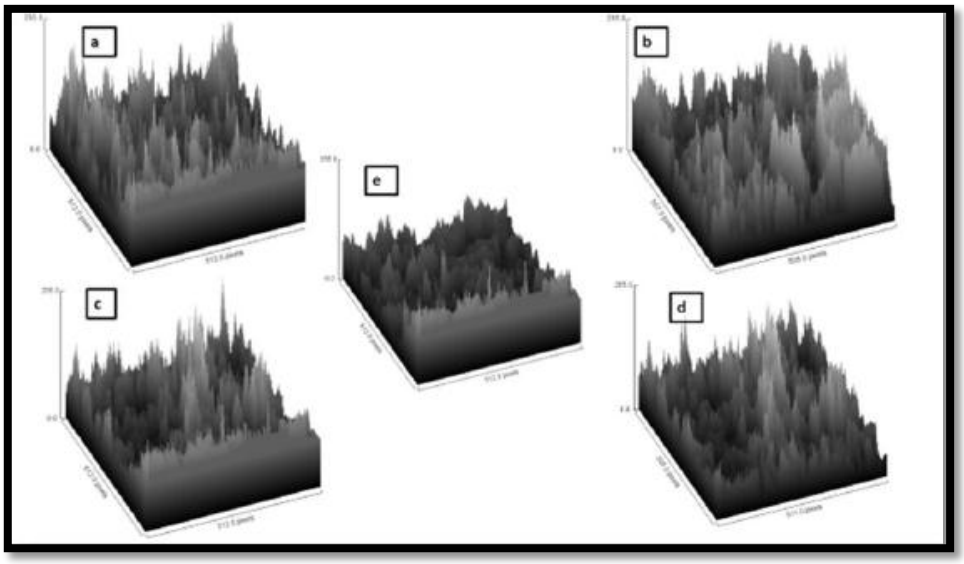

Figure (4.21) surface roughness of CNTs+CoO samples
a) CNTs+CoO (0.50). b) CNTs+CoO (0.75) c) CNTs+CoO (1.00)
d) CNTs+CoO (1.25) e) CNTs+CoO (1.50)

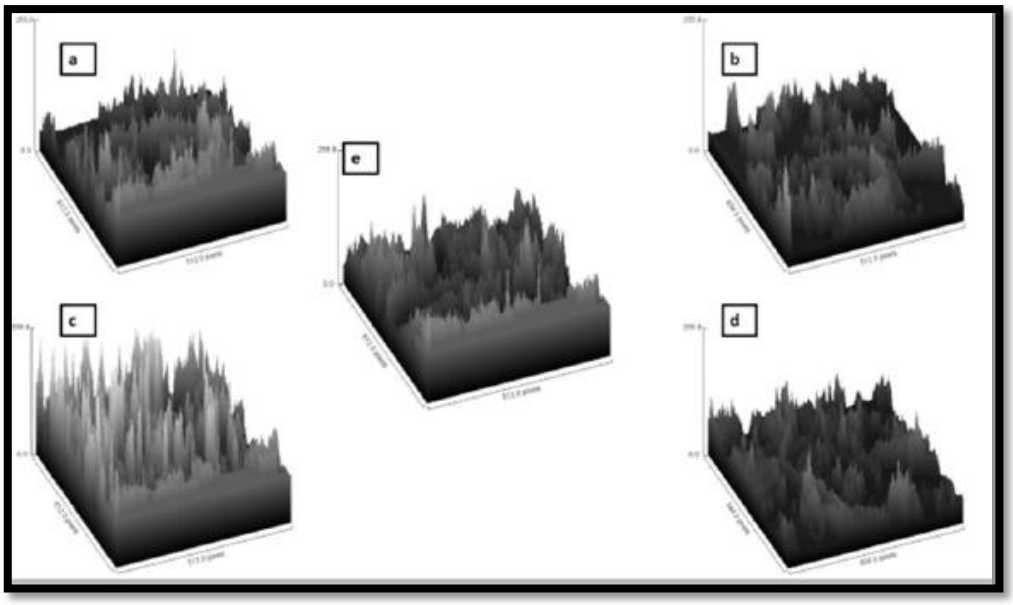

Figure (4.22) surface roughness of CNTs+CoO samples
a) CNTs+TiO2 (0.50). b) CNTs+TiO2 (0.75) c) CNTs+TiO2 (1.00)
d) CNTs+TiO2 (1.25) e) CNTs+TiO2 (1.50)

Imagej software was used to obtain surface roughness from SEM images for reference sample, CNTs+CoO and CNTs+ TiO_2 at concentrations (0.5, 0.75, 1.00, 1.25 and 1.5) molar as shown in fig (4.21), (4.22) and (4.23) respectively. It is determine the variation of cobalt oxide and titanium dioxide molarity at prepared carbon nanotubes, white color refer to treated by cobalt oxide or titanium dioxide while black color refer to untreated area.

4.4 FTIR results

Fourier transforms infrared spectroscopy (FTIR) used to study the vibrational frequencies of chemical bonds and structural properties of Carbon nanotubes (CNT) doping by with cobalt Oxide (CoO) and titanium dioxide (TiO_2) at concentration (0.5, 1.00 and 1.5) molar as showing in the results below:

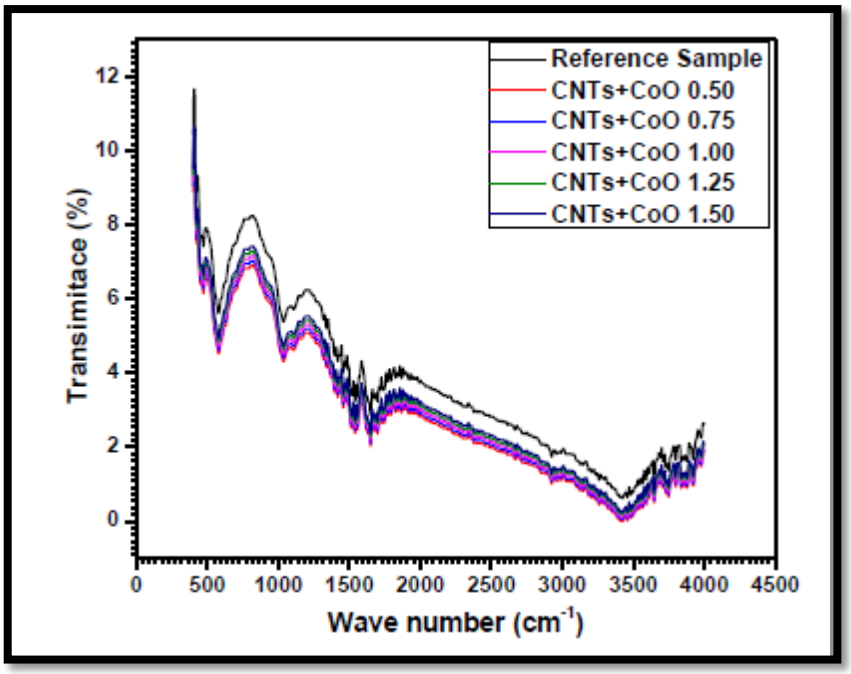

Figure (4.23) IR spectrum of CNTs +CoO samples

Table (4.4) Table of Characteristic IR of CNTs + CoO (0.00, 0.5, 0.75, 1.00, 1.25 and 1.50) Molar

No	Wavenumber (cm^{-1})	Functional Group	Type of Vibration
1	471	meta disubstituted aromatic	C-H bend patterns for aromatics
2	547	alkyl halides	C–Br stretch
3	1040	Esters	(C-O Stretch)
4	1530	Aromatic Compounds	C=C stretch
5	1650	Carboxylic Acids	C=O Stretch
6	2920	Alkanes	C-H stretch
7	3440	Phenols & Alcohols	Hydrogen-bonded O-H Stretch
8	3740	alcohols	O–H stretch
9	3930	alkynes (terminal)	–C ≡ C–H: C–H stretch

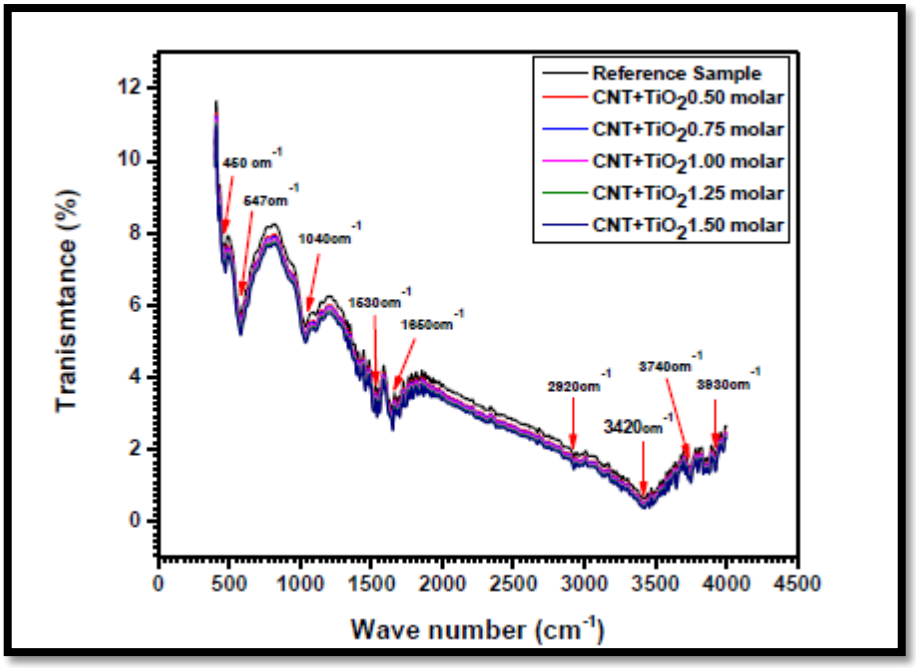

Figure (4.24) IR spectrum of CNTs +TiO_2 samples

Table (4.5) Table of Characteristic IR of CNTs + TiO_2 (0.00, 0.5, 0.75, 1.00, 1.25 and 1.50) Molar

No	Wavenumber (cm^{-1})	Functional Group	Type of Vibration
1	450	meta disubstituted aromatic	C-H bend patterns for aromatics
2	547	alkyl halides	C–Br stretch
3	1040	Esters	(C-O Stretch)
4	1530	Aromatic Compounds	C=C stretch
5	1650	Carboxylic Acids	C=O Stretch
6	2920	Alkanes	C-H stretch
7	3420	Phenols & Alcohols	Hydrogen-bonded O-H Stretch
8	3760	alcohols	O–H stretch
9	3930	alkynes (terminal)	–C ≡ C–H: C–H stretch

Fourier Transform Infrared spectroscopy is a technique used to measure the vibrational frequencies of bonds in the molecule. Figure (4.23) show IR spectrum of CNTs +CoO (0.50, 0.75, 1.00, 1.25 and 1.5) molar compared to reference sample, all values listed in table (4.4). The strong intensity peak at 3930 cm^{-1} refer to alkynes (terminal) –C ≡ C–H: C–H stretch, at 3740 cm^{-1} refer to O–H stretch vibration of alcohol group, the strong broad band at 3440 cm^{-1} refer to Alcohols group (O-H stretch).the very intense peak positioned at 2920 cm^{-1} refer to alkanes (C-H stretch) . The peaks at 1650 cm^{-1} refer to vibration of Carboxylic Acids (C=O Stretch). The peaks at 1530 cm^{-1} refer to C=C stretch vibration of Aromatic Compounds ,the band at 1040 cm-1 refer to Esters group (C-O Stretch)vibration. Peak at 547 cm^{-1} refer to alkyl halides C–Br stretch, finally the very intense peak at 471 cm^{-1} refer to cobalt oxide(CoO) vibrations. And the FTIR spectra of CNTs+ TiO_2 (0.50, 0.75, 1.00, 1.25 and 1.5) compared to reference sample shown in fig (4.24) and the results listed in table (4.5), It observed that CNTs +CoO and of CNTs+ TiO_2 have same value of intensity expect at peak position 471 cm^{-1} which refer to cobalt oxide (CoO) vibrations and 450 cm^{-1} which refer titanium dioxide (TiO_2).

4.5 Optical Results of CNTs doping by CoO and TiO_2 at different concentration (0.5, 1.00 and 1.5) molar

After made Carbon nanotubes (CNT) doping by with cobalt Oxide (CoO) and titanium dioxide (TiO_2) at different concentration (0.5, 1.00 and 1.5) molar used UV-VS spectrophotometer to study the optical parapets (absorbance, transmission, reflection, absorption coefficient, extinction coefficient, refractive index, real dielectric constant, imaginary dielectric constant, optical energy band gap, optical conductivity and electrical conductivity) as showing in the results blow:

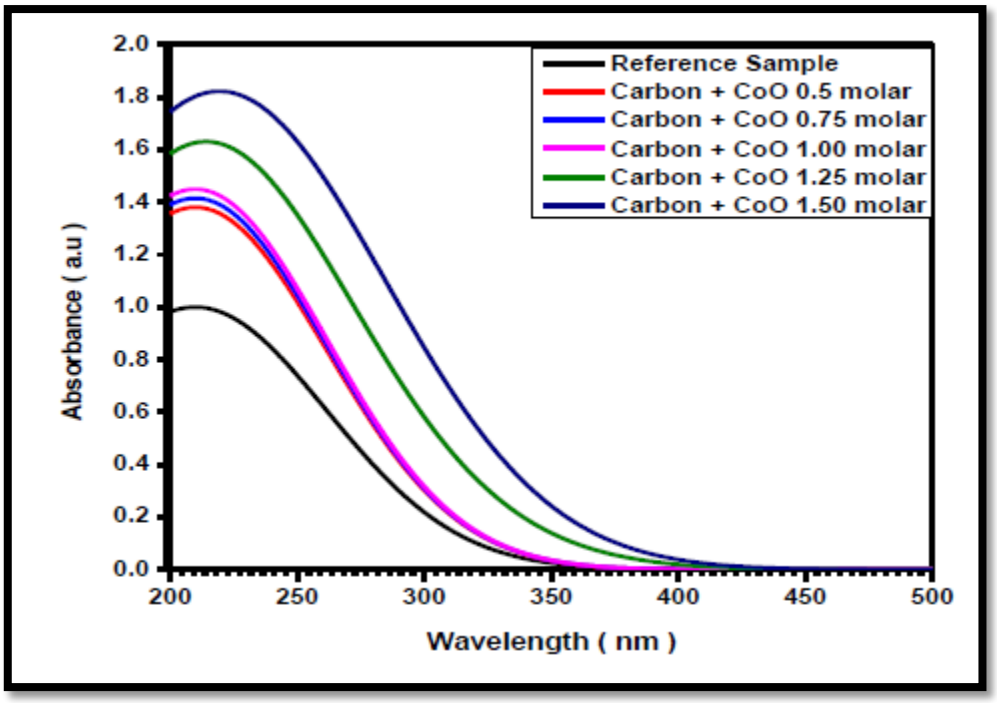

Figure (4.25) the relation between absorbance and wavelengths of CNTs + CoO (0.5, 0.75, 1.00, 1.25 and 1.5) molar

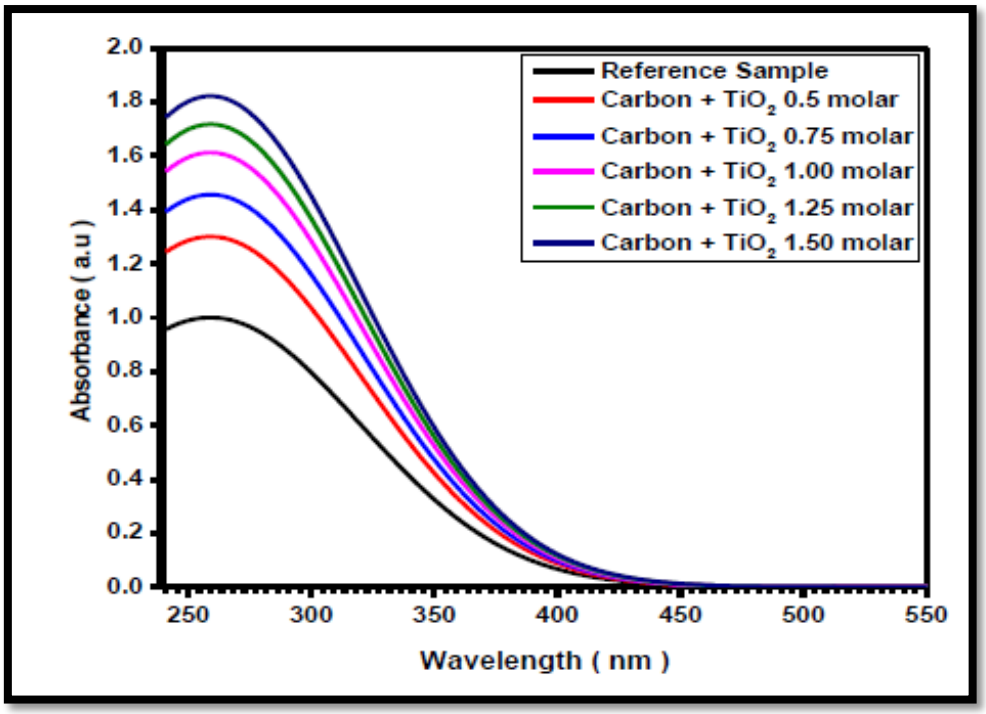

Figure (4.26) the relation between absorbance and wavelengths of CNTs + TiO_2 at (0.5, 0.75, 1.00, 1.25 and 1.5) molar

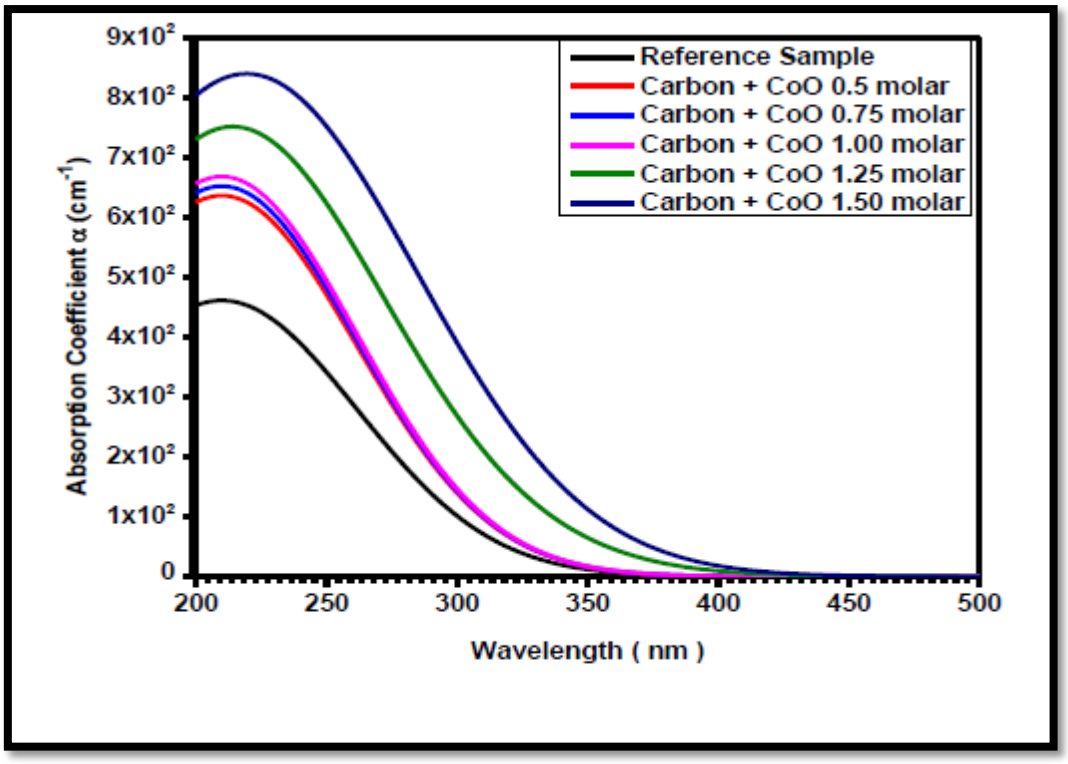

Figure (4.27) the relation between absorption coefficient and wavelengths of CNTs + CoO (0.5, 0.75, 1.00, 1.25 and 1.5) molar

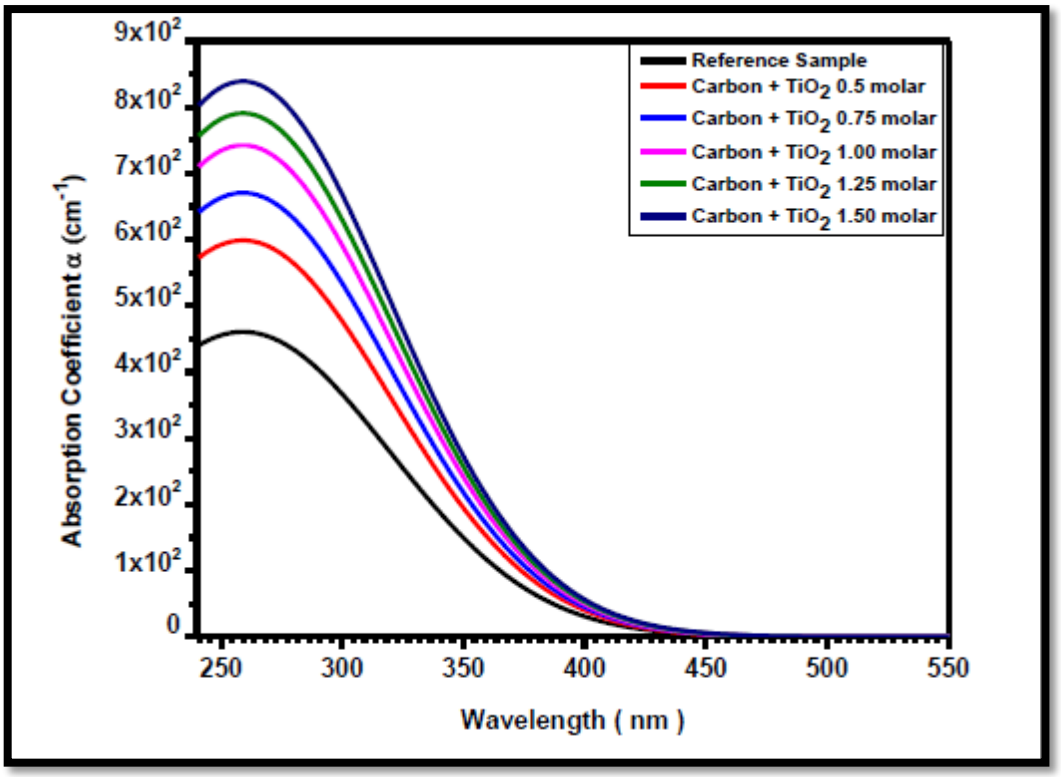

Figure (4.28) the relation between absorption coefficient and wavelengths of CNTs+TiO_2 (0.5, 0.75, 1.00, 1.25 and 1.5) molar

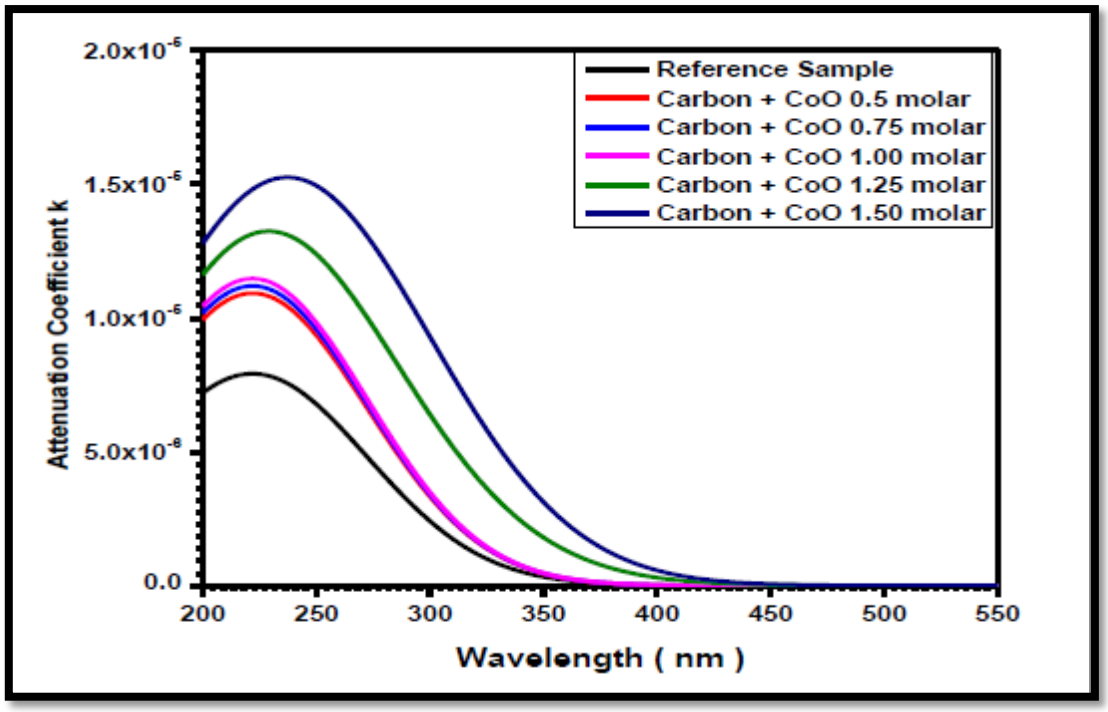

Figure (4.29) the relation between extinction coefficient and wavelengths of CNTs + CoO (0.5, 0.75, 1.00, 1.25 and 1.5) molar

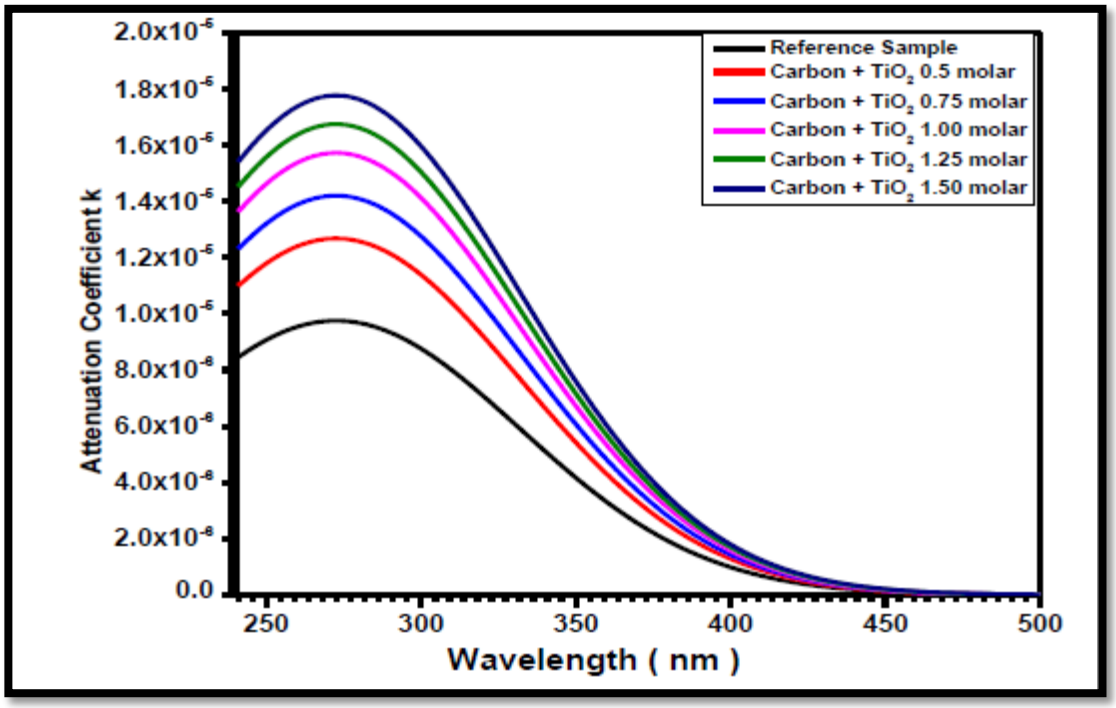

Figure (4.30) the relation between extinction coefficient and wavelengths of CNTs + TiO2 (0.5, 0.75, 1.00, 1.25 and 1.5) molar

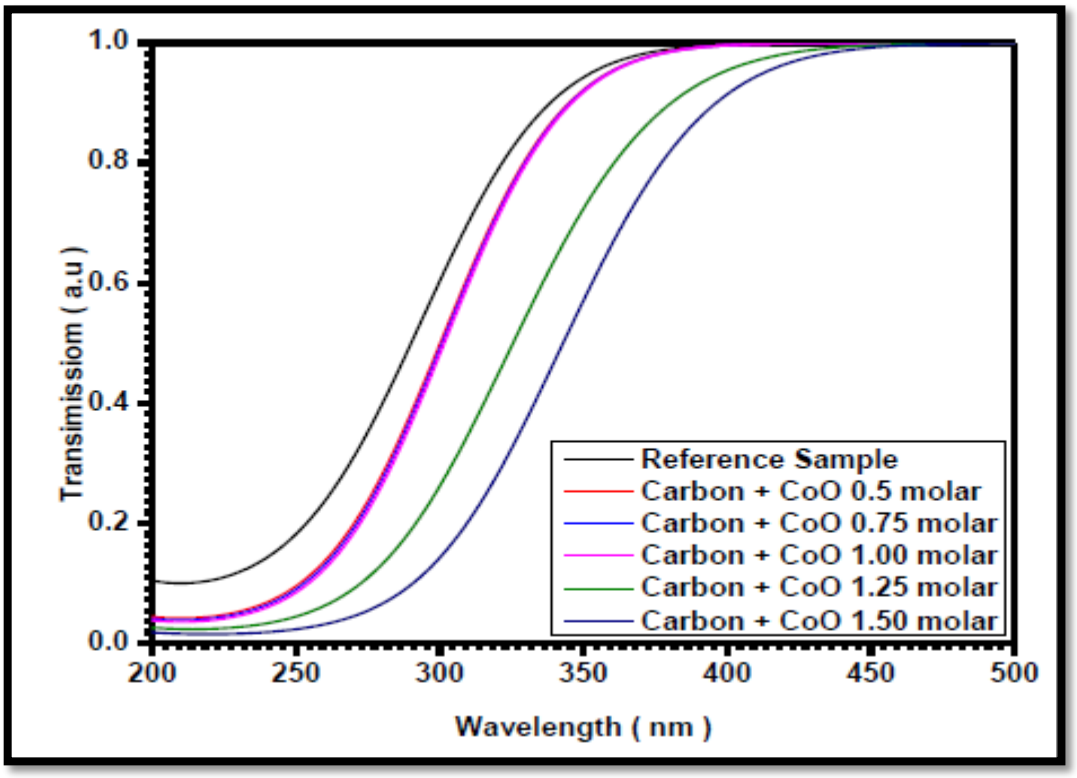

Figure (4.31) the relation between transmission and wavelengths of CNTs +CoO (0.5, 0.75, 1.00, 1.25 and 1.5) molar

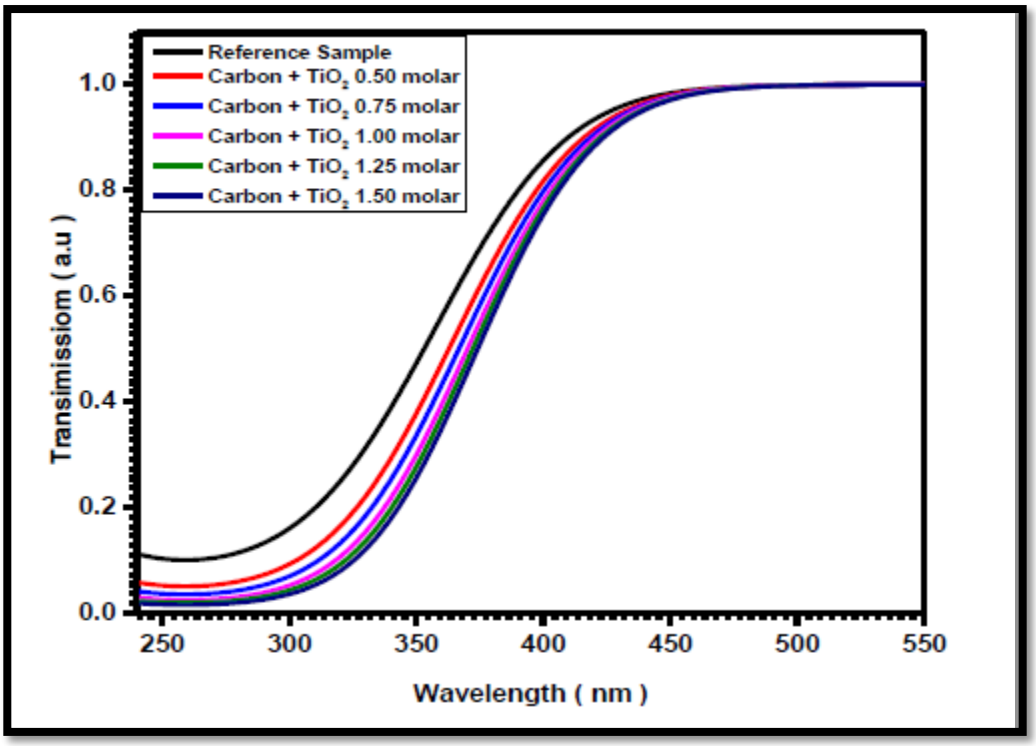

Figure (4.32) the relation between transmission and wavelengths of CNTs + TiO2 (0.5, 0.75, 1.00, 1.25 and 1.5) molar

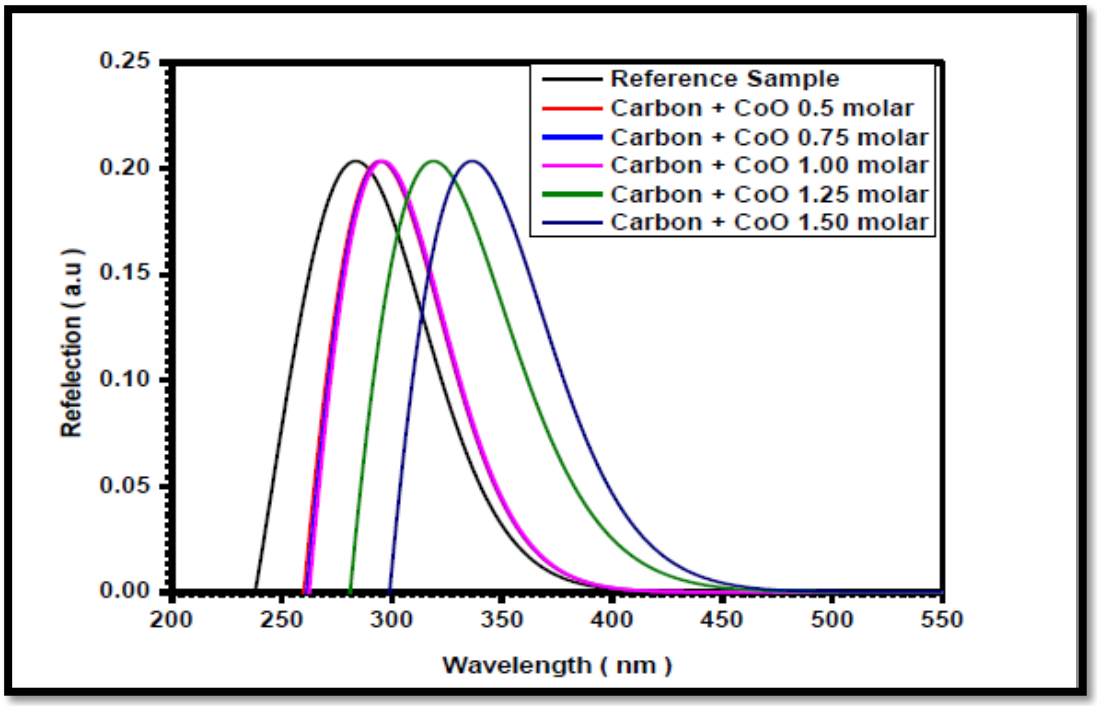

Figure (4.33) the relation between reflection and wavelengths of CNTs + CoO (0.5, 0.75, 1.00, 1.25 and 1.5) molar

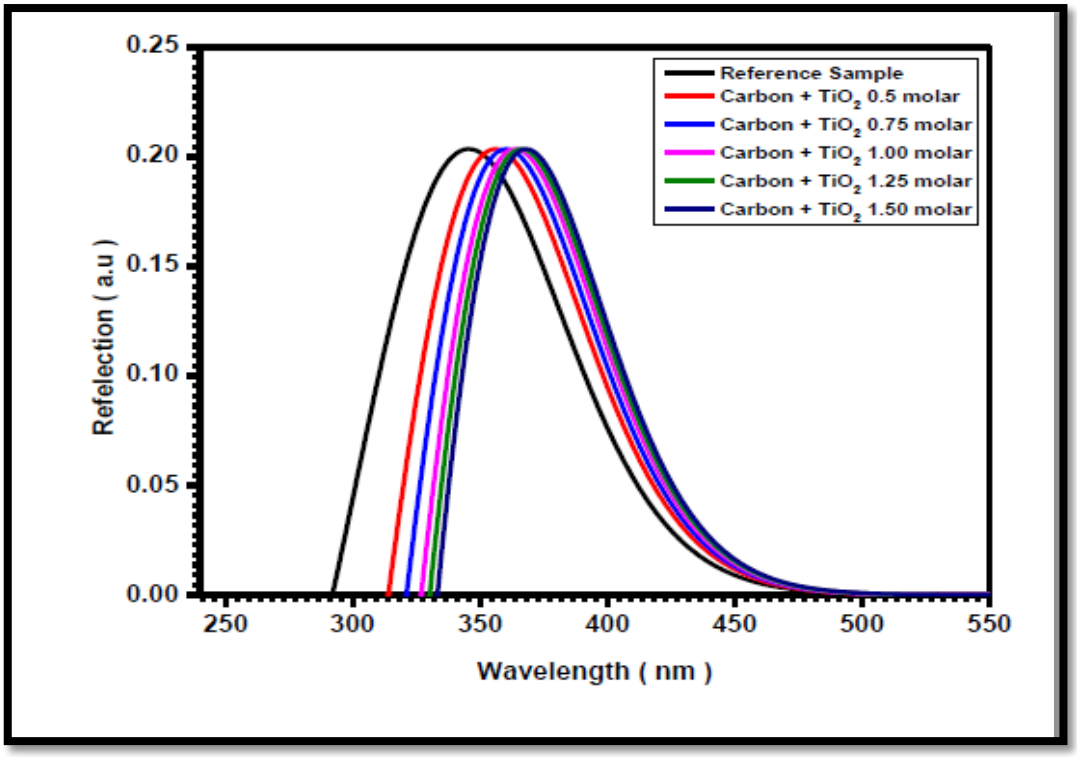

Figure (4.34) the relation between reflection and wavelengths of CNTs + TiO_2 (0.5, 0.75, 1.00, 1.25 and 1.5) molar

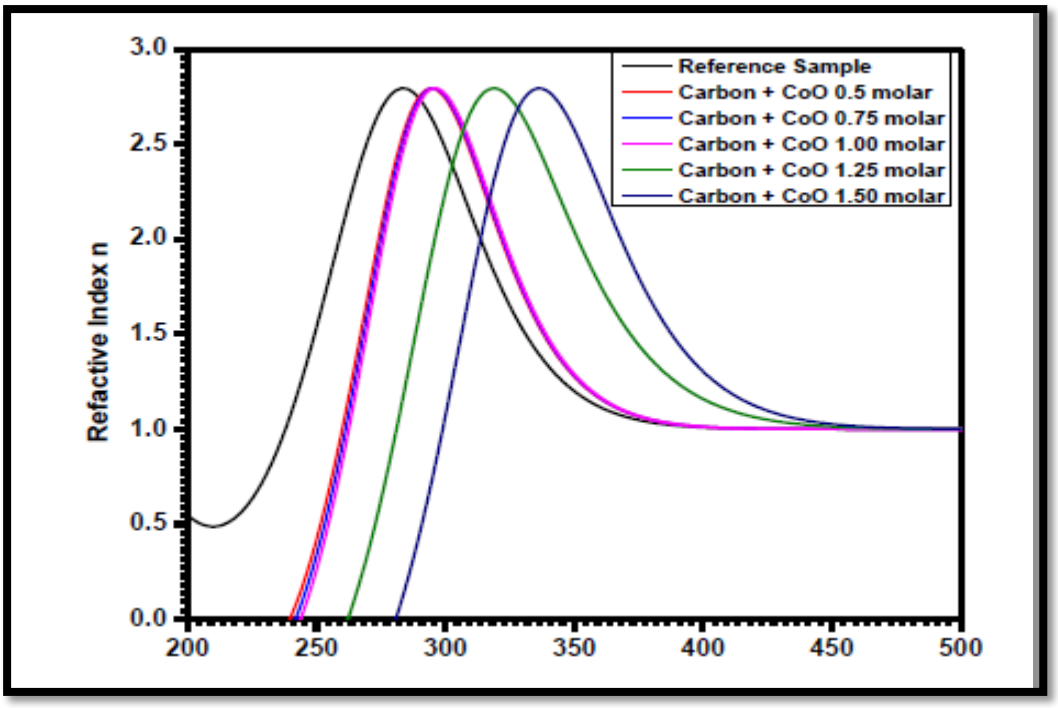

Figure (4.35) the relation between refractive index and wavelengths of CNTs + CoO (0.5, 0.75, 1.00, 1.25 and 1.5) molar

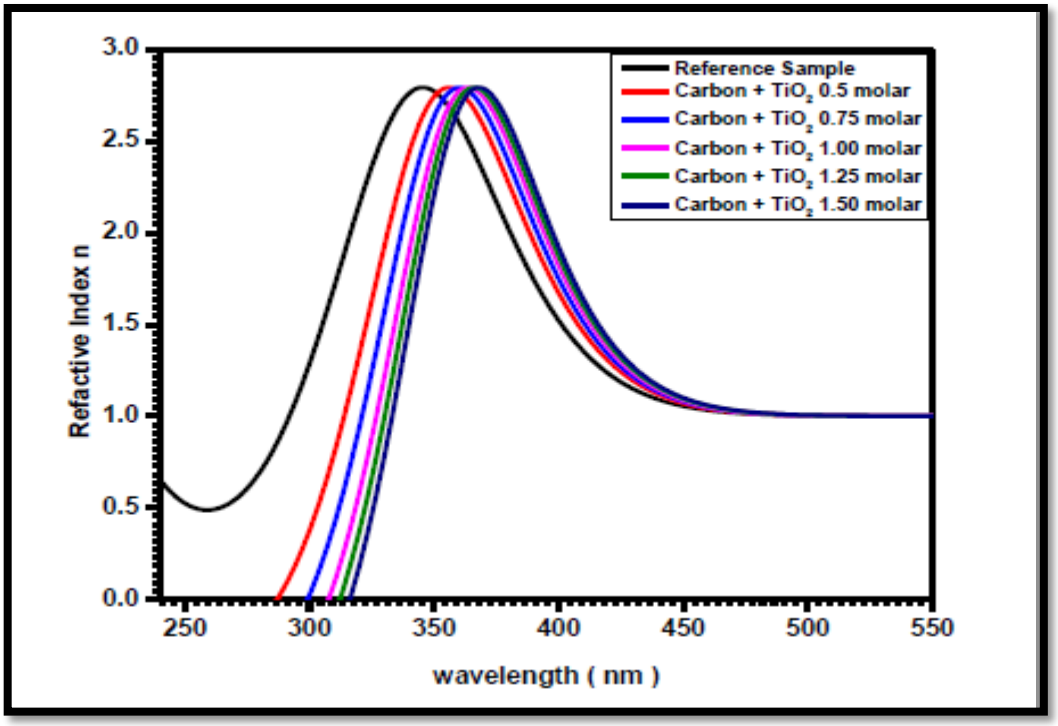

Figure (4.36) the relation between refractive index and wavelengths of CNTs + TiO_2 (0.5, 0.75, 1.00, 1.25 and 1.5) molar

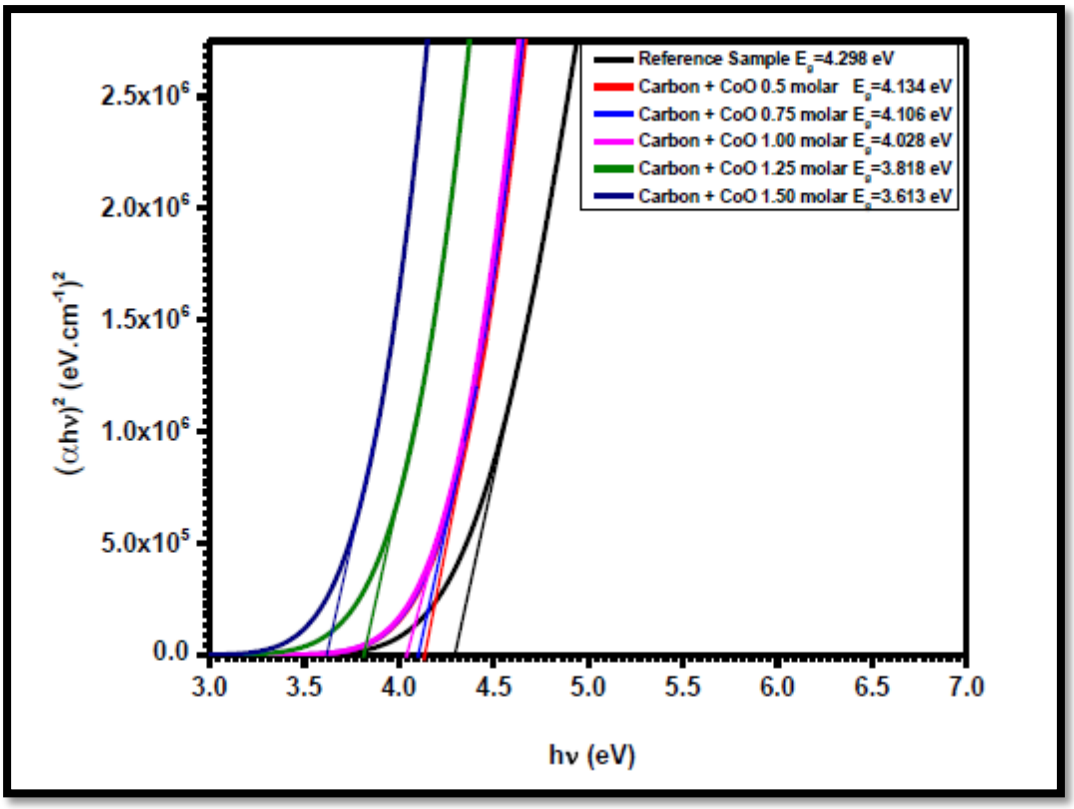

Figure (4.37) the optical energy band gap of CNTs + CoO (0.5, 0.75, 1.00, 1.25 and 1.5) molar

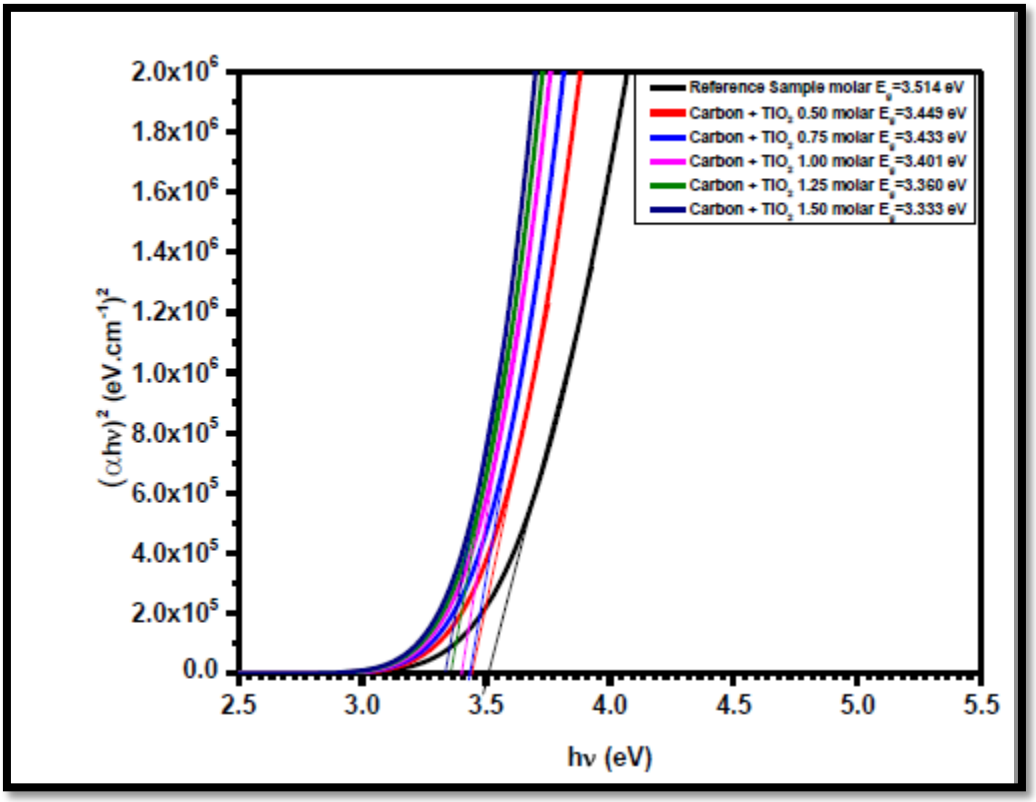

Figure (4.38) the optical energy band gap of CNTs + TiO2 (0.5, 0.75, 1.00, 1.25and 1.5) molar

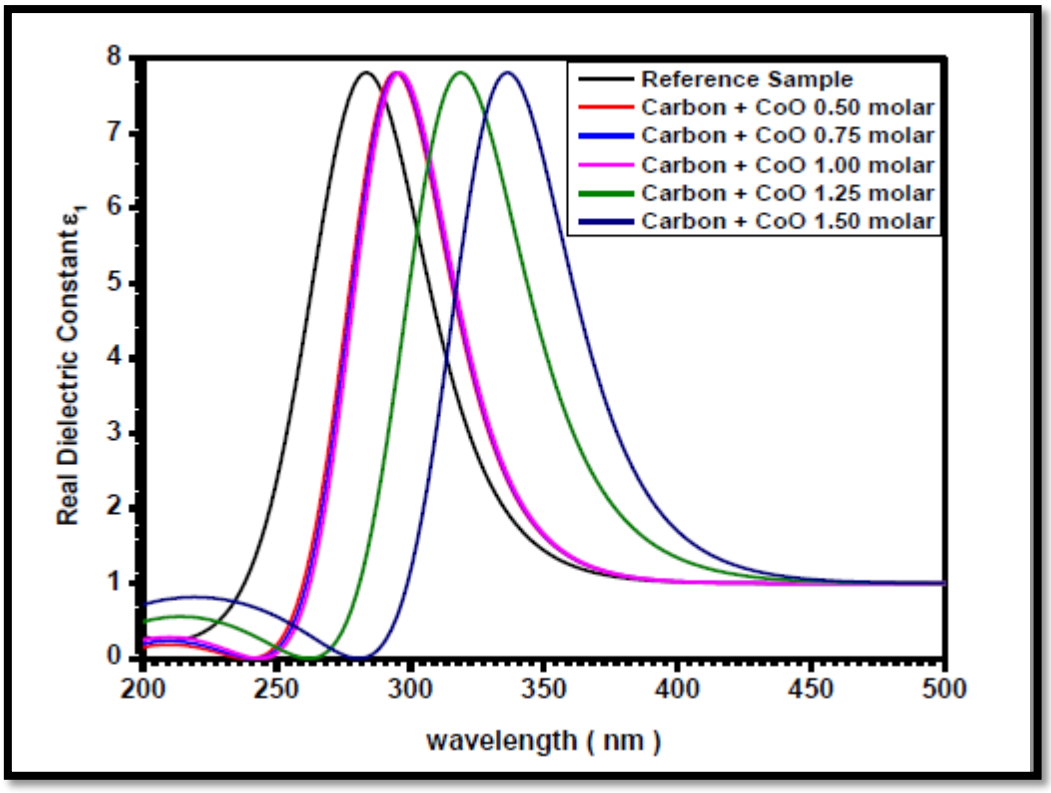

Figure (4.39) the relation between real dielectric constant and wavelengths of CNTs + CoO (0.5, 0.75, 1.00, 1.25 and 1.5) molar

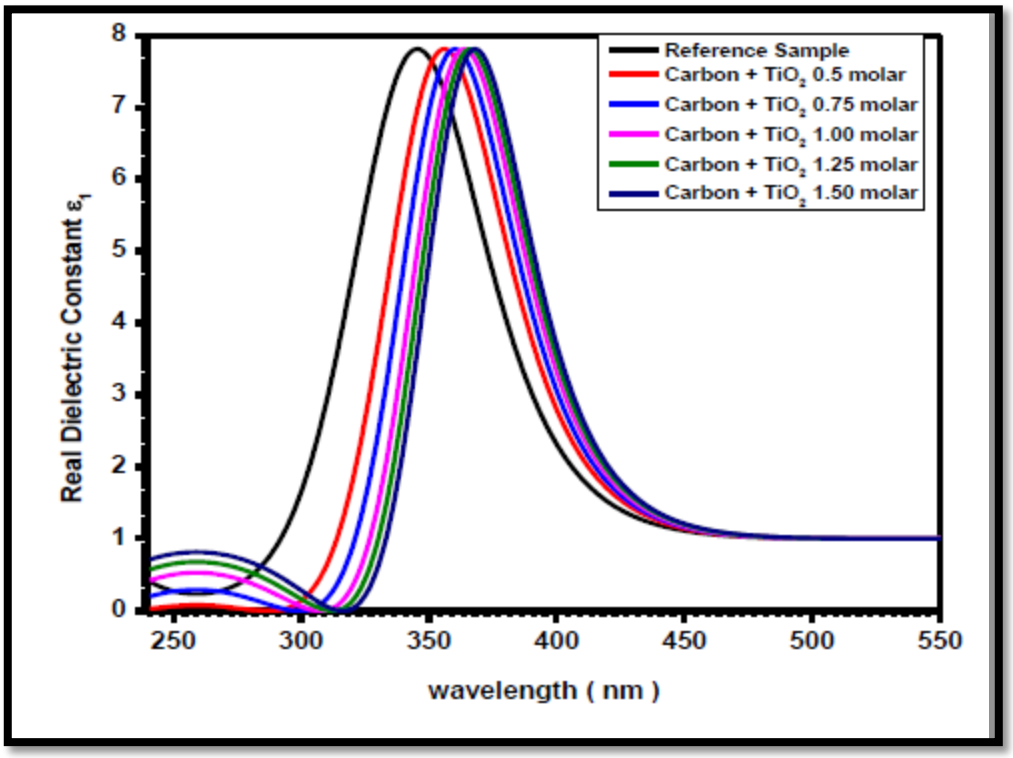

Figure (4.40) the relation between real dielectric constant and wavelengths of CNTs + TiO2 (0.5, 0.75, 1.00, 1.25 and 1.5) molar

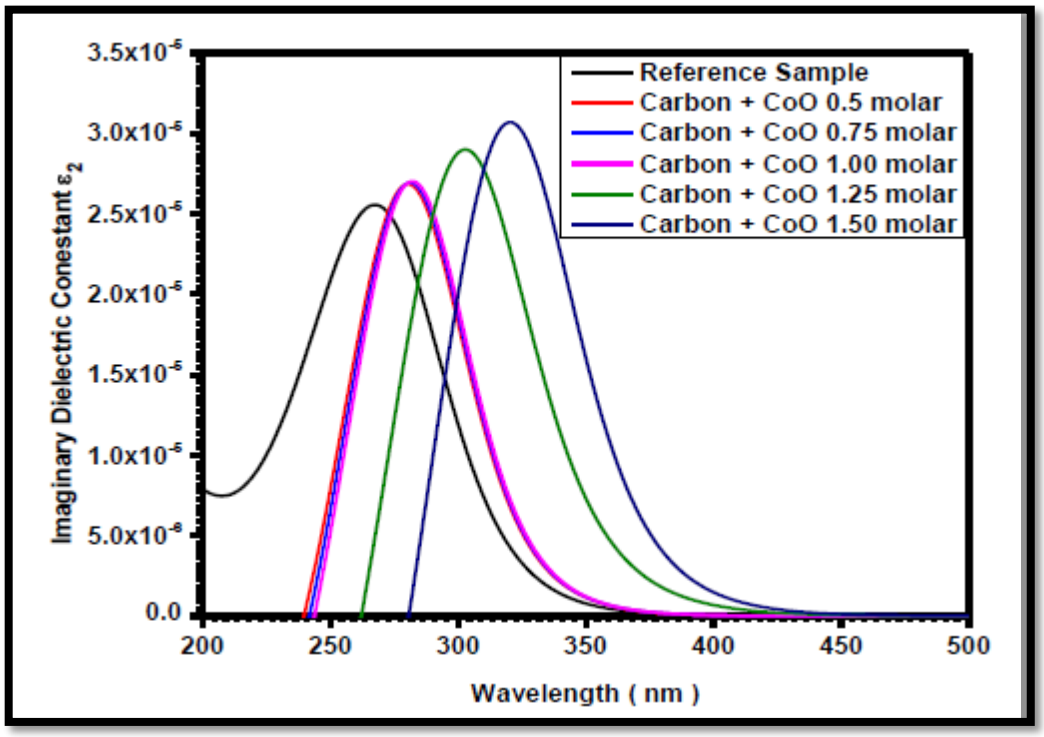

Figure (4.41) the relation between imaginary dielectric constant and wavelengths of CNTs + CoO (0.5, 0.75, 1.00, 1.25 and 1.5

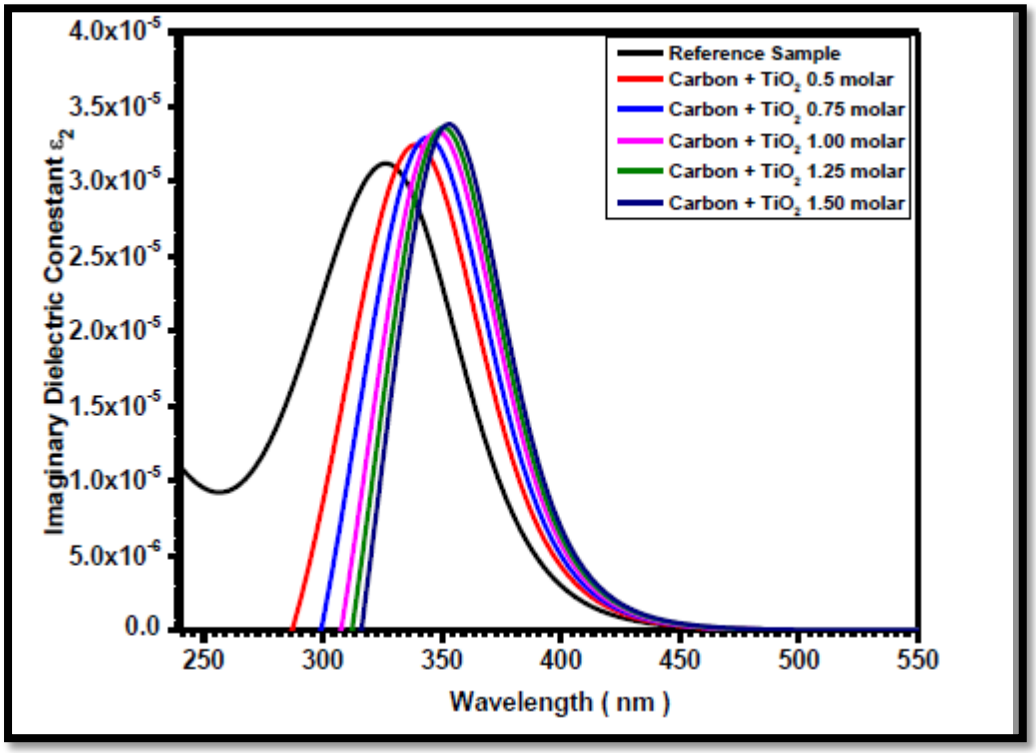

Figure (4.42) the relation between imaginary dielectric constant and wavelengths of CNTs + TiO_2 (0.5, 0.75, 1.00, 1.25 and 1.5

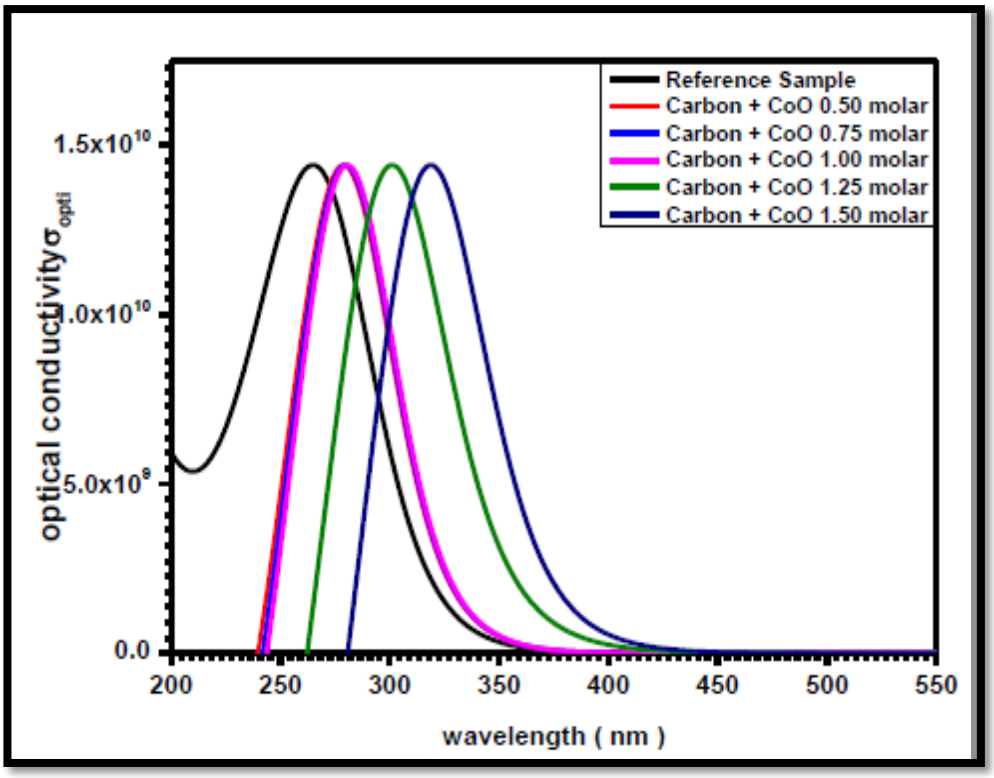

Figure (4.43) the optical conductivity and wavelengths of CNTs + CoO at (0.5, 0.75, 1.00, 1.25 and 1.5

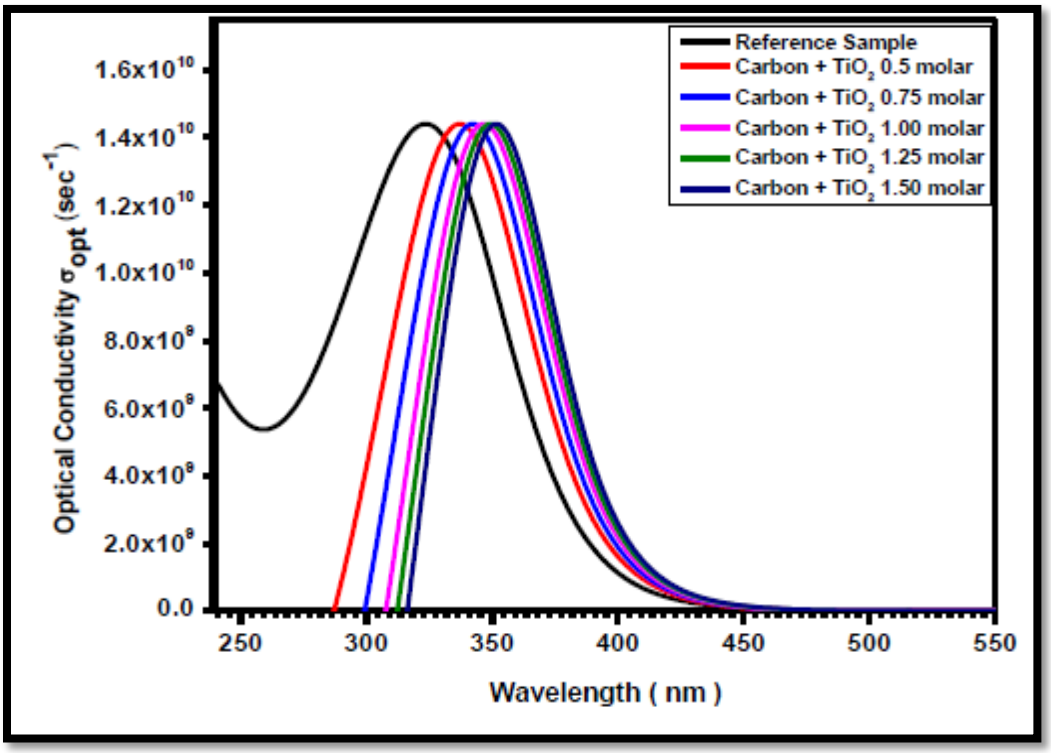

Figure (4.44) the optical conductivity and wavelengths of CNTs + TiO_2 (0.5, 0.75, 1.00, 1.25 and 1.5

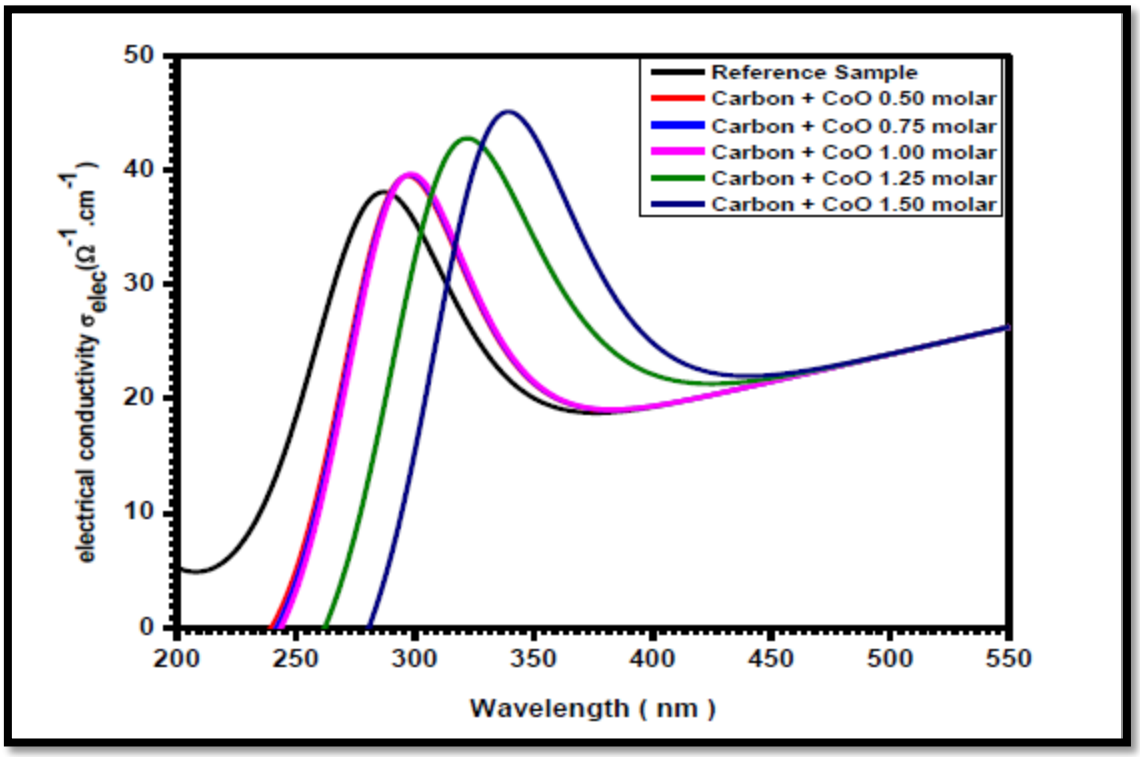

Figure (4.45) the electrical conductivity and wavelengths of CNTs + CoO (0.5, 0.75, 1.00, 1.25 and 1.5

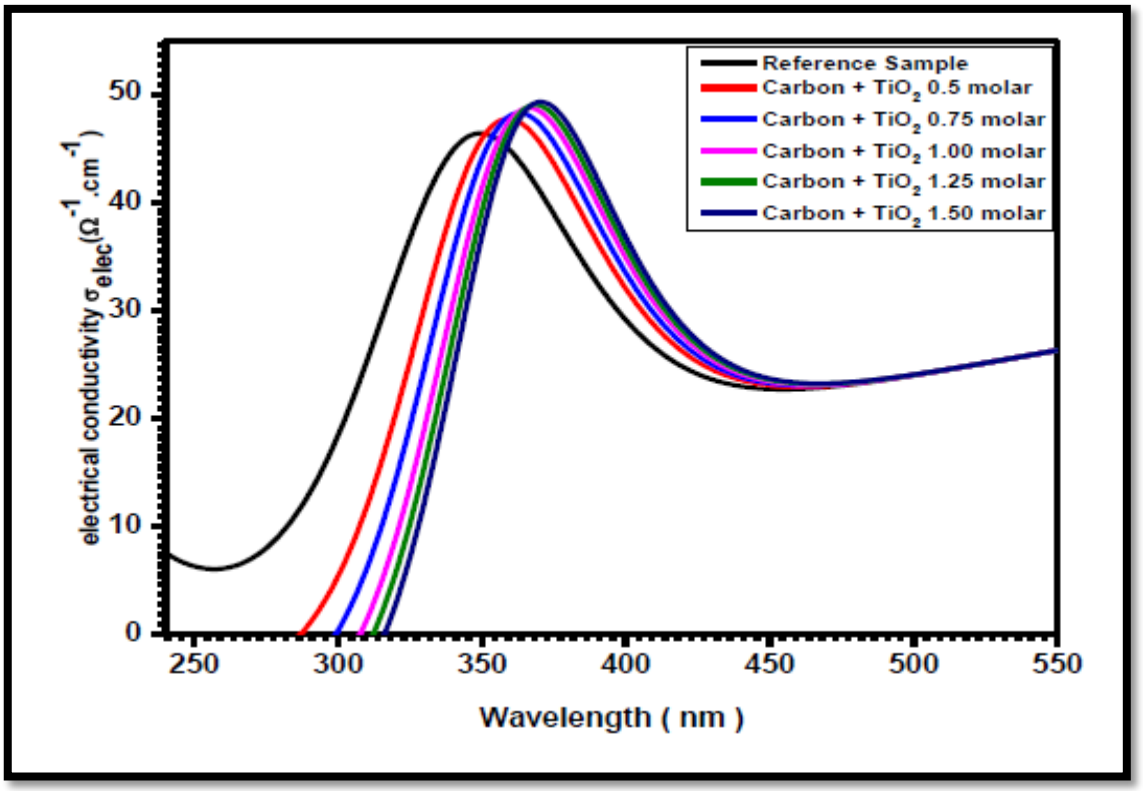

Figure (4.46) the electrical conductivity and wavelengths of CNTs + TiO_2 at (0.5, 0.75, 1.00, 1.25 and 1.5

From the above curves the behaviour of Carbon Nano Tube (CNT) doping with cobalt Oxide (CoO) and titanium dioxide (TiO_2) at concentration (0.5,0.75. 1.00,1.25 and 1.5) molar has been studied using UV-VS spectrophotometer. Fig (4.25) and (4.26) shows the absorbance of CNTs+CoO and CNTs+ TiO_2 at different concentration, the maximum value of absorbance is 1.83 (a.u) at wavelength (220) nm corresponding photon energy 3.613 eV for CNTs + CoO $_{(1.5)}$ and the minimum value is 1.002 (a.u) at the same wavelength for reference sample corresponding photon energy 4.298 eV ,while the maximum value of absorbance is 1.82 (a.u) at wavelength (258) nm corresponding photon energy 3.333 eV for carbon +TiO_2 $_{(1.5)}$ and the minimum value is 0.99 (a.u) at the same wavelength for reference sample corresponding photon energy 3.514 eV. The relation between absorption coefficient (α) and wavelength for CNTs+CoO and CNTs+ TiO_2 at concentration (0.5, 0.75. 1.00, 1.25 and 1.5) molar show in Fig (4.27) and (4.28) respectively that has been calculated using the formula:

$$\alpha = \frac{2.303xA}{l}$$

Where (A) is the absorbance and (l) is the optical length in the samples. The maximum value of (α) is $8.44x10^2$ cm^{-1} at wavelength 220nm for CNTs + $CoO_{(1.5)}$ while the minimum value is $4.61x10^2$ cm^{-1} at the same wavelength for CNTs +$CoO_{(0.50)}$. The maximum value of (α) is $8.42x10^2$ cm^{-1} at wavelength (258) nm for CNTs + TiO_2 $_{(1.5)}$ while the minimum value is $8.62x10^2$ cm^{-1} at the same wavelength for CNTs + TiO_2 $_{(0.5)}$.

Fig (4.29) and (4.30) shows the relation between extinction coefficient and wavelengths for CNTs+CoO and CNTs+ TiO_2 at concentration (0.5, 0.75. 1.00, 1.25 and 1.5) molar respectively. Extinction coefficient (K) was calculated using the relation:

$$\mathrm{K} = \frac{\alpha\lambda}{4\pi}$$

The maximum value of (K) is 1.53x10^{-5} at wavelength (236) nm for CNTs+CoO (1.5) while the minimum value is 7.98x10^{-6} at the same wavelength for CNTs +CoO (0.50). The maximum value of (K) is 1.77x10^{-5} at wavelength (236) nm for CNTs +TiO_2 (1.5 molar) while the minimum value is 9.82x10-6 at the same wavelength for CNTs + TiO2 (0.5 molar). It observed that the absorption coefficient and the extinction coefficient have the same spectrum shape. Fig (4.31) and (4.32) shows the relation between transmission (T) and wavelengths for all sample that treated by CoO and TiO_2 at different concentration (0.5, 0.75. 1.00, 1.25 and 1.5) molar, the treatment at range of (300-476) nm, it is observed that the value of transmission increase by molarity decrease. For the reflection of CNTs+CoO and CNTs+ TiO2 the results was shown in Fig (4.34) and (4.35) respectively, the reflection has been calculated using this formula

$$R = 1 - A - T$$

The maximum value of (R) is 0.2 (a.u) for all samples at the wavelength 283 nm for CNTs+CoO (0.00)and 336 nm for CNTs+CoO (1.5),the maximum value of (R) is 0.2 (a.u) for all samples at wavelength 345 nm for CNTs+CoO (0.00) and 365 nm for CNTs+CoO (1.50).

Fig (4.35) and (4.36) shows the refractive index (n) of the sample of CNTs+CoO and CNTs+ TiO_2, (n) is defined as the ratio between the speeds of light in a vacuum to its speed in material, and the value of n was calculated from the equation

$$n = \left[\left(\left(\frac{(1+R)}{(1-R)} \right)^2 - (1+k^2) \right)^{\frac{1}{2}} + \left(\frac{(1+R)}{(1-R)} \right) \right]$$

The value of (n) equal (2.80) for all samples at wave length (283 nm) for CNTs+ CoO (0.00 molar) and 336 nm for CNTs+ TiO_2 (1.5 molar), the value of (n) equal (2.79) for all samples at wave length (345 nm) for CNTs+ TiO_2 (0.00 molar) and 368 nm for CNTs+ TiO_2 (1.5 molar).

The optical energy band gab which has been calculated using the relation for CNTs+CoO and CNTs+ TiO_2 at concentration (0.5, 0.75. 1.00, 1.25 and 1.5) molar have been calculated from relation

$$(\alpha h\upsilon)^n = C(h\upsilon - Eg)$$

Where C = constant and n = type of transition, optical energy band gab which has been by plotting $(\alpha h\upsilon)^2$ VS photon energy ($h\upsilon$) as shown in fig (4.39) and (4.30) for CNTs+CoO and CNTs+TiO_2 respectively, the value of E_g for reference samples is 4.298 eV, CNTs+$Co_{(0.50)}$ is 4.134 eV, CNTs+$Co_{(0.75)}$ is 4.106 eV, CNTs+$Co_{(1.00)}$ is 4.028eV, CNTs+$Co_{(1.25)}$ is 3.818 eV and for CNTs+$Co_{(1.50)}$ is 3.613 eV while E_g for CNTs+ $TiO_{2\,(0.00)}$ is 3.514 eV, CNTs+ $TiO_{2\,(0.50)}$ is 3.449 eV, CNTs+ $TiO_{2\,(0.75)}$ is 3.433 eV, CNTs+ $TiO_{2\,(1.00)}$ is 3.401 eV, CNTs+ $TiO_{2\,(1.25)}$ is 3.360 eV and for CNTs+ $TiO_{2\,(1.50)}$ is 3.333 eV, it is observed that optical energy gap decrease due to concentration of cobalt oxide and titanium dioxide increase. Fig (4.41) and (4.42) shows the relation between real dielectric constant and wavelengths of CNTs + CoO and CNTs + TiO_2 at concentration (0.5, 0.75, 1.00, 1.25 and 1.5) molar respectively that has been calculated by relation

$$\varepsilon_1 = n^2 - k^2$$

The value of ε_1 equal 7.811 at wavelength 283 nm for CNTs +$CoO_{(0.00)}$, the same value at 337nm for CNTs +$CoO_{(1.5)}$, the value of ε_1 equal 7.82 at wavelength 345 nm for CNTs +$TiO_{2\,(0.00)}$, the same value at 368 nm for CNTs +$TiO_{2\,(1.5)}$. Fig (4.42) and (4.43) shows the relation between imaginary dielectric constant and wavelengths of CNTs + CoO and CNTs + TiO_2 at concentration (0.5, 0.75, 1.00, 1.25 and 1.5) molar respectively that has been calculated by relation

$$\varepsilon_2 = 2nk$$

The value of ε_2 equal $2.56x10^{-5}$ at 267.5 nm for CNTs +$CoO_{(0.00)}$ and $3.05x10^{-5}$ at 320 nm for CNTs +CoO (1.5), the value of ε_2 equal 3.48×10^{-5} at 345 nm for CNTs +TiO2 $_{(0.00)}$, the 2.98×10^{-5} value at 368 nm for CNTs +TiO2 (1.5).

The optical conductivity is a measure of frequency response of material when irradiated with light which is determined using the following relation

$$\sigma_{opt} = \frac{\alpha n c}{4\pi}$$

Where(c) is the light velocity, fig (4.43) and (4.44) shows the relation optical conductivity and wavelengths of CNTs + CoO and CNTs + TiO_2 at concentration (0.5, 0.75, 1.00, 1.25 and 1.5), the value of σ_{opt} is $1.44x10^{10}$ sec^{-1} at 265 nm for CNTs +CoO (0.00) and the same value at 320nm for CNTs +CoO (1.5) while for CNTs +TiO_2 (0.00) is $1.45x10^{10}$ sec^{-1} 324 nm and the same value at 350nm for CNTs +TiO_2 (1.5).

Fig (4.46) and (4.47) shows the relation electrical conductivity and wavelengths of CNTs + CoO and CNTs + TiO_2 at concentration (0.5, 0.75, 1.00, 1.25 and 1.5), the electrical conductivity can be estimated using the following relation

$$\sigma_{ele} = \frac{2\lambda\delta_{opt}}{\alpha}$$

The value of σ_{ele} is 38.15 ($\Omega.cm^{-1}$) at 287 nm for CNTs +CoO (0.00) 45.2 ($\Omega.cm^{-1}$) at 340 nm for CNTs +CoO (1.5) while for CNTs +TiO_2 (0.00) is 46.5($\Omega.cm^{-1}$) at 348 nm and 49.4 at 370 nm for CNTs +TiO_2 (1.5).

4.6 Discussion

According to XRD analysis we found that the concentration was change in of the CNTs +CoO and CNTs+TiO_2 structure. It is observed that the grain size affected by concentration and molecular weight, grain size decreased when concentration and molecular weight increase due to number of atoms per unit cell increase that's lead to increasing in distance between atomic levels in addition to that the concentration and molecular weight for doping element change the type of crystal (or its parameters) and miller indices, for CNTs+CoO we find that for low concentration (0.5 ,0.75) molar the type of crystal and density are the same(monoclinic-primitive) but when concentration increase (1, 1.25 and 1.5) molar

the type were changed to another types (monoclinic-B-centre and hexagonal-primitive) and the density changed due to angels. For CNTs+TiO_2 the crystal types for all samples also changed due to concentration and molecular weight for doping element (see table (4.3). It observed that the reference sample have grain size and d-space greater than grain size and d-space of CNTs+CoO and CNTs+TiO_2.

FTIR analysis showed that the transmittance of IR spectrum decreasing with Concentration increase, one observed that reference sample, CNTs+CoO and CNTs+TiO_2 approximate have same shape of spectrum except cobalt oxide and Titanium dioxide wavenumbers, this means that the consternation doesn't effect on IR shape spectra but effect on the absorption and transmission of the samples. The optical properties of CNTs were affected by concentration, the concentration lead to increase the absorption coefficient of all samples. It observed that the sample has high value of absorption has low value of transmittance. CNTs+CoO and CNTs+TiO_2 when to compare with the reference have same value of reflection at different wavelengths in red shift that means the polarization have same value in different wavelengths. Refractive index, optical conductivity and real dielectric constant for reference sample, CNTs+CoO and CNTs+TiO_2 have same value with red shift. The optical energy band gap decrease with concentration increase according to atomic level convergence and this confirm with XRD results. It is noted that optical energy band gap of CNTs+TiO2 less than optical energy band gap of CNTs+CoO. The electrical conductivity increase due to concentration increase because increasing concentration leads to increase of number of free electron in CNTs+CoO and CNTs+TiO_2. The diameter of CNTs decreases with concentration of CoO and TiO_2 increase. Average diameter of CNTs+TiO_2 greater than diameter of CNTs+CoO.

Imagej software was used to obtain surface roughness from SEM images for the reference sample CNTs+CoO and CNTs+ TiO_2. It is determine the variation of cobalt oxide and titanium dioxide concentration at prepared carbon nanotubes,

white color refer to treated area by cobalt oxide or titanium dioxide while black color refer to untreated area. For all samples we see that there are inhomogeneous distribution of doping element in samples, then concentration affected on surface roughness of the samples.

The results confirm with pervious study that concentration affected on optical properties and average diameter of carbon nanotubes. The different between this study and previous studies the method of preparing and sources of samples.

4.7 Conclusions

Chemical vapor deposition (CVD) was used to synthase carbon nanotubes doping by cobalt oxide and titanium dioxide at different concentration. X-ray diffraction (XRD) was used to study the structure of carbon nanotubes, scanning electron microscope was used to study the morphology of samples, and Fourier transforms infrared spectroscopy (FTIR) used study the vibrational frequencies of chemical bonds and structural properties, UV-Visible spectrometer used to study optical properties of samples. Diameter was calculated from SEM images by using Imagej and origin software's. The increasing on concentration on cobalt oxide and titanium dioxide leads to change structure parameter of carbon nanotubes samples (grain size, d-space…etc.) which lead to change poetical properties. The increase of concentration of cobalt oxide and titanium dioxide increase the absorption and decrease the optical angry band gab while have Constance reflectance, refractive index, real dielectric and optical conductivity at different wavelengths. Finally, found that the diameter of carbon nanotubes decrease when concentration increase.

4.8 Recommendation

- Use this material for synthase optoelectronic devices such as solar cell, multi-layer diode and gas sensor.
- Study the effect of distribution of doping elements on morphology of material.

- Study additional properties of carbon nanotubes (mechanical, thermal and magnetic)
- Synthase this material by different method.

References

[1] Mohamed Bououdina and J. Paulo Davim, Handbook of Research on Nanoscience, Nanotechnology, and Advanced Materials, IGI Global, ISBN 1466658240, 2016.

[2] Nasir Mahmoud and et al, Handbook of carbon nanotube-polymer nanocomposites, LAP LAMPART Academic Publishing, ISBN 978-3-659-64990-5, 2016.

[3] Simone Morais, Multi-Walled Carbon nanotubes, MDPI AG, published online in the open access journal applied science, 978-3039212293, 2019.

[4] Narendra Kumar and Sunita Kumbhat, Essentials in Nanoscience and Nanotechnology, John Wiley & Sons, 978-1119096115, 2016.

[5] T.Maniecki and et al, Carbon nanotubes: properties, synthesis and applicant, fiber chimestry journal, DOI 10.1007/s10692-019-09979-2, 2018.

[6] Megha Chitranshi and et al, Carbon Nanotube Sheet- Synthesis and Applications, Nanomaterial Journal, doi10.3390/nano10102023, 2020.

[7] Sonia Khanna and Nazmul Islam, Carbon Nanotubes-properties and applications, organic and medical chemistry Journal, DOI 10.19080/OMCIJ.2018.07.555705, 2018.

[8] Vasyle Harik, Mechanics of Carbon Nanotubes- Fundamentals, Modeling and safety, Academic Press, ISBN 978-0128110713,, 2018.

[9] Mechael J.O'Connell, Carbon Nanotubes: Properties and Application, CRC Press, 2018.

[10] Rahoul Rao and et al, Carbon nanotubes and related materials: Critical Advances and Challenges for Syntheses towards Mainstream Commercial Application, American Chemical Society, DOI: 10.1021/acsnano.8b06511, ACS Nano, 2018.

[11] John Edward and et al, An Introduction to Graphene and Carbon Nanotubes, Published online by Cambridge University, ISBN978-1498751797, 2018.

[12] Yury Gogotsi, Nanomaterial Handbook, CRC Press, ISBN 9781498703062, 2017.

[13] Lee Li Theng and et al, First Principle Study of Graphene Carbon Nanotubes Hybrid (GCH) Structure for Advanced Nanoelectronics Devices, IEEE International Conference of Semiconductors Electronics (ICSE), 2018.

[14]Beat Krause and et al, Nitrogen-Doped Carbon Nanotube/Polypropylene Composites Krause with Negative Seebeck Coefficient, Journal of Composite Science, doi: 10.3390/jcs4010014, 2020.

[15] H. Idriss and et al, Effect of Acetylene Rates and Temperature Variations of Iron Nanoparticles in Carbon nanotubes, INTERNATIONAL JOURNAL OF SCIENTIFIC & TECHNOLOGY RESEARCH, ISSN 2277-8616, 2017.

[16] Ibtehag Ali Sanosy1 Optical Properties of Barium Borate (BaB_2O_4) Compound for Current Optoelectronic Applications, Journal of Materials & Metallurgical Engineering, ISSN: 2321-4236, 2020.

[17] Azza Abdalwahab Abdalla and et al, The Effect of Annealing Temperature, Doping Carbon Nanotubes with TiO_2, CuO, ZnO and MgO on Its Conductivity and Electrical Primitively, GLOBAL JOURNAL OF ENGINEERING SCIENCE AND RESEARCHES, DOI- 10.5281/zenodo.3229422, 2019.

[18] Joydip Sengupta and Chacko Jacob, The effect of Fe and Ni catalysts on the growth of multiwalled carbon nanotubes using chemical vapor deposition, Journal of Nanoparticles Research 2019.

[19] Ali Nakhaei Pour and et al, Effects of metallic cobalt crystal phase on catalytic activity of cobalt catalysts supported on carbon nanotubes in Fischer–Tropsch synthesis. Reaction Kinetics and Mechanism, Vol. 44(4) 316–323, 2019.

[20] Maria Teresa Caccamo and et al, Thermal Investigations on Carbon Nanotubes by Spectroscopic Techniques, Journal of Materials, doi: 10.3390/app10228159, 2020.

[21] T. Arunkumar and et al, Synthesis and Characterization of Multi Walled Carbon Nanotubes (MWCNT), International Journal of Ambient Energy, ISSN: 0143-0750, 2018.

[22] Monika Rdest and et al, Effective Doping of Single-Walled Carbon Nanotubes with Polyethyleneimine, Journal of Materials, .doi.org/10.3390/ ma14010065, 2021.

[23] George Trakakis and et al, Mechanical, Electrical, and Thermal Properties of Carbon Nanotube Buckypapers/Epoxy Nanocomposites Produced by Oxidized and Epoxidized Nanotubes, Journal of Materials, doi: 10.3390/ma13194308, 2020.

[24] Salma Fath Alrahman Ahmed and et al, Study of the Optical Properties of Isonitrosoacetophenone (C8H7NO2) Using UV-Vis Spectroscopy, Journal of Photonic Materials and Technology, ISSN: 2469-8431 (Online), 2019

[25] Guohai Chen and et al, Diameter control of single-walled carbon nanotube forests from 1.3–3.0 nm by arc plasma deposition, Scientific Reports, DOI: 10.1038/srep03804, 2014.

[26] Megha Chitranshi and et al, Carbon Nanotube Sheet-Synthesis and Applications, Journal of Nanomaterials, 2023; doi: 10.3390/nano10102023, 2020.

[27] Dinesh K. Patel and et al, Carbon Nanotubes-Based Nanomaterials and Their Agricultural and Biotechnological Applications, Journal of Materials, doi:10.3390/ma13071679,2020.

[28] Timur Saliev, The Advances in Biomedical Applications of Carbon Nanotubes, Journal of Carbon Research, doi: 10.3390/c5020029, 2019.

[29] Wenquan Zhu and et al, Multi-walled carbon nanotube-based systems for improving the controlled release of insoluble drug dipyridamole, EXPERIMENTAL AND THERAPEUTIC MEDICINE 17: 4610-4616, 2019 DOI: 10.3892/etm.2019.7510, 2019.

[30] Ruhul Amin and et al, Carbon Nanotubes: Applications to Energy Storage Devices, Published online in IntechOpen, 2020.
[31] Yang Liu, and et al, Facile growth of carbon nanotubes using microwave ovens: the emerging application of highly efficient domestic plasma reactors, the Royal Society of Chemistry, DOI: 10.1039/c9na00538b, 2019.
[32] Kamelia Banihashemi and et al, The Construction of Carbon Nanotubes Containing an Anti-Bacterial Chemical Component and its Effect on MDR and XDR Isolates of Pseudomonas Aeruginosa, Reports of Biochemistry & Molecular Biology, Vol.9, No.1, 2020.
[33] Natalia P. Stepina and et al, Preparation and transport properties of oriented buckypapers with single walled carbon nanotubes, Modern Electronic Materials Journal, DOI 10.3897/j.moem.5.1.39452, 2019.
[34] B. B. Zhang, P. F. and et al, Microwave Absorption and Magnetic Properties of Cobalt Ferrites/Carbon Nanotubes Nanocomposites, World Scientific Publishing Company, DOI: 10.1142/S1793292015500708, 2015.
[35] Department of P.G. Studies & Research in Materials Science, G. U. K. Introduction to Nanoscience and Nanotechnology, CRC Press, 2016.
[36] Tawfik A. Saleh, Nanomaterials: Classification, Properties, and Environmental Toxicities, Environmental Technology & Innovation Journal, S2352-1864(20)31367-5, 2020.
[37] Ibrahim Khan and et al, Nanoparticles: Properties, applications and toxicities, Arabian Journal of Chemistry, 2017.
[38] Sulabha K. Kulkarni, Physics Department Indian Institute of Science Education and Research Nanotechnology: Principles and Practices, Third Edition, 2015.
[39] Chetna Dhand, and et al, Methods and Strategies for the Synthesis of Diverse Nanoparticles and their Applications: A Comprehensive Overview, RSC Advances, And DOI: 10.1039/C5RA19388E. 5. Hans-Georg Braun, Electron beam lithography, (2016).

[40] M. Braun, Handbook of Manufacturing Engineering and Technology, Springer-Verlag London, 2015.
[41] Yuan Lin and Xin Chen, Advanced Nano Deposition Methods, First Edition, Wiley-VCH Verlag GmbH & Co. KGaA,2016.
[42] Hans-Ulrich Krebs and, Pulsed Laser Deposition (PLD) - a Versatile Thin Film Technique, Advances in Solid State Physics, 2003. ·
[43] M. C. RAO, Department of Physics, Andhra Loyola College, PULSED LASER DEPOSITION — ABLATION MECHANISM AND APPLICATIONS, International Conference on Ceramics, Bikaner, India International Journal of Modern Physics: Conference Series, Vol. 22 (2013) 355–360, World Scientific Publishing Company, 2015.
[44] R. L. Boxman and V. N. Zhitomirsky, Vacuum arc deposition devices, EVIEW OF SCIENTIFIC INSTRUMENTS 77, 021101, 2017.
[45] Amit Kumar and et al, Sol-Gel Derived Nanomaterials and its Applications: A Review, Research Journal of Chemical Sciences, Vol. 5(12), 98-105, December (2015).
[46] Antonio Cid, Synthesis of NPs by Microemulsion Method, Microemulsion - A Chemical Nanoreactor, DOI: http://dx.doi.org/10.5772/intechopen.80633, 2017.
[47] Radu-Robert Piticescu and et al, Hydrothermal Synthesis of Nanostructured Materials for Energy Harvesting Applications, International Journal of Materials Chemistry and PhysicsVol. 1, No. 1, 2015.
[48] Guijun Yang and Soo-Jin Park, Conventional and Microwave Hydrothermal Synthesis and Application of Functional Materials: A Review, MDPI. Journal/material, 2019.
[49] Xinhe Zhao and et al, Chemical vapor deposition and its application in surface modification of nanoparticles, Institute of Chemistry, Slovak Academy of Sciences, 2019.

[50] Monaliben Shah and et al, Green Synthesis of Metallic Nanoparticles via Biological Entities, MDPI. Journal/material, 2015.

[51] Kadircan H Keskinbora and Muslim A Jameel, Nanotechnology Applications and Approaches in Medicine: A Review, iMedPub Journals, Vol.2 No.2:6, 2018.

[52] Amra Bratovcic, Different Applications of Nanomaterials and Their Impact on the Environment, SSRG International Journal of Material Science and Engineering (IJMSE) - Volume 5 Issue, 2019.

[53]Robert E. Camley, Robart L.stamps, Solid State Physics, Elsevier Inc, ISBN 978-0-12-815242-3 2018.

[54] Quinn, John J.,Yi, Kyung-soo, Solid State Physics Principle And Modern Application, Springer ISBN 978-3-319-7999-1,2018.

[55] Patterson, James, Bailey Bernard C., Solid State Physics, Introduction to the Theory, Springer, ISBN 978-319-75322-5, 2018.

[56] Dr. Prathap Haridodd, Physics of Materials: Essential Concepts of Solid State Physics, Willey, ISBN 978-8126557875, 2015.

[57] Augusta Lawrence, Solid State Physics, Larsen and Keller Education, ISBN 978-1641721479, 2019.

[58]Wolfram Hergert and R.Matthias Geilhufe Group Theory in the Solid State Physics and Photonic, Willey, ISBN 978-3527411337, 2018.

[59] Siegmar Roth and David Carroll, Foundation of Solid State Physics, Willey, ISBN 978-3527345045, 2019.

[60] Mark.F.Vitha, Spectroscopy: Principle and Instrumentation, Willey, ISBN 1119436648, 2018.

[61] Farrmukh M A, Advanced Aspects of Spectroscopy, IntechOpen, ISBN 978-9535107156, 2015.

[62]Colin N. Banwell and Eliaine M.McCash,Fundamental of Molecular Spectroscopy, Mc Graw Hill India, ISBN 978-9352601738, 2016.

[63] Dr. Ashima Kathuria, Dr.Agarwala and Dr. Keemti Lal, Jak Prakash &Co, ISBN 978-819292900582, 2017.

[64] Catherine E. Housecroft, Inorganic Chemistry, Person Education, ISBN 978-1292139913, 2018.

[65] Lucarini and et al, Application of Infrared Spectroscopy for functional Compound Evaluation, Journal of Spectroscopy, doi.org/10.1155/2019/5319024, 2019.

[66] Marwa Elazazy, Infrared Spectroscopy: Principle, Advanced and Application, IntechOpen, ISBN 978-1-78984969-1, 2019.

[67] Marcello and et al, UV-Visible Spectroscopy, De Gruyter, Published online doi.org/10.1515/psr-2018-008, 2018.

[68] Azad Mohammed and Avin Abdullah, Scanning Electron Microscope (SEM): A Review, International Conference on Hydraulics and Pneumatics-HERVEX, ISSN 1454-8003, 2018.

[69] E.s.Ameh, A review of basic X-ray diffraction application, The International of Advanced Manufacturing Technology, Springer, doi 10.1007/s00170-019-04508-1, 2020.

[70] Dogllas R. Powell, Review of X-ray Crystallography, Journal of Chemical Eduction, doi 10.1021/acs.jchemed.5b00893, 2016.

[71] Tiago Ferreira and Wayne Rasband, ImageJ User Guide, ImageJ User Guide IJ 1.46r ImageJ/Fiji 1.46, 2020.

[72] Origin User Guide, Origin Lab Corporation, 2016.